Fall 2010

Characterization of diamond thin films and related materials

Travis K. McKindra

Department: Materials Science and Engineering

CHARACTERIZATION OF DIAMOND THIN FILMS AND RELATED MATERIALS

by

TRAVIS KYLE MCKINDRA

A DISSERTATION

Presented to the Faculty of the Graduate School of the

MISSOURI UNIVERSITY OF SCIENCE AND TECHNOLOGY

In Partial Fulfillment of the Requirements for the Degree

DOCTOR OF PHILOSOPHY

in

METALLURGICAL ENGINEERING

2010

Approved by

Matthew J. O'Keefe, Advisor
F. Scott Miller
Wayne Huebner
Richard Brow
Hai-Lung Tsai

PUBLICATION DISSERTATION OPTION

This dissertation has been prepared in the form of four manuscripts for publication. The first manuscript (pages 13-33) is a reviewed and revised manuscript that has been submitted to and formatted in the style of Diamond and Related Materials. The second manuscript (pages 34-54) has been published in Applied Surface Science in February 2009. The third manuscript (pages 55-75) was published in Materials Characterization in June 2010. The fourth manuscript (pages 76-95) has been formatted in the style of and submitted to Surface Coatings and Technology. Appendix A (pages 101-113) has been prepared as additional work complimentary to the first manuscript. Appendix B (pages 114-130) has been prepared as additional work related to the third and fourth manuscript. Appendix C (pages 131-177) contains unpublished results.

ABSTRACT

Thin carbon films including sputtered deposited graphite and CO_2 laser-assisted combustion-flame deposited graphite and diamond thin films were characterized using optical and electron microscopy, X-ray diffraction and micro-Raman spectroscopy.

Amorphous carbon thin films were deposited by DC magnetron sputtering using Ar/O_2 gases. The film morphology changed with the oxygen content. The deposition rate decreased as the amount of oxygen increased due to oxygen reacting with the growing film. The use of oxygen in the working gas enhanced the crystalline nature of the films.

Graphite was deposited on WC substrates by a CO_2 laser-assisted O_2/C_2H_2 combustion-flame method. Two distinct microstructural areas were observed; an inner core of dense material surrounded by an outer shell of lamellar-like material. The deposits were crystalline regardless of the laser power and deposition times of a few minutes.

Diamond films were deposited by a CO_2 laser-assisted $O_2/C_2H_2/C_2H_4$ combustion-flame method with the laser focused parallel to the substrate surface. The laser enhanced diamond growth was most pronounced when deposited with a 10.532 μm CO_2 laser wavelength tuned to the CH_2-wagging vibrational mode of the C_2H_4 molecule.

Nucleation of diamond thin films deposited with and without using a CO_2 laser-assisted combustion-flame process was investigated. With no laser there was nucleation of a sub-layer of grains followed by irregular grain growth. An untuned laser wavelength yielded nucleation of a sub-layer then columnar grain growth. The 10.532 μm tuned laser wavelength caused growth of columnar grains.

ACKNOWLEDGMENTS

This dissertation as the culmination of my graduate studies would not have been completed without the guidance and support of many special people. Without taking the time to thank everyone individually, I would like to express my deepest thanks and gratitude for all of your help.

I would like to thank my advisor, Dr. Matthew O'Keefe, for giving me the opportunity to learn from him. I would also like to express my gratitude for his patience, guidance and motivation during the entire process.

I would like to acknowledge my dissertation committee for their efforts. My sincere appreciation goes to Dr. F. Scott Miller, Dr. Wayne Huebner, Dr. Richard Brow and Dr. Hai-Lung Tsai for their insight and assistance.

To my colleagues and friends without whom this would not be possible: Jeff Wight, Eric Bohannon, Clarissa Wisner, Ron Haas, Kenny Allison and Elizabeth Kulp.

Special thanks to my parents, sisters and extended family for their love and support during my graduate studies.

TABLE OF CONTENTS

Page

PUBLICATION DISSERTATION OPTION iii

ABSTRACT iv

ACKNOWLEDGMENTS v

LIST OF ILLUSTRATIONS ix

LIST OF TABLES xii

SECTION

1. INTRODUCTION 1

1.1. DEPOSITION TECHNIQUES 2

1.2. EFFECT OF OXYGEN ON DIAMOND AND DLC GROWTH AND DEPOSITION 4

1.3. APPLICATIONS 6

1.4. CHARACTERIZATION 7

1.5. RESEARCH OBJECTIVE 9

1.6. REFERENCES 10

PAPER

1. REACTIVE SPUTTER-DEPOSITION OF OXYGENATED AMORPHOUS CARBON THIN FILMS IN AR/O_2 13

Abstract 13

Introduction 14

Material and methods 15

Results and Discussion 16

Conclusions 22

Acknowledgements 22

References 23

2. CHARACTERIZATION OF ULTRA-FAST DEPOSITED POLYCRYSTALLINE GRAPHITE BY A CO_2 LASER-ASSISTED COMBUSTION-FLAME METHOD 34

Abstract 34

1. Introduction 35

2. Experimental details 36
3. Results and discussion 38
4. Conclusions 42
Acknowledgements 42
References 43
3. CHARACTERIZATION OF DIAMOND THIN FILMS DEPOSITED BY A CO_2 LASER-ASSISTED COMBUSTION-FLAME METHOD 55
Abstract 55
1. Introduction 56
2. Experimental 58
3. Results and discussion 59
4. Conclusion 66
Acknowledgments 66
References 73
4. NUCLEATION AND GROWTH OF DIAMOND THIN FILMS DEPOSITED BY A CO_2 LASER-ASSISTED COMBUSTION-FLAME METHOD 76
Abstract 76
1. Introduction 77
2. Material and methods 78
3. Results and discussion 79
4. Conclusion 85
Acknowledgments 86
References 87
SECTION
2. SUMMARY AND CONCLUSIONS 96
3. FUTURE WORK 99
APPENDICES
A. DEPOSITION OF CARBON THIN FILMS IN Ar/CO_2 101
B. NUCLEATION AND INTIAL GROWTH OF DIAMOND THIN FILMS ON SILICON 114
C. UNPUBLISHED RESULTS 131

VITA 178

LIST OF ILLUSTRATIONS

INTRODUCTION

Figure 1.1. Ternary phase diagram of diamond-like carbon species 1

1. REACTIVE SPUTTER DEPOSITION OF OXYGENATED AMORPHOUS CARBON THIN FILMS IN Ar/O_2

Figure 1. Deposition rate versus percentage of O_2 for a given working pressure. 26

Figure 2. Comparison of XRD spectra for selected samples and the crystalline features..... 27

Figure 3. SEM images from selected films deposition parameters (a) 5% O_2 – 2 mTorr, (b) 5% O_2 – 5 mTorr, (c) 10% O_2 – 2 mTorr and (d) 25% O_2 – 2 mTorr. 28

Figure 4. AFM images showing morphology of carbon thin films deposited under varying oxygen partial pressures (a) 5% O_2 - 2 mTorr, (b) 5% O_2 - 5 mTorr, (c) 10% O_2 - 2 mTorr, and (d) 25% O_2 - 2 mTorr. All images are 1 μm × 1 μm. The black to white grayscale is 15 nm in (a) through (c) and 6 nm in (d)..... 29

Figure 5. XPS spectra of C 1s from films deposited with (a) 0% O_2 at 2 mTorr, (b) 0% O_2 at 5 mTorr, (c) 5% O_2 at 2 mTorr, (d) 5% O_2 at 5 mTorr, (e) 10% O_2 at 2 mTorr, and (f) 25% O_2 at 2 mTorr. 30

Figure 6. The Raman spectra from the carbon films deposited at (a) 2 mTorr and (b) 5 mTorr..... 32

Figure 7. Variation of the I_D/I_G ratio and G peak position with oxygen in the sputtering gas at both working pressures. 33

2. CHARACTERIZATION OF ULTRA-FAST DEPOSITED POLYCRYSTALLINE GRAPHITE BY A CO2 LASER-ASSISTED COMBUSTION-FLAME METHOD

Fig 1. Schematic drawing of as-deposited structure. 45

Fig.2. SEM micrographs of as-deposited carbon pillars, processed with CO_2 laser power of (a) 400 W, and (b) 800 W showing the pillar base (A) and pillar (B) 46

Fig. 3. XRD spectra of carbon pillar and pillar base which shows a (002) graphite peak..... 47

Fig. 4. Plan view TEM micrographs with inset electron diffraction pattern of particles from (a) graphite pillar, (b) bulk graphite, and (c) large grain from graphite pillar..... 498

Fig. 5. SEM micrographs of cross-sections of CO_2 laser-assisted combustion-flame deposited carbon pillars with laser power of (a) 400 W and (b) 800 W showing the “shell” (A) and “core” (B) 50

Fig. 6. SEM micrographs of alternate cross-section of CO_2 laser-assisted combustion-flame deposited carbon pillars with laser power of (a) 400 W and (b) 800 W showing the “shell” (A) and “core” (B)..... 51

Fig. 7. SEM micrographs of cross-section of CO_2 laser-assisted combustion-flame deposited carbon pillar with laser power of 600 W (a) entire pillar with arrows ‘A’ and ‘B’ denoting areas of interest, (b) higher magnification image displaying the outer shell labeled ‘A’, inner “core” labeled ‘B’, the pillar base labeled ‘C’ and (c) higher magnification image contrasting the growth direction of the outer shell labeled ‘A’ and the pillar base labeled ‘B’ of the carbon pillar 52

3. CHARACTERIZATION OF DIAMOND THIN FILMS DEPOSITED BY A CO_2 LASER-ASSISTED COMBUSTION-FLAME METHOD

Fig. 1. Optical micrograph of as-deposited film with the center of the deposit labeled ‘A’. 67

Fig. 2. XRD spectra from films deposited at CO_2 laser wavelength of (a) 10.591 μm and (b) 10.532 μm. 68

Fig. 3. Comparison laser wavelength effect on X-ray diffraction peak associated with diamond (111) planes from films deposited without laser irradiation and at each laser power. 69

Fig 4. Comparison of Raman spectra from films deposited with CO_2 laser wavelength of (a) 10.591 μm and (b) 10.532 μm. 70

Fig. 5. Dark-field STEM images from diamond films deposited with CO_2 laser wavelength of 10.591 μm and laser power of (a) no laser, (b) 100 W, (c) 400 W and (d) 800 W. 71

Fig. 6. Dark-field STEM images from diamond films deposited with CO_2 laser wavelength of 10.532 μm and laser power of (a) no laser, (b) 100 W, (c) 400 W and (d) 800 W. 72

4. NUCLEATION AND GROWTH OF DIAMOND THIN FILMS DEPOSITED BY A CO_2 LASER-ASSISTED COMBUSTION FLAME METHOD

Fig. 1. XRD spectra from films deposited for (a) 1, (b) 2, (c) 5 minutes with (d) 2θ range associated with diamond (111) planes from films deposited for 5 minutes. 89

Fig 2. Comparison of Raman spectra from films deposited (a) 1, (b) 2 and (c) 5 minutes. 90

Fig 3. SEM micrographs from the center of films deposited for 1 minute with (a) no laser irradiation, (b) untuned laser irradiation and (c) tuned laser irradiation. 91

Fig 4. SEM micrographs from the center of films deposited for 2 minutes with (a) no laser irradiation, (b) untuned laser irradiation and (c) tuned laser irradiation. 92

Fig 5. SEM micrographs from the center of films deposited for 5 minutes with (a) no laser irradiation, (b) untuned laser irradiation and (c) tuned laser irradiation. 93

Fig 6. Dark-field STEM images from cross-sections of diamond films deposited for 1 minute with (a) no laser, (b) untuned and (c) tuned laser irradiation..... 94

Fig 7. Dark-field STEM images from cross-sections of diamond films deposited for 5 minutes with (a) no laser, (b) untuned and (c) tuned laser irradiation. Some individual grains have been outlined for clarity. 95

LIST OF TABLES

1. REACTIVE SPUTTER DEPOSITION OF OXYGENATED AMORPHOUS CARBON THIN FILMS IN Ar/O_2

Table I. Summary of oxygen content from XPS chemical quantification 31

2. CHARACTERIZATION OF ULTRA-FAST DEPOSITED POLYCRYSTALLINE GRAPHITE BY A CO2 LASER-ASSISTED COMBUSTION-FLAME METHOD

Table I. Summary of measured d-spacings for the carbon pillar with comparisons to a bulk graphite sample and calculated values 54

1. INTRODUCTION

The simplest distinguishing characteristic between diamond and its related materials (diamond-like carbon) is the type of bonding. The bonding lies between that of diamond and graphite and can described as elemental (carbon) network solids joined by covalent bonding. Graphite contains layers of covalently bonded hexagons of carbon atoms with weak Van der Waals bonds between the layers. Crystalline graphite has a hexagonal crystal structure and has P63mc symmetry. The carbon atoms in diamond are covalently bonded by sp^3 hybrid bonds that extend throughout the solid in a tetrahedral framework. Cubic diamond lies in the Fd3m symmetry group.

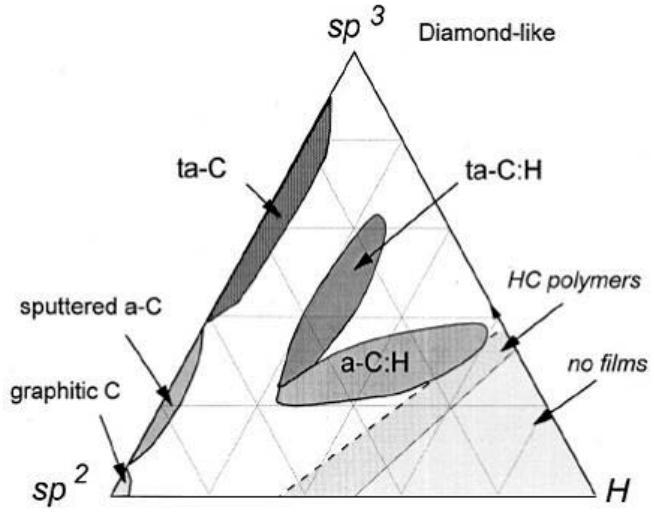

Figure 1.1. Ternary phase diagram of diamond-like carbon species (from Ref. [1]).

Diamond-like carbon is a term used to classify a variety of carbon species. In general, these materials are amorphous and may contain 1 at% up to 50 at% hydrogen. The hydrogenated form (a-C:H) typically contains less than 50% sp^3 bonds, while the non-hydrogenated form (a-C or ta-C) may contain as much as 85% C-C sp^3 bonds. The diamond-like carbon (DLC) materials contain a significant fraction of sp^3 bonds, which imparts the mechanical and physical properties similar to diamond such as high hardness (5-80 GPa), low friction coefficient (<0.01-0.7), visible and IR transparency and chemical inertness [1].

1.1. DEPOSITION TECHNIQUES

Diamond and DLC films have been deposited by several different processes based on chemical (CVD) or physical (PVD) vapor deposition techniques. CVD has been used to produce synthetic diamond and DLC films. These films have been hydrogenated as hydrocarbons or used hydrogen gas as the precursor sources. The substrate temperature was in the range of 800-900°C which limited the type of substrates to those unaffected by the high temperature [1]. The plasma-enhanced (PECVD) and microwave plasma-enhanced (MPECVD) CVD techniques have been shown to successfully deposit DLC at lower substrate temperatures (300-500°C) [1]. The combustion-flame CVD method has been used to deposit diamond films and used a commercial oxy-acetylene torch [2-4]. Other combustion gases have been used [5,6]. A recent application of the process included the addition of CO_2 laser energy [7,8]. An KrF excimer laser has been used in combination with the combustion flame also [9].

The filtered cathodic vacuum arc (FCVA) process has been used to deposit many hard thin films like ta-C. These films have a high sp^3 fraction approaching 87%, which contributes to the properties of high hardness and high internal stress that limits the film thickness. Metals have been incorporated in these films to increase the adhesion and lower the internal stress. The metal incorporation lowered the sp^3 fraction and the stress, while the hardness remained [10].

Lasers have also been used in the deposition processes in the form of laser ablation of a graphite target. Amorphous carbon, a-C:H, and microcrystalline diamond films have been formed in a hydrogen atmosphere on silicon substrates by the pulsed excimer laser ablation of a graphite target. Higher substrate temperatures produced superior uniformity as well as a cubic morphology. These temperatures were reported to be as low as 150°C [11]. In addition, it has been reported that a femtosecond laser ablation process produced hydrogen free DLC thin films with good scratch resistance, chemical inertness, and high optical transparency. The films were produced at room temperature under high vacuum using a polycrystalline graphite disk [12].

Sputter deposition has been used extensively to deposit DLC films including direct current (DC), radio frequency (RF), and ion beam deposition. Typically, Ar has been used as the source gas with a pure graphite target, but reactive sputtering with hydrocarbon gases has also been done. Variations on dual ion beam sputtering have shown the ability to deposit highly tetrahedral amorphous carbon (ta-C) at substrate temperatures below 70°C. This film deposition combined rf magnetron sputtering with bombardment with energetic (100 eV) Ar ions during deposition. The ratio of Ar ion flux to neutral carbon flux was approximately five, producing a film density of 2.7 g/cm^3 with a maximum compressive stress of 16 GPa. This produced strong clustering of sp^3 carbon [13].

There have been many instances of RF magnetron sputtered DLC films from a graphite target. In the case of an inert source gas (Ar), transparent, a-C films with a structure close to that of amorphous diamond were deposited at room temperature. The main parameters that affected the films were sputtering power, working pressure, bias voltage, and substrate to target distance [14]. Another case typically produced a-C films with 62% sp^2 and 38% sp^3 content. As the substrate temperature was increased an ordering of the films was observed, but the sp^2/sp^3 ratio did not change with temperature, indicating high thermal stability. In the substrate temperature range of room temperature to 450°C, the deposition rate varied from 100 nm/h to 1600 nm/h [15].

Asymmetric bipolar pulsed-DC magnetron sputtering produced DLC films at room temperature using a graphite target and a source gas of Ar with 7.5% methane. A DC bias was applied to the substrate, which affected the deposition rate, intrinsic compressive stress, and abrasive wear. Pulsed DC power increased the plasma ionization compared to RF power, resulting in higher ion and electron density, producing more energetic carbon species [16].

Other studies on the effect of substrate bias with DC magnetron sputtering produced pure a-C films with a constant versus a graded bias [17]. The bias-graded deposition lowered the coefficient of friction by 20% and doubled the adhesion of the film. The effect of the source gas was studied with DC magnetron sputtering using a graphite target with Ar/C_2H_2 and Ar/CH_4 gas mixtures. In both cases when the partial pressure of the hydrocarbon was increased the atoms bonding configuration was

modified. The lower molecular weight hydrocarbon (CH_4) produced superior films, which may make it more attractive for use in MEMS applications [18]. Another case involved the addition of nitrogen to a mixture of argon and methane. The increased nitrogen content increased the deposition rate and dielectric constant [19].

1.2. EFFECT OF OXYGEN ON DIAMOND AND DLC GROWTH AND DEPOSITION

Hydrogen plays an important role in the growth of synthetic diamond, but recent research suggests that oxygen may also prove useful [20-23]. The oxygen present during DLC deposition will preferentially etch away the sp^2 species present leaving sp^3 and a more diamond-like film [24, 25]. Similar to use of hydrocarbons as source gases for the deposition of diamond and DLC, oxygen has been used with a variety of deposition techniques. The most popular technique has been laser ablation. An experiment with a KrF excimer pulsed laser deposition (PLD) utilizes the laser ablation of a graphite target in a low-pressure (0.15 Torr) oxygen atmosphere [23]. The technique produced epitaxially grown high quality diamond crystals on sapphire without diamond seeding of the substrate at temperatures below 600°C. The researchers concluded that the oxygen gas played a role in the preferential etching of the graphitic phase. A similar experiment produced hexagonal and cubic diamond in a non-uniform, discontinuous film with particle sizes in the nanometer range. X-ray diffraction confirmed the presence of cubic and hexagonal diamond. The growth conditions for diamond deposition were more critical in the presence of oxygen compared to previous work in a hydrogen atmosphere. The important parameters were substrate temperature, the oxygen pressure and the “mold effect” of the sapphire [20]. In addition to traditional PLD, plasma-assisted PLD (PAPLD) has produced a-C thin films. An oxygen RF plasma with an ArF excimer laser was used to deposit nanometer-sized particles up to an sp^3 content of 58% at a substrate temperature of 410°C. Nanocrystalline diamond films have been deposited by KrF excimer laser PLD and PAPLD with a graphite target on silicon and sapphire substrates [22]. The substrate temperature ranged from 20-660°C and the working pressure ranged

from 1-270 Pa [22]. XRD of the films revealed no peaks attributed to diamond, but Raman spectroscopy showed nanocrystalline diamond features.

Amorphous carbon and diamond films were deposited at temperatures lower than 500°C by MPECVD with the addition of oxygen to the precursor of CH_4/H_2 [21]. Water cooling or decreasing the gas pressure and microwave power were used to achieve the substrate temperatures below 500°C. The research concluded that the addition of oxygen was instrumental to the ability to lower the critical temperature for diamond growth, improving the quality of the Raman peaks, and increased film transparency.

The sp^2/sp^3 carbon ratio and surface chemistry of detonation-synthesized nanodiamond powders has been controlled by selective oxidation in air. Amorphous and graphitic carbon species were selectively removed from nanodiamond powders with an optimal temperature range of 400-430°C. XANES results indicated an increase in sp^3 content from 23-81% for a selected sample, which is a purity approaching that of microcrystalline diamond. This process also allowed metal impurities encased in carbon prior to oxidation to be removed by treatment in diluted acids after oxidation [25]. An experiment of the oxygen plasma etching of magnetron sputtered DLC films (a-C and a-C:H) showed Raman results indicating oxygen reactive ion etching (RIE) preferentially etched the non-crystalline carbon atoms. The remaining film had higher sp^3 content [24].

The combustion-flame CVD method relies heavily on the oxygen to fuel ratio regardless of the hydrocarbon used for the fuel. A theoretical prediction of the suitable O_2/C_2H_2 ratio and substrate temperature ranges for diamond deposition discovered that the widest temperature range existed when the oxygen/fuel ratio was approximately one [26]. Additionally, the researchers discovered that diamond synthesis was thermodynamically favorable at $O_2/C_2H_2 > 1.1$, but the deposition rate (kinetically) may be very low comparatively. Another study investigated the fuel/oxygen ratio for premixed oxygen-acetylene and oxygen-ethylene flames [6]. Raman spectroscopy of the films indicated that diamond formed over a range of temperatures when the flame was neutral (O_2/fuel ~ 1.0). Graphite formation was promoted with lower oxygen/fuel ratios and higher substrate temperatures, while lower substrate temperatures and oxygen/fuel ratios favored amorphous carbon growth.

1.3. APPLICATIONS

The various deposition techniques produce films with different properties applicable to a wide variety of uses. When DLC films are deposited by sputtering, another material can be co-sputtered such as Ti or Al. These additions created a nanocomposite and increased the adhesion of the films [17]. Metals have typically been added to DLC films to lower the internal stress of the films. Reactive DC magnetron sputtering has been used to produce metal containing DLC films (Me-DLC). Transition metals or transition metal carbides in conjunction with acetylene produced films with composition and structure nearly identical to films produced by the glow discharge with similar mechanical and tribological properties. This process could be up-scaled due to the economic viability in the lower cost of graphite [27]. There have been several instances of "doping" of DLC films. Metals such as titanium have been added by ion implantation to alter the tribological properties [28]. The addition of silicon in DLC films has been shown to be a successful etch stop for oxygen reactive ion etching of DLC, as well as lowering film stress and increasing biocompatibility [29].

There has been interest in using DLC materials in integrated circuit fabrication as low-k dielectrics ($k<4.0$), as components in microelectromechanical systems (MEMS) [30], and as an antireflective coating [31]. Dielectric films include the incorporation of fluorine into amorphous carbon films. The dielectric constant (k) for the films was varied between 2.7 and 3.3. The thermal stability of the films correlated with the dielectric constant; as k decreased the films became less stable at high temperature (~400°C) [32]. DLC films have also been investigated as a hard coating and a resist material for lithography [33]. Amorphous carbon films with high sp^3 content and smooth surfaces were determined to be suitable for MEMS applications. Thin DLC films were used as antireflective and protective coatings on GaAs devices. The films had excellent adhesion and increased the IR transmittance and microhardness when compared to an uncoated substrate [31].

DLC, a-C, and ta-C films have found uses in the biomedical field as possible biocompatible coatings on stainless steel components. Films between 50nm and 100nm were found to stimulate less inflammatory activity than uncoated materials [34]. Nitinol

(NiTi) alloys that are used in biomedical applications due to its shape memory, superelasticity, and biocompatibility have been coated with DLC films. The films suppressed the diffusion of Ni atoms. In addition, coated NiTi samples showed increased corrosion resistance and hemocompatibility compared to uncoated samples. The DLC films also appeared to have no effect on the transformation temperature and superelasticity of the NiTi [34].

Diamond-like carbon (DLC) films have been shown to possess tribological properties similar to diamond such as high hardness, wear resistance and low coefficient of friction. DLC films have been used as protective coatings for various substrates including ceramic, glass [35], various steel and titanium alloys [36-38].

1.4. CHARACTERIZATION

The characterization of amorphous carbon thin films uses a myriad of techniques to determine the bonding nature of the carbon atoms as well as structural and mechanical properties. One of the most commonly used techniques is Raman spectroscopy due to its ability to distinguish between different forms of carbon (sp^2 and sp^3) and the fact that it is non-destructive [39]. Raman spectroscopy is used to examine quantized molecular resonances by the observation of transitions between vibrational energy levels caused by inelastic scattering of high-energy photons. The Raman spectrum for diamond (sp^3 carbon) shows a single peak at 1332 cm^{-1}. The distinguishable types of sp^2 carbon are crystalline graphite and disordered or microcrystalline graphite. The spectrum for crystalline graphite shows a peak at 1580 cm^{-1}, while the spectrum for disordered graphite shows two broad peaks at 1580 cm^{-1} and 1350 cm^{-1}. Some peak position shift and linewidth fluctuation can occur due to film stress, sample temperature, or due to disorder in the bonding environment [40].

X-ray diffraction (XRD) is a non-destructive technique used to determine the crystalline structure and confirm diamond synthesis. In addition, XRD can provide quantitative measurements of d-spacings and information about preferential orientation, residual strain and grain size. Amorphous or nanocrystalline films may yield little to no

information due to their small grain size which results in broad peaks in the XRD spectrum [40].

Several techniques can be used to investigate the bonding characteristics of these films including x-ray photoelectron spectroscopy (XPS). XPS is a surface chemistry technique used for determining the chemical binding of atoms. X-rays incident on the sample interact with atoms via quantum energy absorption causing the ejection of an inner shell electron. The kinetic energy of this electron is related to the binding state (binding energy) of the atom. The peak intensities from the XPS spectra can be used to obtain quantitative information, but peak ratios are more reliable [40]. The sp^2 and sp^3 components in carbon films can be determined from the C 1s core photoelectron peak that is near 285 eV [28,41]. The absolute values of these peaks are somewhat subjective and dependent on the individual instrument, but the separation of the sp^2 and sp^3 peaks is generally accepted to be ~ 1 eV. Other characterization techniques such as electron energy-loss spectroscopy (EELS) and nuclear magnetic resonance (NMR) can be used to determine the sp^3 content in the films.

Microscopy techniques used to characterize carbon films include scanning electron (SEM), transmission electron (TEM) and atomic force (AFM) microscopy. SEM is used to investigate the surface morphology of the films including the crystallite size and faceting. Amorphous and microcrystalline films may appear featureless. Energy dispersive spectroscopy (EDS) conducted with the SEM may provide information about non-trace elements in the films. AFM provides a high magnification three-dimensional image of a solid surface and can examine the film morphology, roughness, and grain size. TEM can be difficult to employ with bulk samples since the sample must be electron transparent, but thin films can be readily observed. TEM can yield pertinent information about grain boundaries and growth interfaces and electron diffraction can be used to determine lattice parameters [40]. Mechanical properties such as hardness and elastic modulus of carbon films can be determined by nanoindentation. Substrate effects can be difficult to avoid during indentation, thus scratch testing is a useful alternative for mechanical and adhesion properties [42]. Optical properties of these films can be determined by Fourier transform infrared spectroscopy (FTIR), IR transmittance, or ellipsometry.

1.5. RESEARCH OBJECTIVE

Based on the success of the laser ablation to produce diamond-like films, sputtering has the potential to deposit diamond-like thin films in the presence of oxygen by investigating the process atmosphere. The process atmosphere relates to the precursor gases used to supply carbon and oxygen atoms to react with the carbon atoms removed from the surface of the sputtering target. This atmosphere must be controlled such that the critical combination of C and O is reached to facilitate the formation of sp^3 bonds (characteristic of diamond) and the etching of sp^2 bonds (characteristic of graphite). The chemical bonding nature of the films will be investigated by x-ray photoelectron spectroscopy (XPS) and Raman spectroscopy. The sputtering power must be optimized such that deposition rate, dissociation and ionization of the reactant gases may be controlled. Determining the effect of the substrate temperature on the nucleation and growth of the film will allow for tailoring film properties such as surface morphology and crystallinity characterized by electron microscopy techniques.

The research efforts will also include the characterization of films from a deposition process that is a laser-assisted combustion-flame CVD method deposited at the University of Nebraska-Lincoln. The films are deposited in open atmosphere. Characterization techniques including scanning electron microscopy (SEM), transmission electron microscopy, x-ray diffraction, x-ray photoelectron spectroscopy and focused-ion beam (FIB) manufactured scanning transmission electron microscopy (STEM) will be used to correlate precursor and process conditions in terms of the deposited phases, film morphology. The characterization will allow for the study of the relationship between process parameters and film microstructural development.

1.6. REFERENCES

[1] Grill, A., Diamond and related materials, (1999) 8(2-5) 428-434.

[2] Hirose, Y., S. Amanuma, and K. Komaki, Journal of Applied Physics, (1990) 68(12) 6401-6405.

[3] Matsui, Y., H. Yabe, and Y. Hirose, Jpn. J. Appl. Phys, (1990) 29(8) 1552–1560.

[4] Matsui, Y., A. Yuuki, M. Sahara, and Y. Hirose, Jpn. J. Appl. Phys, (1989) 28(9) 1718-1724.

[5] Carrington, W., L. Hanssen, K. Snail, D. Oakes, and J. Butler, Metallurgical and Materials Transactions A, (1989) 20(7) 1282-1284.

[6] Snail, K.A., D.B. Oakes, J.E. Butler, and L.M. Hanssen, New diamond science and technology, (1991) 503-509.

[7] Han, Y.X., H. Ling, J. Sun, M. Zhao, T. Gebre, and Y.F. Lu, Applied Surface Science, (2008) 254(7) 2054-2058.

[8] Ling, H., Y.X. Han, and Y.F. Lu, Proceedings of SPIE 6459, 2007, p. 64590Y-1-64590Y-7.

[9] Han, Y.X., H. Ling, and Y.F. Lu, Journal of Applied Physics, (2006) 100(12) 124911-5.

[10] Liu, E., L. Li, B. Blanpain, and J.P. Celis, Journal of Applied Physics, (2005) 98 073515.

[11] Bourdon, E.B.D., P. Kovarik, and R.H. Prince, Diamond and related materials, (1993) 2(2-4) 425-431.

[12] Qian, F., V. Craciun, R.K. Singh, S.D. Dutta, and P.P. Pronko, Journal of Applied Physics, (1999) 86(4) 2281-2290.

[13] Schwan, J., S. Ulrich, H. Roth, H. Ehrhardt, S.R.P. Silva, J. Robertson, R. Samlenski, and R. Brenn, Journal of Applied Physics, (1996) 79(3) 1416-1422.

[14] Logothetidis, S., Applied Physics Letters, (1996) 69(2) 158-160.

[15] Nakazawa, H., T. Mikami, Y. Enta, M. Suemitsu, and M. Mashita, Japanese Journal of Applied Physics, (2003) 42(6B) 676.

[16] Rubio-Roy, M., C. Corbella, J. Garcia-Céspedes, M.C. Polo, E. Pascual, J.L. Andújar, and E. Bertran, Diamond and related materials, (2007) 16(4-7) 1286-1290.

[17] Zhang, S., X. Lam Bui, X.T. Zeng, and X. Li, Thin Solid Films, (2005) 482(1-2) 138-144.

[18] Libardi, J., K. Grigorov, M. Massi, C. Otani, S.P. Ravagnani, H.S. Maciel, M. Guerino, and J.M.J. Ocampo, Thin Solid Films, (2004) 459(1-2) 282-285.

[19] Guerino, M., M. Massi, H.S. Maciel, C. Otani, R.D. Mansano, P. Verdonck, and J. Libardi, Diamond and related materials, (2004) 13(2) 316-319.

[20] Chen, Z.Y., J.P. Zhao, T. Yano, and J. Sakakibara, Physical Review B, (2000) 62(11) 7581.

[21] Liou, Y., R. Weimer, D. Knight, and R. Messier, Applied Physics Letters, (1990) 56(5) 437-439.

[22] Ono, T., Y. Suda, M. Akazawa, Y. Sakai, and K. Suzuki, Japanese Journal of Applied Physics, (2002) 41 4651-4654.

[23] Yoshimoto, M., M. Furusawa, K. Nakajima, M. Takakura, and Y. Hishitani, Diamond and related materials, (2001) 10(3-7) 295-299.

[24] Massi, M., R.D. Mansano, H.S. Maciel, C. Otani, P. Verdonck, and L. Nishioka, Thin Solid Films, (1999) 343 381-384.

[25] Osswald, S., G. Yushin, Y. Gogotsi, V. Mochalin, and S.O. Kucheyev, Journal of the American Chemical Society, (2006) 128(35) 11635-11642.

[26] Zhang, D.W., Z.J. Liu, Y.Z. Wan, and J.T. Wang, Applied Physics A: Materials Science & Processing, (1998) 66(1) 49-51.

[27] Bewilogua, K., R. Wittorf, H. Thomsen, and M. Weber, Thin Solid Films, (2004) 447-448 142-147.

[28] Mérel, P., M. Tabbal, M. Chaker, S. Moisa, and J. Margot, Applied Surface Science, (1998) 136(1-2) 105-110.

[29] Maguire, P.D., J.A. McLaughlin, T.I.T. Okpalugo, P. Lemoine, P. Papakonstantinou, E.T. McAdams, M. Needham, A.A. Ogwu, M. Ball, and G.A. Abbas, Diamond and related materials, (2005) 14(8) 1277-1288.

[30] Grill, A., Diamond and related materials, (2001) 10(2) 234-239.

[31] Klibanov, L., N. Croitoru, A. Seidman, M. Gilo, and R. Dahan, Optical Engineering, (2000) 39 989.

[32] Oh, T., C.K. Choi, and K.M. Lee, Thin Solid Films, (2005) 475(1-2) 109-112.

[33] Komatsu, Y., A. Alanazi, and K.K. Hirakuri, Diamond and related materials, (1999) 8(11) 2018-2021.

[34] Sui, J.H. and W. Cai, Diamond and related materials, (2006) 15(10) 1720-1726.

[35] Eryilmaz, O.L., J.A. Johnson, O.O. Ajayi, and A. Erdemir, Journal of Physics: Condensed Matter, (2006) 18(32) S1751-S1762.

[36] Erdemir, A., G.R. Fenske, J. Terry, and P. Wilbur, Surface and Coatings Technology, (1997) 94-95 525-530.

[37] Platon, F., P. Fournier, and S. Rouxel, Wear, (2001) 250(1-12) 227-236.

[38] Tillmann, W., E. Vogli, and F. Hoffmann, Thin Solid Films, (2007) 516(2-4) 262-266.

[39] Ferrari, A.C. and J. Robertson, Physical Review B, (2000) 61(20) 14095-14107.

[40] Gleason, K.M.R.a.K.K., Characterization methods for natural and synthetic diamonds, in Handbook of industrial diamonds and diamond films. 1998. p. 413-480.

[41] Díaz, J., G. Paolicelli, S. Ferrer, and F. Comin, Physical Review B, (1996) 54(11) 8064-8069.

[42] Fisher, A.C., Nanoindentation. 2002.

PAPER

1. REACTIVE SPUTTER-DEPOSITION OF OXYGENATED AMORPHOUS CARBON THIN FILMS IN AR/O_2

Travis McKindra[a1], Matthew J. O'Keefe[a] and Rebecca Cortez[b]

[a]Department of Materials Science and Engineering, Missouri University of Science and Technology, Rolla, MO 65409, United States

[b]Department of Mechanical Engineering, Union College, Schenectady, NY 12308, United States

Abstract

Oxygenated amorphous carbon thin films were deposited by DC magnetron sputtering using various argon and oxygen gas mixtures in the process gas. The X-ray diffraction data indicated that the predominantly amorphous films had more defined peaks with a higher partial pressure of oxygen. Scanning electron microscopy revealed that the morphological features of the films increased with the addition of oxygen. The film surface chemistry was examined by X-ray photoelectron spectroscopy where increased oxygen content was found with higher levels of oxygen in the working gas. Growth rate (deposition rate) decreased as the amount of oxygen increased due to oxygen reacting (etching) the growing carbon film. Raman spectroscopy results suggested that the increased oxygen in the process gas and films led to a higher percentage of sp^3-bonded carbon atoms. Results indicated that use of oxygen in the working gas enhanced the crystalline nature of the films.

Keywords: amorphous carbon; diamond-like carbon; sputtering; surface characterization; morphology

Introduction

Amorphous carbon (a-C) or diamond-like carbon (DLC) thin films are engineering materials with many unique properties such has high hardness, density, electrical resistivity and corrosion resistance [1-5]. DLC films have various technical applications as protective coatings on magnetic hard disks, razor blades and biomedical components and as low-k dielectrics and microelectromechanical systems (MEMS) devices [6]. The films are comprised of an amorphous network of sp^2 bonded carbon with islands of sp^3 bonded material. It is the fraction of sp^3 bonds which impart the physical properties reminiscent of diamond [7].

The films can be deposited by a variety of methods including plasma-enhanced chemical vapor deposition (PECVD) [8], laser ablation [9] or sputter deposition [10-15] from a graphite target. Typically, argon gas is used during sputter deposition, but reactive gases such as C_2H_2 and CH_4 have been added [14,15]. The hydrogenated DLC films may contain up to 50 at% hydrogen, but be comprised of less than 50% sp^3 bonds. Conversely, the non-hydrogenated films may contain 85% or more sp^3 bonds. Some research has investigated the use of oxygen in the deposition of DLC films using various methods including CVD [8] and pulsed laser deposition [16]. The post-treatment of a-C films with an oxygen plasma [17] has been studied as well as oxidation of non-diamond species in a furnace [18]. The consensus was that the oxygen preferentially etches away

[1] Corresponding Author, Tel: 573-341-4349, Fax: 573-341-2071, Email: mckindra@mst.edu

the sp^2 species in the films leaving a higher fraction of sp^3 bonds. Little work has focused on the impact of oxygen during the sputter deposition process.

The work presented here investigates the use of oxygen in the room temperature reactive DC magnetron sputter deposition of a-C thin films. It shows the effect of the oxygen partial pressure in the sputtering gas mixture and subsequent oxygen content in the film on the structure and bonding of the film. Also included is a discussion of the film growth rate, surface chemistry and morphology of carbon films sputtered in an Ar/O_2 atmosphere.

Material and Methods

Carbon thin films were deposited onto Si substrates by DC magnetron sputtering of a graphite target. The substrates were cleaned by a standard wet chemical wafer cleaning procedure. The base vacuum was approximately 5×10^{-7} Torr and the total working pressure was maintained at 2 and 5 mTorr. The sputtering gas was high-purity (99.999%) argon. The partial pressure of oxygen in the working gas was variable at levels of 5, 10 and 25% of the total working pressure. A film was deposited with only Ar for comparison. The films were deposited at a power of 300 W for 1.5 - 3.0 hours to obtain films of at least 100 nm for characterization.

The film thickness was measured with a Tencor Alpha-step 100 profilometer. The film structure was studied with X-ray diffraction (XRD) using a Philips X-Pert X-ray diffractometer operating in glancing angle mode with Cu Kα radiation. Surface roughness measurements were obtained using a Veeco Dimension V Scanning Probe Microscope. The system's atomic force microscope (AFM) was used in tapping mode to obtain RMS roughness measurements. The film structure and morphology was further

studied using scanning electron microscopy (SEM) with a Hitachi S-4700 Field Emission Scanning Electron Microscope (FESEM). The surface chemistry of the films was investigated with X-ray photoelectron spectroscopy (XPS) using a Kratos Axis 165 with a Mg source. Micro-Raman spectroscopy was conducted with a Horiba ARAMIS system. The Raman spectra were measured using the 632.8 nm wavelength of a He-Ne laser in the range of 50-2000 cm^{-1}. After 13-point Savitzky-Golay smoothing and manual linear background subtraction the spectra were fitted with multiple Gaussian curves.

Results and Discussion

The effect of the oxygen partial pressure in the working gas on the deposition rate, at both 2 and 5 mTorr working pressures, is shown in Figure 1. The effect of the oxygen content on the deposition rate at each working pressure showed a similar trend. The highest rate (~250 nm/hr) occurred when no oxygen was added to the sputtering gas. At both working pressures, with the addition of only 5% O_2, the deposition rate was decreased by as much as one-half (~125 nm/hr). There was little change in the rate when the oxygen content was doubled to 10%. The addition of 25% O_2 at 2 mTorr yielded a deposition rate of approximately 125 nm/hr, but there was no measurable film deposited at 25% O_2 and 5 mTorr despite a visible plasma during deposition. It was also evident that the deposition rate decreased when the working pressure was increased from 2 mTorr to 5 mTorr with the exception of the Ar only case. The decreased deposition rate could be attributed to an oxide build-up on the surface of the graphite target which resulted in a condition known as target poisoning. The target poisoning phenomenon is a known complication of the reactive sputtering technique [19, 20] where a more resistive oxide layer on the surface of the target exhibits a significantly lower sputtering yield and target

self-bias compared to the elemental target. However, a decrease in the target self-bias was not seen in the work presented here which suggests that there is another cause for the reduced deposition rate such as the oxygen reacting with the carbon in the vapor phase or on the growing film surface.

Glancing angle XRD techniques were used for phase identification of the as-deposited films. The XRD spectra of the deposited films are shown in Figure 2. For a baseline comparison, the films deposited without oxygen at both working pressures were characterized and the XRD spectra are shown in Figure 2(a). The spectra showed the films to be amorphous. Several film deposition conditions exhibited broad peaks and are presented in Figures 2(b) – 2(e). A broad peak at ~28° was identified in the spectra for the films deposited with 5% and 10% O_2 at 2 mTorr, Figure 2(b) and 2(d) respectively. The peak corresponds to the graphite (002) plane. When the oxygen was increased to 25% at 2 mTorr, a broad peak at ~48° became evident in the spectra (Figure 2(e)). That peak was also visible in the spectra from the film deposited with 5% O_2 at 5 mTorr, which corresponds to the graphite (101) plane. The XRD results suggest that the addition of oxygen to the plasma during deposition caused some structural changes in the form of more highly ordered (crystalline) species. There is no basis for the oxygen to improve the crystallinity in the films, though it is possible that the oxygen preferentially etched the amorphous species prior to the more highly-ordered species in the film. The crystalline features of the selected XRD spectra from films deposited with oxygen in the plasma were considered significant.

Scanning electron microscopy was used to determine changes in film morphology caused by the amount of oxygen in the deposited films. Carbon thin films sputter deposited at room temperature are generally smooth and exhibit the Zone 1 structure proposed by Thornton [21]. The XRD spectra from the films deposited with 5, 10 and 25% O_2 at 2 mTorr as well as the film deposited with 5% O_2 at 5 mTorr suggests a higher order arrangement. The SEM images from the selected films are shown in Figure 3 and are similar to other reactively sputtered carbon thin films [22-24]. The films deposited with Ar only were smooth and essentially featureless, as very little surface topography was detected. The film deposited with 5% O_2 at 2 mTorr (Fig. 3(a)) shows a smooth, predominantly featureless film very reminiscent of the films deposited with only Ar. The morphology became coarser when the working pressure was increased to 5 mTorr, as shown in Fig. 3(b). Irregularly-shaped agglomerated particles less than 50 nm in size were visible. When the parameters were adjusted to 10% O_2 and 2 mTorr, there was another change in the morphology to more rounded particles (Fig. 3(c)) that were also less than 50 nm in diameter. Finally, at the highest percentage of oxygen (Fig. 3(d)) there was a slight change to more equiaxed, almost spherical particles that were similar to metallic sputtered films [24]. The reasons for the changes in morphology are difficult to discern, but do correlate with the XRD findings in that the films with the most surface topography had the most predominate diffraction peaks in the XRD spectra. As suggested previously, the decrease in the measured film thickness was linked to the possibility of oxygen etching away material on the surface of the growing film. It is also possible that the oxygen etching was responsible for the increased surface topography, as

the surface features were similar in appearance to DLC and amorphous carbon films exposed to mixed Ar/O_2 plasmas [17, 25].

Further investigation of the surface effects included using AFM to determine the surface roughness. Figure 4 provides AFM images over an area of 1 μm x 1 μm and corroborates several of the morphology observations made through SEM surface characterization. For instance, the well rounded particles in Figure 3(c) are also clearly shown in Figure 4(c). The surface roughness for each of the four selected films was taken from four different locations. The average RMS values ranged from 0.87 nm (5 % O_2 and 2 mTorr), 0.76 nm (5 % O_2, 5 mTorr), 1.30 nm (10 % O_2, 2 mTorr) and 0.34 nm (25 % O_2, 2 mTorr). The trend in the surface roughness seemed to correspond with the SEM images in that the film with the most surface topography had the highest RMS value (10% O_2 at 2 mTorr). The decrease in the surface roughness for the films deposited with oxygen may be another indication that the carbon films were etched (Figure 4(d)).

From the SEM images and AFM data alone it was difficult to determine whether the oxygen affected the growth mechanism of the film as opposed to just the film surface. Surface chemistry analysis of the deposited films was investigated by XPS. The films were Ar sputter cleaned for 60 seconds in the XPS chamber prior to examination in order to remove any surface contamination. XPS spectra for selected samples are shown in Figure 5. The spectra from the C 1s electron for each sample exhibited a broad, asymmetric peak that was resolved by two curves. The first curve was centered at 285 eV for each sample and was assigned to the C-C bond. Research has shown that this

curve can be separated into two curves and can be used to delineate between sp^2 and sp^3 bonded carbon atoms [26-28]; however, that approach was not taken here due to the subjective nature of that analysis. The second curve was centered at approximately 286.2 eV and assigned to C-O bonding [29-31]. The summary of the chemical quantification analysis is shown in Table I. There appeared to be some oxygen contamination in the films deposited with only Ar that was most likely nascent oxygen that was not removed by the Ar sputter cleaning. There was a general trend that as the oxygen content in the plasma increased the oxygen content in the film increased, especially at 2 mTorr. At a the working pressure of 5 mTorr, the highest oxygen content was found with 5% O_2 in the plasma. The cause of the lower oxygen content in the 5% O_2 at 10 mTorr film is unclear, but it is possible that a saturation limit was reached. The trend lends credence to the earlier assertion that the morphological and structural changes in the films were due to the presence of oxygen.

The Raman spectra of the carbon thin films deposited with varying amounts of oxygen are shown in Figure 6. In general the spectra all have a shape typical of amorphous carbon or DLC films sputter deposited from a graphite target at room temperature. Specifically, each spectrum exhibits a relatively broad band ranging from 900 cm^{-1} to 1800 cm^{-1} and centered near 1460 cm^{-1} [32, 33]. The broad band was fitted with two Gaussian peaks corresponding to the G peak (1560-1580 cm^{-1}) and the D peak (~1380-1400 cm^{-1}). Both the G and D peaks are caused by vibrations from only sp^2 sites in the films. The G peak is due to bond stretching of pairs of sp^2 atoms while the D peak is due to breathing modes of carbon rings [33] and bond disorder [34]. Consider the

changes in the shape of the spectra from the films deposited at 2 mTorr and shown in Figure 6(a). As the oxygen was increased from 0% to 25%, the width of the broad band decreased and a pronounced shoulder from the D peak became visible (especially in the 10% and 25% spectra). A similar trend was visible in the spectra from the films deposited at 5 mTorr, shown in Figure 6(b). There is a significant change in the spectrum of the film deposited with 5% O_2 at 5 mTorr where it appeared that a doublet was forming.

The visible Raman spectrum from a-C is said to depend on clustering of the sp^2 phase, bond disorder, presence of sp^2 rings or chains and the sp^3/sp^2 ratio according to Ferrari and Robertson [34]. A proposed phenomenological three-stage model of an amorphization trajectory, ranging from pure graphite to ta-C (ta-C is defined as a DLC with upwards of 85% sp^3-bonding), based on variations of the G-peak position and I_D/I_G ratio (integrated peak intensities from the D and G peaks) [34, 35] was used to explain the phenomena from the Raman spectra from the oxygenated films. The three stages are as follows: (1) graphite to nanocrystalline graphite, (2) nanocrystalline graphite to a-C and (3) a-C to ta-C (~100% sp^3 or defected diamond). The plot of the I_D/I_G ratio and G peak position versus the amount of oxygen in the films is shown in Figure 7. In general, the intensity ratio decreased, while the G peak position increased, with the oxygen content of the film. According to the model, the results indicate the films lie in the third stage, where there is an increase in the sp^3 content. The plot of the I_D/I_G does appear to level out or even begin to rise suggesting that the addition of too much oxygen leads to graphitization.

Conclusions

Carbon thin films were reactively sputtered in an Ar/O_2 gas mixture. The deposition rate decreased with increasing O_2 partial pressure and the system working pressure. X-ray photoelectron spectroscopy of C 1s spectra taken from the films exhibited broad peaks that were separated into components corresponding to C-C and C-O species and indicated that there was retained oxygen in the films. X-ray diffraction results revealed the films were predominantly amorphous with broad peaks indicative of a nano-crystalline phase. The crystalline features in the spectra were only evident when oxygen was added to the process gas. The RMS surface roughness values varied between 0.34 and 1.30 nm. Scanning electron microscopy of the films indicated a surface morphology change with changes in the oxygen content of the films. As the oxygen content in the plasma increased, the surface features of the films became more defined. Raman spectroscopy showed a change in the spectra with increased oxygen and a decreasing I_D/I_G ratio indicated a higher percentage of sp^3-bonding in the films. The characterization results revealed that the oxygen affected the deposition and growth of the amorphous carbon thin films. There was a consistent trend with the films that the increasing oxygen content enhanced the long-range order in the films while suppressing the more amorphous species.

Acknowledgements

This work was financially supported by the U.S. Office of Naval Research (ONR) through the Multidisciplinary University Research Initiative (MURI) program under the advice and guidance of Dr. I. Perez. The surface roughness measurements are based on work supported by the National Science Foundation under Grant No. EEC-0824341. The

assistance of Dr. Eric Bohannon with XRD, Clarissa Wisner with SEM and Jeff Wight with XPS from the Materials Research Center at Missouri University of Science and Technology is gratefully acknowledged.

References

[1] Maguire PD, McLaughlin JA, Okpalugo TIT, Lemoine P, Papakonstantinou P, McAdams ET, et al. Mechanical stability, corrosion performance and bioresponse of amorphous diamond-like carbon for medical stents and guidewires. Diam Relat Mater 2005; 14(8):1277-88.

[2] Grill A. Amorphous carbon based materials as the interconnect dielectric in ULSI chips. Diam Relat Mater 2001; 10(2):234-9.

[3] Komatsu Y, Alanazi A, Hirakuri KK. Application of diamond-like carbon films to the integrated circuit fabrication process. Diam Relat Mater 1999; 8(11):2018-21.

[4] Sui JH, Cai W. Effect of diamond-like carbon (DLC) on the properties of the NiTi alloys. Diam Relat Mater 2006; 15(10):1720-6.

[5] Eryilmaz OL, Johnson JA, Ajayi OO, Erdemir A. Deposition, characterization, and tribological applications of near-frictionless carbon films on glass and ceramic substrates. J Phys Condens Matter 2006; 18(32):S1751-62.

[6] Robertson J. Diamond-like amorphous carbon. Mater Sci Eng R 2002; 37:129-281.

[7] Grill A. Diamond-like carbon: state of the art. Diam Relat Mater 1999; 8(2-5):428-34.

[8] Liou Y, Weimer R, Knight D, Messier R. Effect of oxygen in diamond deposition at low substrate temperatures. Appl Phys Lett 1990; 56(5):437-9.

[9] Qian F, Craciun V, Singh RK, Dutta SD, Pronko PP. High intensity femtosecond laser deposition of diamond-like carbon thin films. J Appl Phys 1999; 86(4):2281-90.

[10] Logothetidis S. Hydrogen-free amorphous carbon films approaching diamond prepared by magnetron sputtering. Appl Phys Lett 1996; 69(2):158-60.

[11] Nakazawa H, Mikami T, Enta Y, Suemitsu M, Mashita M. Structure, chemical bonding and these thermal stabilities of diamond-like carbon (DLC) films by RF magnetron sputtering. Jpn J Appl Phys 2003; 42(6B):L676-9.

[12] Rubio-Roy M, Corbella C, Garcia-Cespedes J, Polo MC, Pascual E, Andujar JL, et al. Diamond like carbon films deposited from graphite target by asymmetric bipolar pulsed-DC magnetron sputtering. Diam Relat Mater 2007; 16(4-7):1286-90.

[13] Zhang S, Lam Bui X, Zeng XT, Li X. Towards high adherent and tough a-C coatings. Thin Solid Films 2005; 482(1-2):138-44.

[14] Libardi J, Grigorov K, Massi M, Otani C, Ravagnani SP, Maciel HS, et al. Comparative studies of the feed gas composition effects on the characteristics of DLC films deposited by magnetron sputtering. Thin Solid Films 2004; 459(1-2):282-5.

[15] Guerino M, Massi M, Maciel HS, Otani C, Mansano RD, Verdonck P, et al. The influence of nitrogen on the dielectric constant and surface hardness in diamond-like carbon (DLC) films. Diam Relat Mater 2004; 13(2):316-9.

[16] Ono T, Suda Y, Akazawa M, Sakai Y, Suzuki K. Effects of oxygen and substrate temperature on properties of amorphous carbon films fabricated by plasma-assisted pulsed laser deposition method. Jpn J Appl Phys 2002; 41:4651-4.

[17] Massi M, Mansano RD, Maciel HS, Otani C, Verdonck P Nishioka L. Effects of plasma etching on DLC films. Thin Solid Films 1999; 343-344:381-4.

[18] Osswald S, Yushin G, Gogotsi Y, Mochalin V, Kucheyev SO. Control of sp^2/sp^3 carbon ratio and surface chemistry of nanodiamond powders by selective oxidation in air. J Am Chem Soc 2006; 128(35):11635-42.

[19] Waite MM, Shah SI. Target poisoning during reactive sputtering of silicon with oxygen and nitrogen. Mater Sci Eng B 2007; 140:64-8.

[20] Depla D, De Gryse R. Target poisoning during reactive magnetron sputtering: Part I: the influence of ion implantation. Surf Coat Technol 2004; 183:184-9.

[21] Thornton JA. High rate thick film growth. Annu Rev Mater Sci 1977; 7:239-60.

[22] Ting JM, Lee H. DLC composite thin films by sputter deposition. Diam Relat Mater 2002; 11:1119-23.

[23] Ryu JT, Honda SI, Katayama M, Oura K. Field electron emission from amorphous carbon thin films grown by RF magnetron sputtering. Curr Appl Phys 2005; 5:387-91.

[24] Agarwal S. Structure and morphology of RF sputtered carbon overlayer films. IEEE Trans Magn 1985; 21(5):1527-9.

[25] Massi M, Ocampo JMJ, Maciel HS, Grigorov K, Otani C, Santos LV, et al. Plasma etching of DLC films for microfluidic channels. Microelectronics J 2003; 34:635-8.

[26] Filik J, May PW, Pearce SRJ, Wild RK, Hallam KR. XPS and laser Raman analysis of hydrogenated amorphous carbon films. Diam Relat Mater 2003; 12:974-8.

[27] Diaz J, Paolicelli G, Ferrer S, Comin F. Separation of the sp^3 and sp^2 components in the C 1s photoemission spectra of amorphous carbon films. Phys Rev B 1996; 54(11):8064-9.

[28] Mérel P, Tabbal M, Chaker M, Moisa S, Margot J. Direct evaluation of the sp3 content in diamond-like-carbon films by XPS. Appl Surf Sci 1998; 136:105-10.

[29] Kowbel W, Shan CH. The mechanism of fiber-matrix interactions in carbon-carbon composites. Carbon 1990; 28(2-3):287-99.

[30] Rats D, Vandenbulcke L, Herbin R, Benoit R, Erre R, Serin V, et al. Characterization of diamond films deposited on titanium and its alloys. Thin Solid Films 1995; 270:177-83.

[31] Sumant AV, Gilbert PUPA, Grierson DS, Konicek AR, Abrecht M, Butler JE, et al. Surface composition, bonding, and morphology in the nucleation and growth of ultra-thin, high quality nanocrystalline diamond films. Diam Relat Mater 2007; 16(4-7):718-24.

[32] Chowdhury S, Laugier MT, Rahman IZ. Characterization of DLC coatings deposited by rf magnetron sputtering. J Mater Process Technol 2004; 153-154:804-10.

[33] Irmer G, Dorner-Reisel A. Micro-Raman studies on DLC coatings. Adv Eng Mater 2005; 7(8):694-705.

[34] Ferrari AC, Robertson J. Interpretation of Raman spectra of disordered and amorphous carbon. Phys Rev B 2000; 61(20): 14095-107.

[35] Ferrari AC, Robertson J. Resonant Raman spectroscopy of disordered, amorphous, and diamondlike carbon. Phys Rev B 2001; 64(7):075414-1-075414-13.

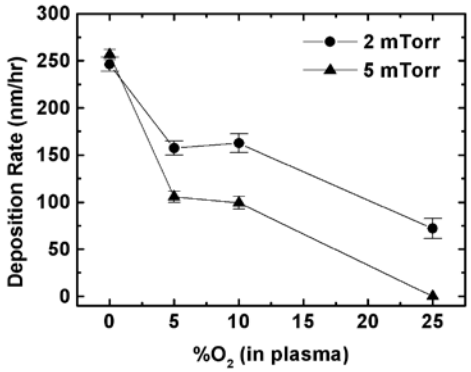

Figure 1: Deposition rate versus percentage of O_2 for a given working pressure.

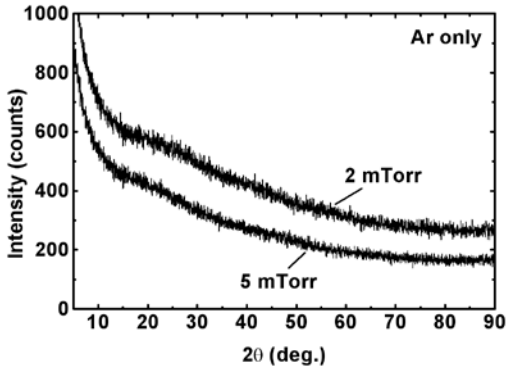

(a)

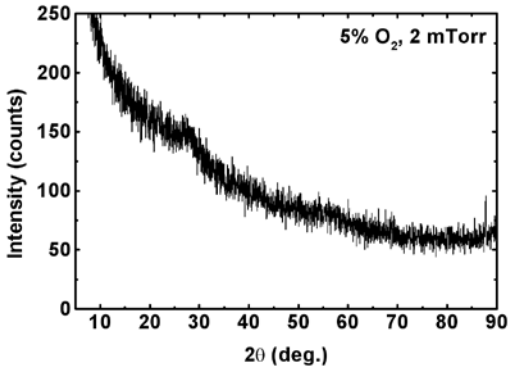

(b)

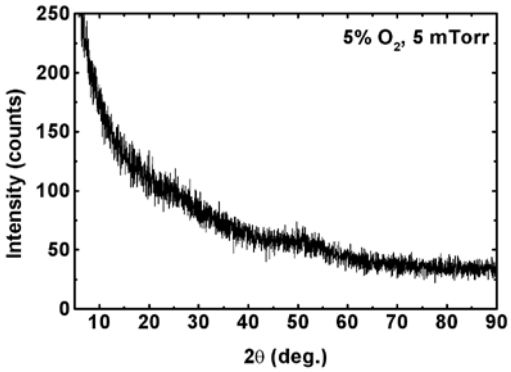

(c)

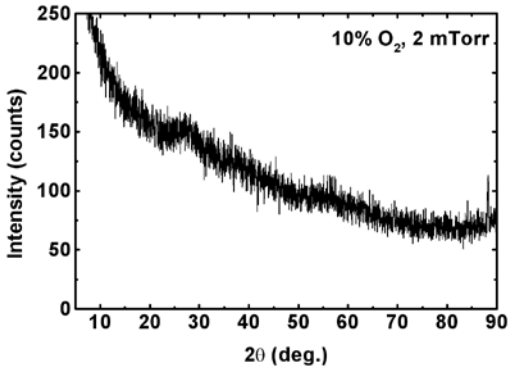

(d)

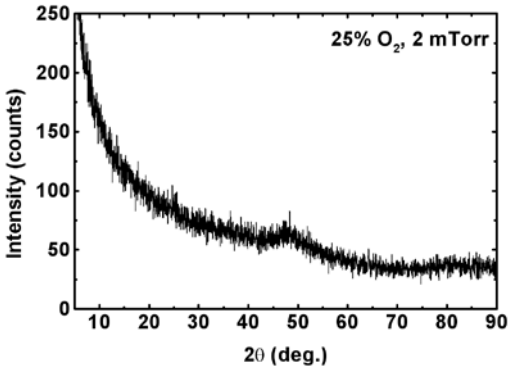

(e)

Figure 2: Comparison of XRD spectra for selected samples and the crystalline features.

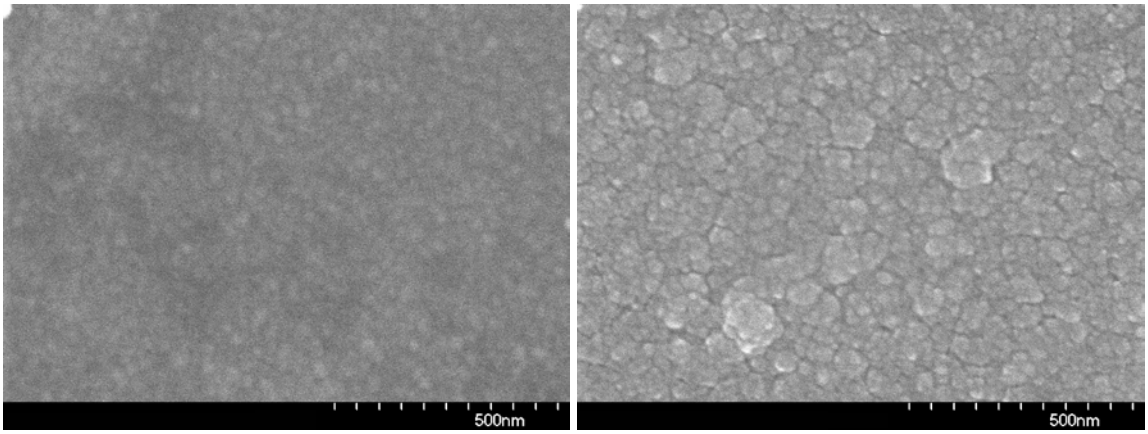

(a) (b)

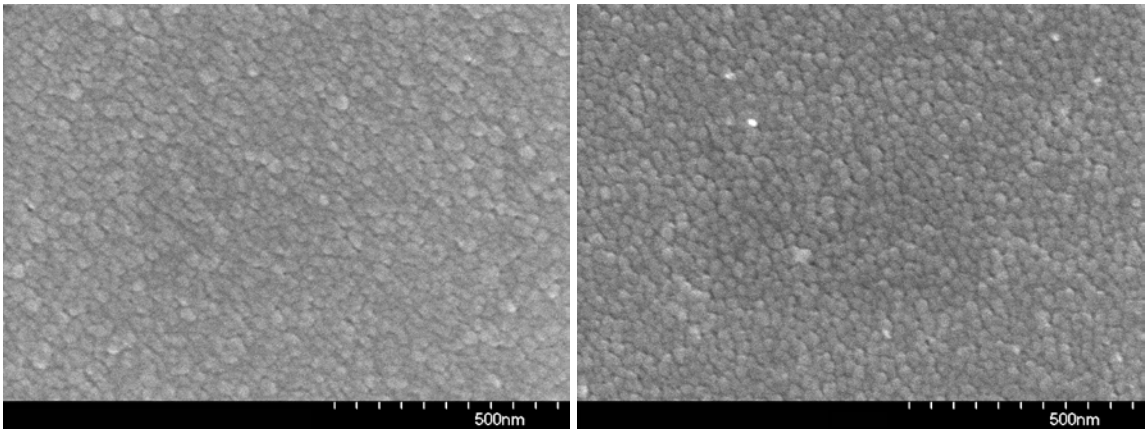

(c) (d)

Figure 3: SEM images from selected films deposition parameters (a) 5% O_2 – 2 mTorr, (b) 5% O_2 – 5 mTorr, (c) 10% O_2 – 2 mTorr and (d) 25% O_2 – 2 mTorr.

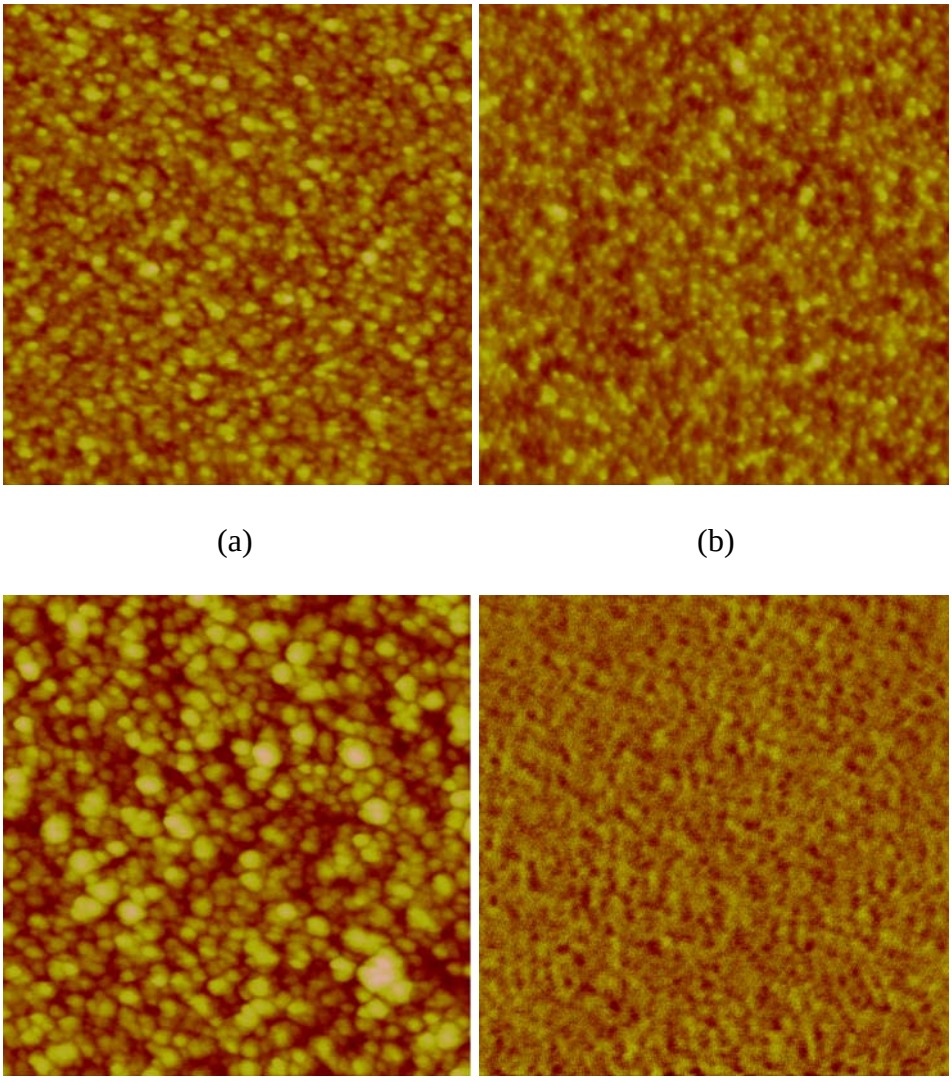

(a) (b)

(c) (d)

Figure 4: AFM images showing morphology of carbon thin films deposited under varying oxygen partial pressures (a) 5% O_2 - 2 mTorr, (b) 5% O_2 - 5 mTorr, (c) 10% O_2 - 2 mTorr, and (d) 25% O_2 - 2 mTorr. All images are 1 μm × 1 μm. The black to white grayscale is 15 nm in (a) through (c) and 6 nm in (d).

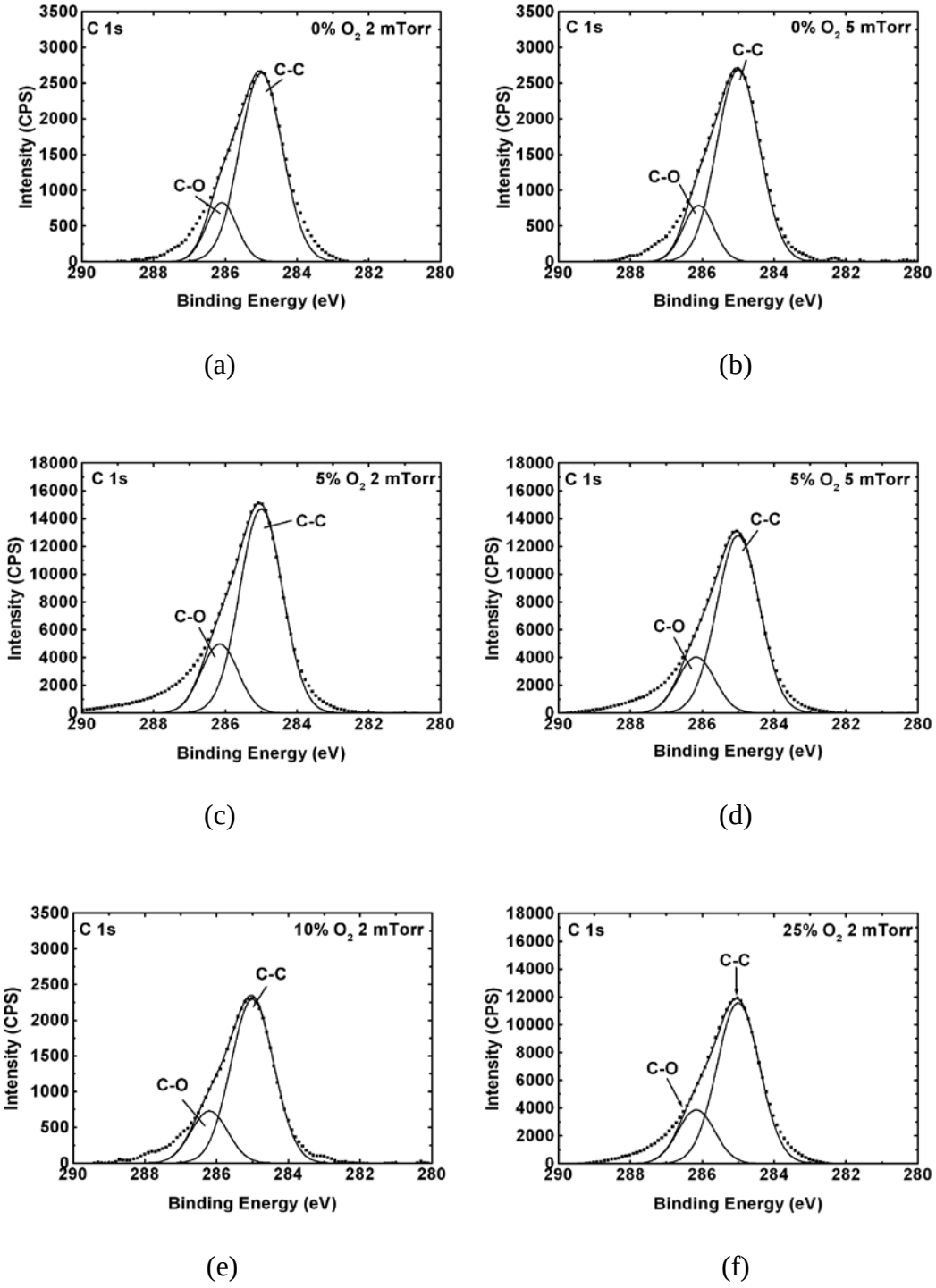

Figure 5: XPS spectra of C 1s from films deposited with (a) 0% O_2 at 2 mTorr, (b) 0% O_2 at 5 mTorr, (c) 5% O_2 at 2 mTorr, (d) 5% O_2 at 5 mTorr, (e) 10% O_2 at 2 mTorr, and (f) 25% O_2 at 2 mTorr.

Table I: Summary of oxygen content from XPS chemical quantification

Working Pressure (mTorr)	% O_2 in plasma	O in film (at%)
2	0	3.0
	5	3.8
	10	5.2
	25	6.5
5	0	2.9
	5	6.4
	10	4.7

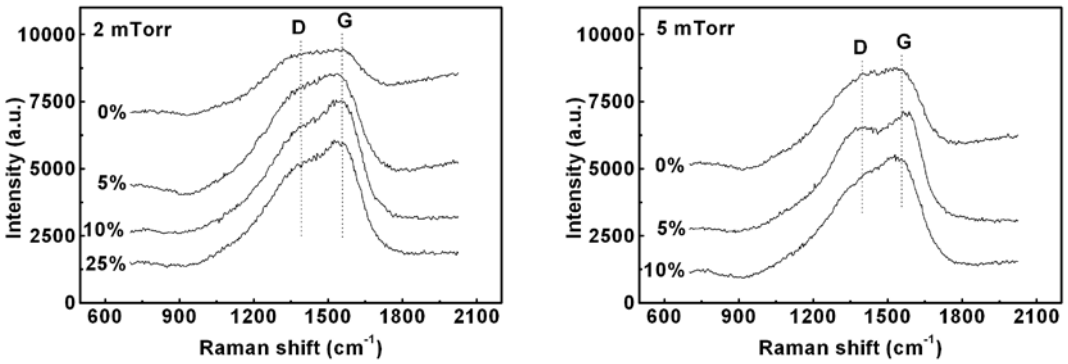

(a) (b)

Figure 6: The Raman spectra from the carbon films deposited at (a) 2 mTorr and (b) 5 mTorr.

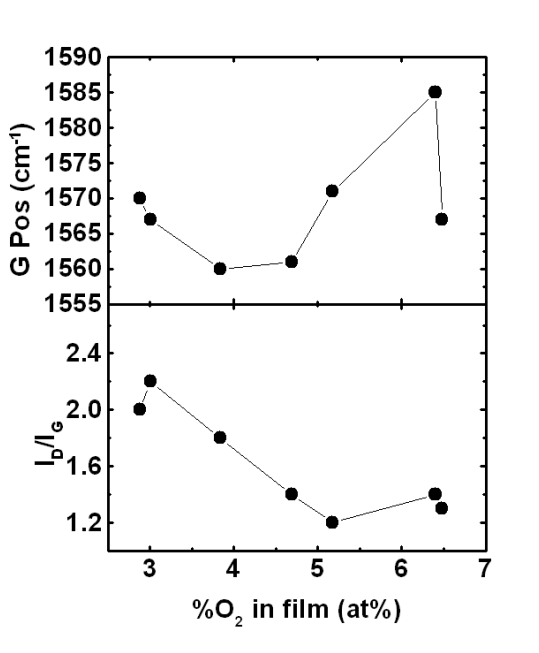

Figure 7: Variation of the I_D/I_G ratio and G peak position with oxygen in the sputtering gas at both working pressures.

2. CHARACTERIZATION OF ULTRA-FAST DEPOSITED POLYCRYSTALLINE GRAPHITE BY A CO_2 LASER-ASSISTED COMBUSTION-FLAME METHOD

Travis McKindra[a], Sandeep Patil[a], Matthew J. O'Keefe[a], Yaoxuan Han[b], Hao Ling[b],Yongfeng Lu[b]

[a]*Department of Materials Science and Engineering, Missouri University of Science and Technology, Rolla, MO 65409, United States*

[b]*Department of Electrical Engineering, University of Nebraska-Lincoln, Lincoln, NE 68588, United States*

Abstract

High deposition rate, 750 μm/minute, crystalline graphite was deposited on WC substrates by a CO_2 laser-assisted combustion-flame method at laser powers between 300 and 800 W. The structures, which were identified as pillars, were characterized by various methods. The pillars were cylindrical in shape and grew to a size of approximately 3 mm in length and in a few minutes. The laser power did not affect the overall length of the pillar, but caused changes in the physical shape. X-ray and electron diffraction results revealed the pillars to be crystalline graphite regardless of the laser power. Investigation of the pillars by scanning electron microscopy showed two distinct microstructural areas: an inner core of dense material surrounded by an outer shell of lamellar-like material. The core/shell microstructure was unaffected by the level of CO_2 laser power.

PACS : 81.05.Uw; 81.16.Mk; 68.37.Hk

Keywords: high deposition rate; crystalline graphite; laser-assisted combustion-flame deposition

1. Introduction

Diamond is a promising material in many applications because of its excellent wear resistance [1], thermal conductivity, electrical and optical properties. Diamond films are deposited in many ways including laser ablation [2,3] and plasma discharge [4,5], but chemical vapor deposition (CVD) is the foremost technique for diamond synthesis. Several CVD based methods are also employed such as hot filament techniques [6,7], plasma enhanced CVD (PECVD) [8,9] and the use of a combustion-flame [10-16]. The most significant contribution towards synthesis of diamond at atmospheric pressure by use of oxygen-acetylene combustion-flame came through the work of Hirose [17,18]. The method introduced by Hirose *et.al.,* has been widely reported because of its simplicity and cost effectiveness, with possibly the high growth rate of 100-200 $\frac{\mu m}{hour}$ [19]. A body of work followed which expanded on this initial discovery with identification of accurate experimental conditions [11,13], growth of diamond at less than atmospheric pressures [20], *in situ* measurements to identify the chemical species present in the transformation during this process [10,18], and deposition of diamond films with high resistivity [15]. Snail *et.al* comprehensively studied diamond crystal morphology through examination using Raman spectroscopy and scanning electron microscopy as a function of oxidizer/fuel ratio and substrate temperature. The generally accepted C_2H_2/O_2 gas ratio for diamond growth is 0.9-1.2 [16] in the temperature range of 400-1200^oC [21].

The search for higher deposition rates led to the investigation of many other techniques. Primarily techniques such as direct current (DC) plasma [5] and DC plasma jet [22] were explored without achieving any significant increase in the deposition rate as compared to that of the combustion-flame process. In fact, a new hot filament process

reports a growth rate of 9 $\frac{\mu m}{hour}$ which is 9 times higher than a conventional hot filament CVD process [23].

In this study, a unique approach of combining the combustion-flame deposition process with CO_2 laser energy was explored. The objective was to investigate the deposition of diamond coatings on tungsten carbide substrates. The combination of the CO_2 laser energy with the oxy-acetylene combustion-flame results in the creation of a plasma and the presence of ionized species which lead to deposition of diamond or graphitic films. Previous work by our group demonstrated that CO_2 laser irradiation during combustion-flame deposition of diamond films raised the local temperature to the critical point of diamond growth while keeping the rest of the substrate at a relatively low temperature [24]. It was also found that excessive laser power density leads to the deposition of amorphous carbon while excessive laser power leads to desorption of the carbon species and growth of tungsten oxide on WC substrates [24]. In this paper, polycrystalline graphite pillars deposited by the CO_2 laser-assisted combustion-flame process with varying CO_2 laser power were characterized by various analytical techniques in order to describe and understand the high growth rate at atmospheric pressure.

2. Experimental details

The key parameters in this process with regards to the combustion-flame method were the C_2H_2/O_2 gas ratio, total gas flow rate, substrate temperature, and the distance between the flame's inner cone and the substrate. For the laser processing, the important parameters included laser power, wavelength of laser energy source and incidence angle.

Tungsten carbide (WC) substrates (BC-6S, Basic Carbide Corp) with a cobalt composition of 6 % were placed on a hollow brass block with water cooling. A commercial welding torch was secured at an incidence angle of 55^{o} from normal to the surface of the WC substrate and used to generate a C_2H_2/O_2 combustion flame. The welding torch had an orifice with diameter of 1.1 mm. The gas ratio of C_2H_2/O_2 was controlled by mass-flow control system (B7920V, Spec-Air Gases & Technologies). The inner cone of the flame was in direct contact with the substrate surface. The arrangement of the torch and laser was described in earlier works [24]. The temperature of the substrate was monitored by a pyrometer (OS3752, Omega Engineering, Inc). Purities of the C_2H_2 and O_2 gases were 99.6% and 99.996% respectively. Dimensions of the substrates were 12.7x12.7x1.6 mm^3 with an RMS surface roughness of about 1.6 μm. The substrates were cleaned in a supersonic bath of acetone for 30 minutes prior to deposition. A continuous wave (CW) CO_2 laser beam (PRC Company, 10.6 μm wavelength) was focused normal to the substrate surface by a ZnSe convex lens. The original laser beam diameter was 14 mm and the distance from the substrate to the lens was 241.3 mm. The focal length of the lens was 190 mm that focused the beam to approximately 4 mm on substrate surface. The laser power used was varied between 300 W to 800 W in increments of 100 W. The deposition time was between 3 and 4 minutes. The C_2H_2/O_2 gas ratio was held constant at 1.36 using flowrates of 340 sccm and 250 sccm for the C_2H_2 and O_2 respectively.

The surface morphologies and microstructures were characterized by scanning electron microscopy (SEM) with a Hitachi S-4700 field emission scanning electron microscope (FESEM). The nature of the crystallinity and phase identification of the

pillars was investigated by x-ray diffraction (XRD) using a Philips X-Pert diffractometer in glancing angle mode. Transmission electron microscopy (TEM) was conducted with a Philips EM430T STEM. The carbon pillars were removed from the WC substrate and sectioned for cross-sectional SEM analysis with a commercially available straight-edged razor. The WC substrates were sectioned using an Isomet 11-1180 low speed saw with an Allied High Tech Products low concentration diamond metal bonded wafering blade (5" x .015" x ½"). The TEM samples were prepared by using the razor to shave particles from the pillars onto 300 mesh copper TEM grids with a carbon type-B support film.

3. Results and discussion

A representative sample of all the pillars was used for the XRD and TEM characterization. Figure 1 shows a schematic drawing of the pillar on the WC substrate. Figure 2 presents SEM images of the as-deposited pillars. The material initially deposited, labeled A in Figure 2, was called the pillar base. The pillar base covered a circular area approximately 4 mm in diameter on the surface of the WC substrate. The remaining material, labeled B in Figure 2, was called the pillar. The deposition time resulted in pillars approximately 3 mm tall, yielding a deposition rate of 750 μm/min that was orders of magnitude higher than anything previously reported in the literature. The pillars increased in diameter from the base, vertically towards the combustion-flame. The material appeared to grow horizontally parallel to the substrate surface to form the pillar base, and then vertically at an angle parallel to the incidence angle of the torch (i.e. the combustion-flame). In general, the as-deposited pillars were cylindrical in shape. As the laser power increased from the lowest level (300 W) to the highest level (800 W), a depression appeared on the pillar directly beneath the laser beam. The effects of the laser

on the shape of the pillar became noticeable at 500 W and caused a deepening depression as the laser power increased. The effect of the laser power on the shape of the pillar was clearly evident in Figure 2(b). The radius of curvature of the depression (from plan view) was similar to that of the pillar's base material. This was an indication of the laser-affected area of the pillar. The edge of the depression corresponded roughly to the center of the laser beam, leading to the conclusion that the pillar nucleated directly beneath the center, and most energetic, portion of the focused laser beam.

Figure 3 shows representative XRD spectra for the pillar and the pillar base remaining on the WC substrate. The spectra for the pillar exhibited several peaks corresponding to graphite (JCPDS file 75-1621) thus confirming the crystallinity of the pillars and pillar base. The range associated with the (002) plane for graphite at 26.25° is inset. Peaks were identified for the (100) planes (42.249°), (004) planes (54.021°), and the (110) planes (77.251°). The 26.25° peak was much more intense indicating that the pillars had a strong (002) texture [25]. This result indicated that despite the difference in growth mechanism and direction, the pillar and the pillar base had the same crystallinity and structure. There was a noticeable peak shift between the two spectra. The irregular and uneven surface topography of the pillar lead to the peak shift, a systematic aberration known as specimen-displacement error. The effects of the error on the peak are to cause a shift in 2θ position and asymmetric broadening toward lower 2θ values [26]. The laser power had no effect on the crystalline structure of the pillars as determined by XRD as all of the laser power levels resulted in polycrystalline graphite. The diameter of the laser beam incident on the substrate surface was approximately 4 mm corresponding to the

diameter of deposited crystalline material, suggesting the integral role of the CO_2 laser irradiation on the high deposition rate.

Transmission electron microscopy was used to investigate the crystallinity of the interior of the pillars. Figure 4 shows bright-field TEM images from the representative pillar and a bulk sample of graphite for comparison. Electron diffraction (ED) results showed ring patterns that indicated the particles taken from the interior of the pillars were polycrystalline. Other particles exhibited ED patterns indicative of a single crystal or large-grained material, such as that in Figure 4(c). The inter-atomic spacings (d-spacings) were measured from the ring patterns and compared to calculated spacings for graphite. Table I summarizes the d-spacings for the pillar and the bulk graphite with the d-spacings for the pillar associated with the (002), (100), and (110) planes. The planes identified from the d-spacings coincided with the indexed planes from the XRD analysis.

Due to the high deposition rate and the crystalline nature of the pillars additional characterization was conducted. The entire pillar was removed from the WC substrate and sectioned approximately 1 mm from the end then examined using SEM in order to determine the microstructure of the interior of the pillars. Figure 5 shows the SEM micrographs of the pillar cross-section at a low (400 W) and high (800 W) laser power. In general, the pillar exhibited two separate components, an outer shell material and an inner core, labeled A and B respectively, in Figure 5. The core appeared to have a dense microstructure while the shell had a lamellar-like microstructure in plan view. The cross-section images suggested that the pillars grew radially as well as vertically. The remainder of the pillar below the initial sectioning was also investigated using SEM. Figure 6 presents representative SEM images from pillars deposited at 400 W and 800 W

laser power, respectively. Figure 6(a) more clearly exhibits the shell and core construction common to all of the pillars. The laser power had no effect on the thickness of the core versus the shell in that both components were equally affected. It may be difficult to discern from the limited comparison presented, but it was believed that the increase in laser power increased the diameter of the pillar and the pillar base. Some samples were sectioned again in order to determine the location where the pillar was nucleated. Figure 7 shows SEM images from pillars sectioned a third time. Figure 7(a) shows the entire sectioned pillar with the shell labeled 'A' and the pillar base labeled 'B'. The higher magnification image (Figure 7(b)) showed that the shell and core construction was consistent for the entire length of the pillar down to the pillar base. Another view of the pillar (Figure 7(c)) showed that the pillar base ('B') clearly grew in a direction perpendicular to the outer shell of the pillar.

Finally, a brief discussion on the temperature effects is warranted. Collectively, the XRD and SEM data suggests that crystalline graphite was deposited in a manner that was not as dependent on the substrate surface as it was on the combination of the incident combustion-flame and laser. Specifically, the C_2H_2/O_2 gas ratio combined with the laser irradiation and the subsequent localized heating was critical to the high growth rate. Compared to a phase diagram based on films deposited with more conventional combustion-flame methods [27], the measured substrate temperature and oxygen/acetylene ratio was outside the range associated with microcrystalline graphite. From that it was concluded that the localized substrate temperature at the nucleation sites was raised due to the CO_2 laser irradiation.

4. Conclusions

Graphite pillars deposited on WC substrates in open atmosphere using a novel deposition technique utilizing a C_2H_2/O_2 combustion-flame combined with CO_2 laser irradiation were characterized. The deposition rate, 750 μm/minute, was very high for a crystalline material. X-ray diffraction spectra of the pillars showed that after four minutes of deposition, the pillars were polycrystalline. Transmission electron microscopy of the pillars determined that the particles from the interior of the pillars were generally polycrystalline with some detectable large grains which produced single crystal electron diffraction patterns. Scanning electron microscopy images showed the pillars consisted of an inner core of dense material surrounded by an outer shell of lamellar-like layers. The microstructure was unaffected by the amount of laser power in that it was found from the top of the pillar down to the base material initially deposited. Increased laser power caused a shape change in the pillar, producing a depression near the nucleation site. Additional efforts to investigate the laser effect on substrate and thus the nucleation of the films leading to the high deposition rate would be beneficial. An understanding of the growth mechanism may allow for the application of this process to other materials systems.

Acknowledgements

This work was financially supported by the U.S. Office of Naval Research (ONR) through the Multidisciplinary University Research Initiative (MURI) program under the advice and guidance of Dr. I. Perez. The assistance of Dr. Eric Bohannon with XRD from the Materials Research Center at the Missouri University of Science and Technology is gratefully acknowledged.

References

[1] Amirhaghi, S., H.S. Reehal, E. Plappert, Z. Bajic, R.J.K. Wood, and D.W. Wheeler, Diamond Relat. Mater., (1999) 8(2-5) 845-849.

[2] Bourdon, E.B.D., P. Kovarik, and R.H. Prince, Diamond Relat. Mater., (1993) 2(2-4) 425-431.

[3] Mishra, D.K., X. Tian, T. Soga, T. Jimbo, and M. Sharon, Jpn. J. Appl. Phys, (2003) 42(Part 2, No. 10A) L1164-L1166.

[4] Noda, M., A. Marui, T. Suzuki, and M. Umeno, Diamond Relat. Mater., (2005) 14(11-12) 1757-1760.

[5] Suzuki, K., A. Sawabe, H. Yasuda, and T. Inuzuka, Appl. Phys. Lett., (1987) 50(12) 728-729.

[6] Uppireddi, K., B.R. Weiner, and G. Morell, (2008) 17(1) 55-59.

[7] Yang, Q., C. Xiao, W. Chen, and A. Hirose, Diamond Relat. Mater., (2004) 13(3) 433-437.

[8] Chiorboli, M., M.G. Donato, G. Faggio, M. Marinelli, G. Messina, E. Milani, R. Potenza, S. Santangelo, M. Scoccia, C. Tuve, and G. Verona Rinati, Diamond Relat. Mater., (2006) 15(11-12) 1976-1979.

[9] Wang, L., J. Lu, Q. Su, N. Wu, J. Liu, W. Shi, and Y. Xia, Mater. Lett., (2006) 60(19) 2390-2394.

[10] Cappelli, M.A. and P.H. Paul, J. Appl. Phys., (1990) 67(5) 2596-2602.

[11] Carrington, W., L. Hanssen, K. Snail, D. Oakes, and J. Butler, Metal. Trans. A, (1989) 20(7) 1282-1284.

[12] Donnet, J.B., H. Oulanti, T.L. Huu, and M. Schmitt, (2006) 44(2) 374-380.

[13] Oakes, D.B., J.E. Butler, K.A. Snail, W.A. Carrington, and L.M. Hanssen, J. Appl. Phys., (1991) 69(4) 2602-2610.

[14] Okada, K., S. Komatsu, T. Ishigaki, S. Matsumoto, and Y. Moriyoshi, J. Appl. Phys., (1992) 71(10) 4920-4924.

[15] Tzeng, Y., C.C. Tin, R. Phillips, T. Srivinyunon, and Y. Chen, Appl. Phys. Lett., (1990) 57(8) 789-791.

[16] Zhang, D.W., Z.J. Liu, Y.Z. Wan, and J.T. Wang, Appl. Phys. A, (1998) 66(1) 49-51.

[17] Hirose, Y., S. Amanuma, and K. Komaki, J. Appl. Phys., (1990) 68(12) 6401-6405.

[18] Hirose, Y. and Y. Terasawa, Jpn. J. Appl. Phys, (1986) 25(6) L519-L521.

[19] Matsui, Y., H. Yabe, and Y. Hirose, Jpn. J. Appl. Phys, (1990) 29(8) 1552–1560.

[20] Yarbrough, W.A., M.A. Stewart, and J.A. Cooper, Surf. Coat. Technol., (1989) 39-40 241-252.

[21] Le Huu, T., H. Zaidi, and D. Paulmier, Thin Solid Films, (1997) 308-309 147-153.

[22] Kurihara, K., K. Sasaki, M. Kawarada, and N. Koshino, Appl. Phys. Lett., (1988) 52(6) 437-438.

[23] Shin, S.D., N. M. Hwang, and D.Y. Kim, Diamond Relat. Mater., (2002) 11(7) 1337-1343.

[24] Ling, H., Y.X. Han, and Y.F. Lu, Proceedings of SPIE 6459, 2007, p. 64590Y-1-64590Y-7.

[25] Gleason, K.M.R.a.K.K., *Characterization Methods for Natural and Synthetic Diamonds*, in *Handbook of Industrial Diamonds and Diamond Films*. 1998. p. 455.

[26] Jenkins, R. and R.L. Snyder, *Error Due to Specimen Displacement*, in *Introduction to X-ray Power Diffractometry*. 1996, Wiley-Interscience. p. 194.

[27] Snail, K.A., D.B. Oakes, J.E. Butler, and L.M. Hanssen, New Diam. Sci. Technol., (1991) 503-509.

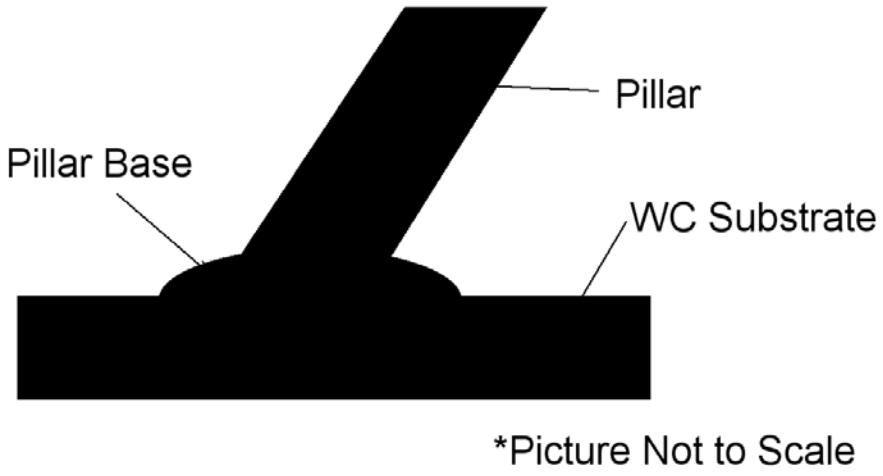

Fig 1. Schematic drawing of as-deposited structure.

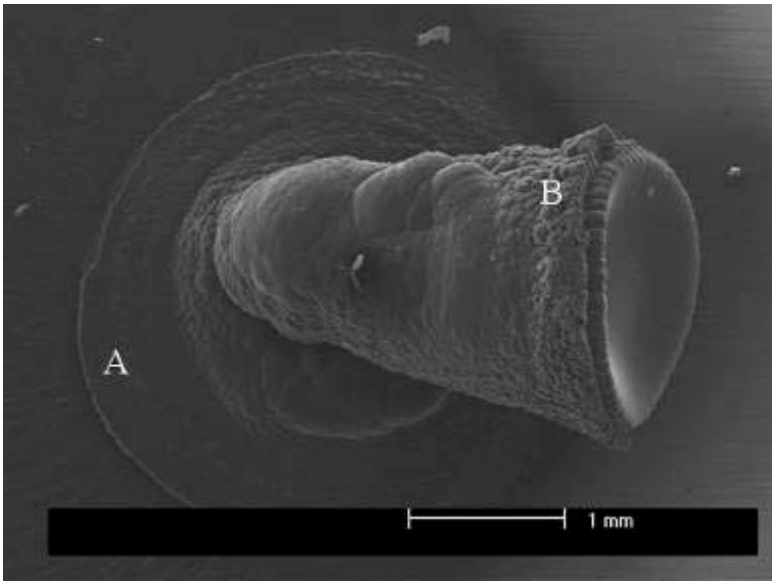

(a)

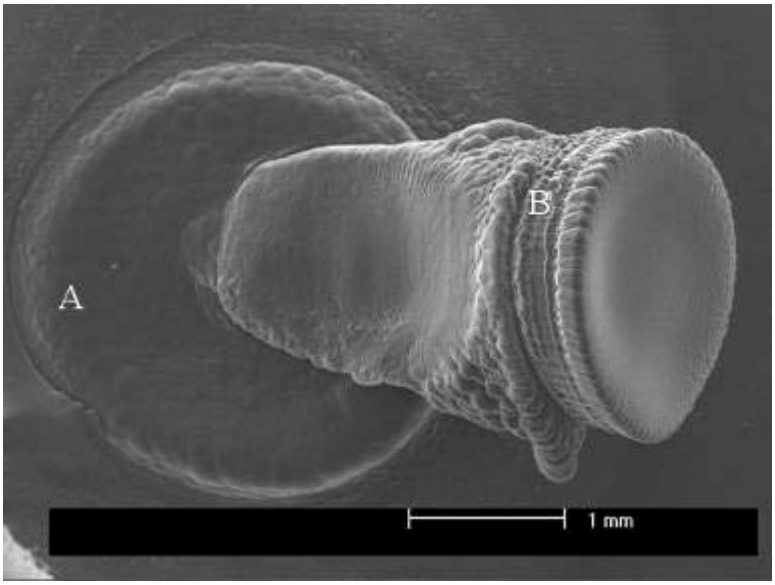

(b)

Fig.2. SEM micrographs of as-deposited carbon pillars, processed with CO_2 laser power of (a) 400 W, and (b) 800 W showing the pillar base (A) and pillar (B)

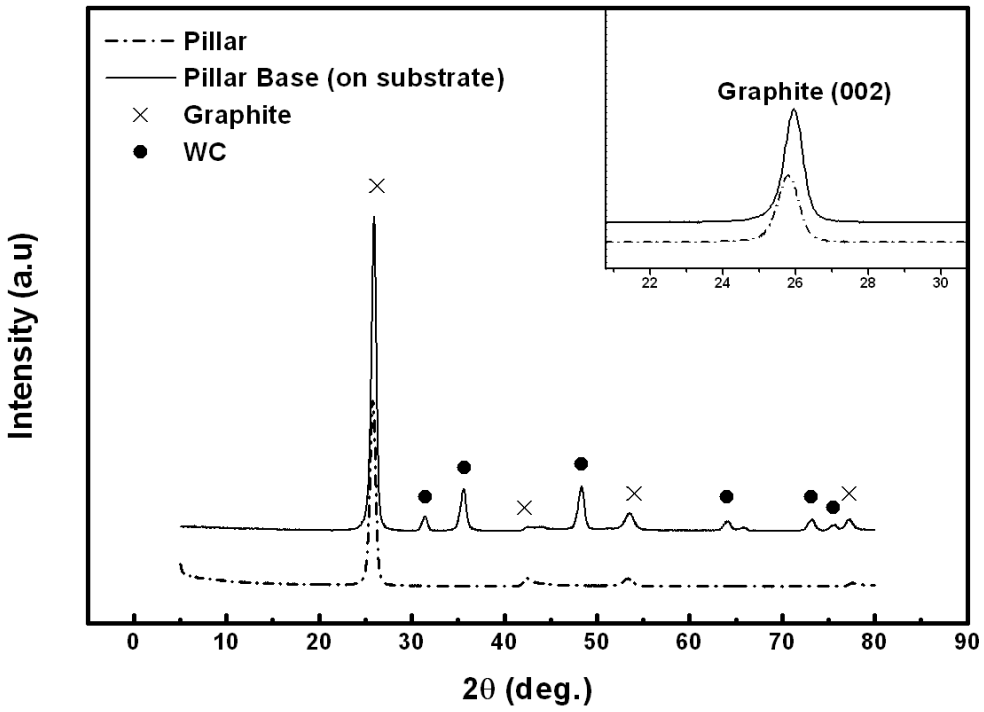

Fig. 3. XRD spectra of carbon pillar and pillar base which shows a (002) graphite peak

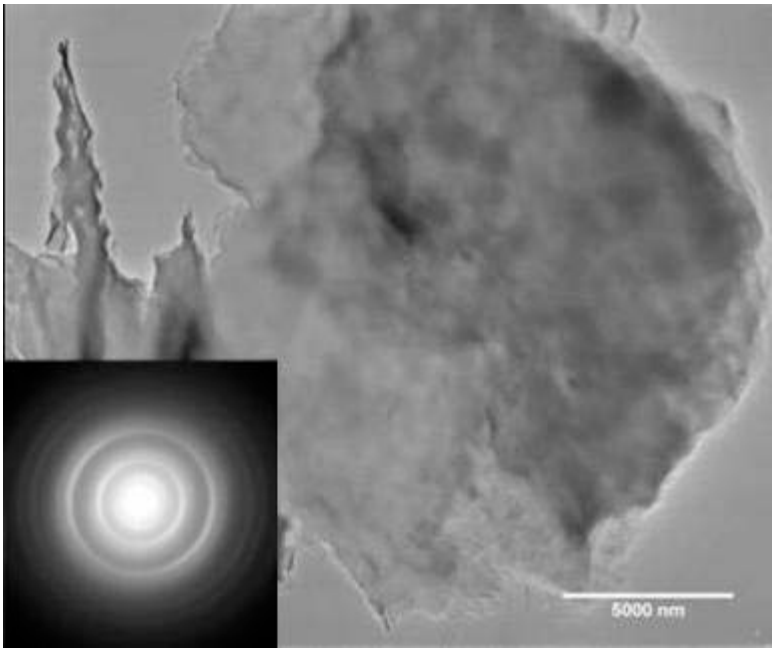

(a)

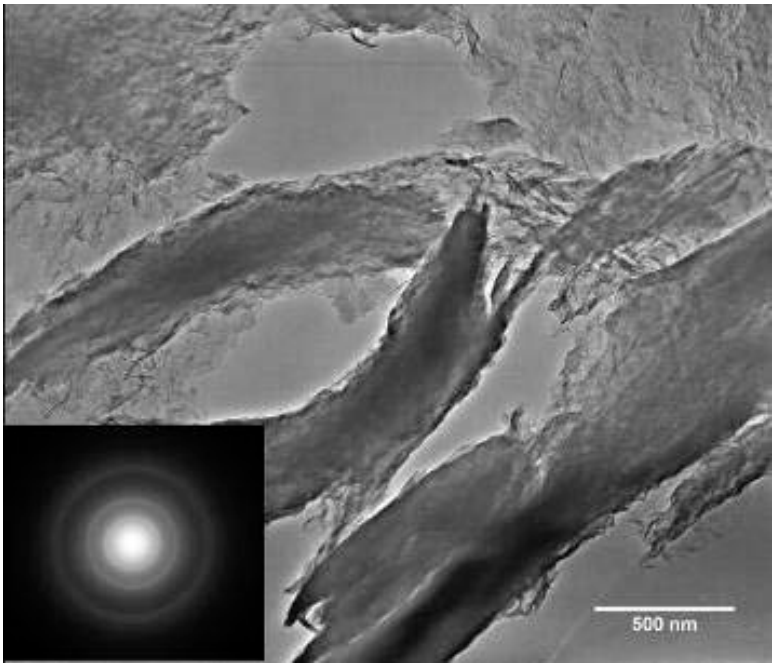

(b)

Fig. 4. Plan view TEM micrographs with inset electron diffraction pattern of particles from (a) graphite pillar, (b) bulk graphite, and (c) large grain from graphite pillar

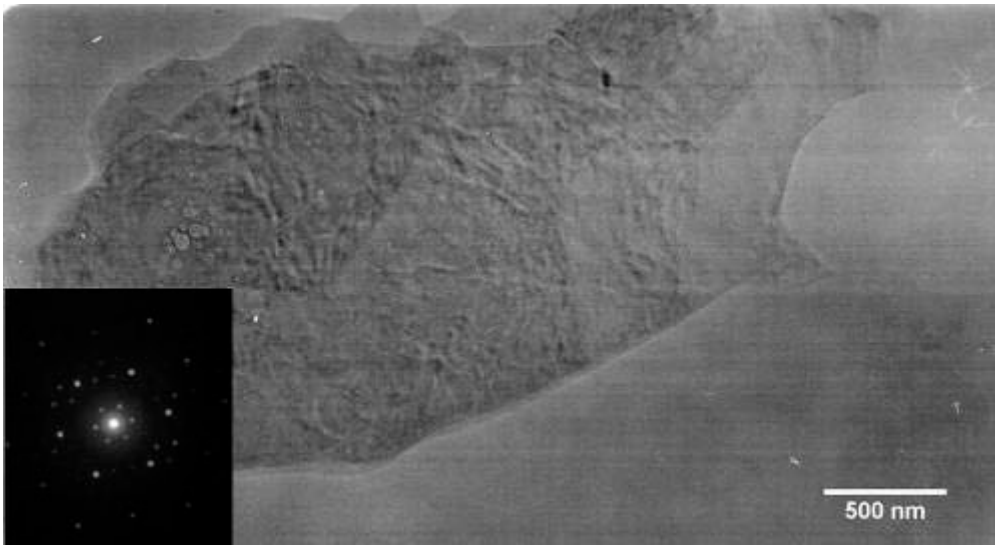

(c)

Fig. 4. (Continued) Plan view TEM micrographs with inset electron diffraction pattern of particles from (a) graphite pillar, (b) bulk graphite, and (c) large grain from graphite pillar

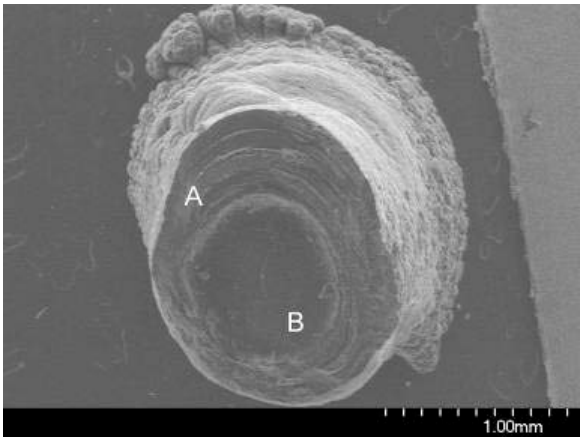

(a)

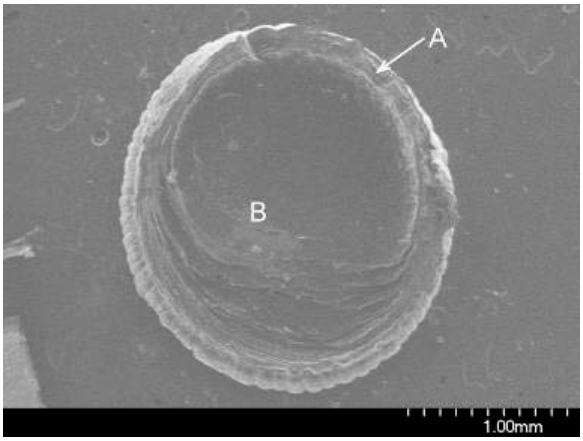

(b)

Fig. 5. SEM micrographs of cross-sections of CO_2 laser-assisted combustion-flame deposited carbon pillars with laser power of (a) 400 W and (b) 800 W showing the "shell" (A) and "core" (B)

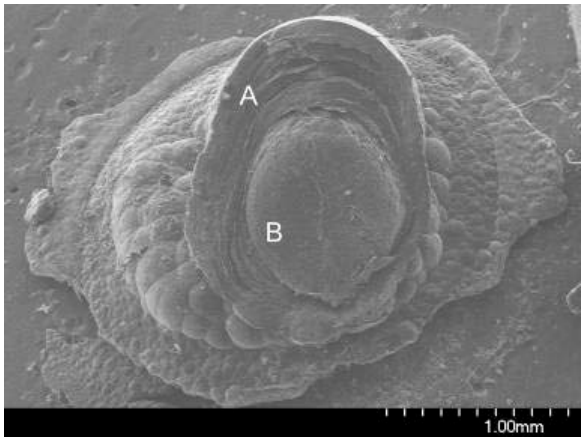

(a)

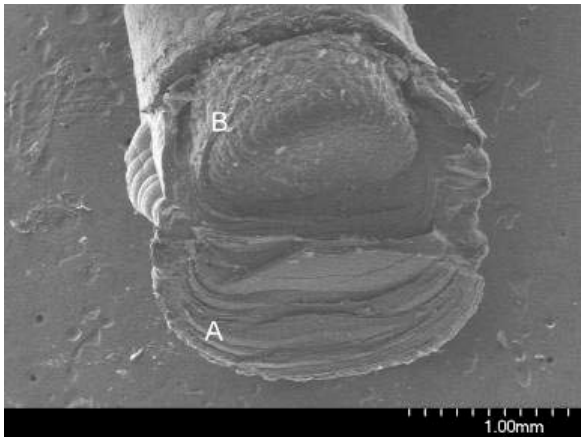

(b)

Fig. 6. SEM micrographs of alternate cross-section of CO_2 laser-assisted combustion-flame deposited carbon pillars with laser power of (a) 400 W and (b) 800 W showing the "shell" (A) and "core" (B)

(a)

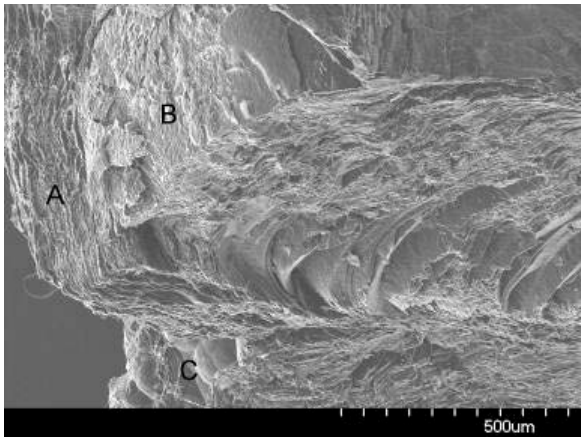

(b)

Fig. 7. SEM micrographs of cross-section of CO_2 laser-assisted combustion-flame deposited carbon pillar with laser power of 600 W (a) entire pillar with arrows ‘A’ and ‘B’ denoting areas of interest, (b) higher magnification image displaying the outer shell labeled ‘A’, inner “core” labeled ‘B’, the pillar base labeled ‘C’ and (c) higher magnification image contrasting the growth direction of the outer shell labeled ‘A’ and the pillar base labeled ‘B’ of the carbon pillar

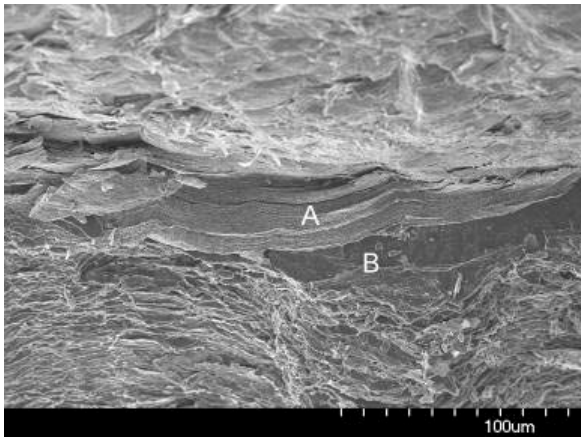

(c)

Fig. 7. (Continued) SEM micrographs of cross-section of CO_2 laser-assisted combustion-flame deposited carbon pillar with laser power of 600 W (a) entire pillar with arrows ‘A’ and ‘B’ denoting areas of interest, (b) higher magnification image displaying the outer shell labeled ‘A’, inner “core” labeled ‘B’, the pillar base labeled ‘C’ and (c) higher magnification image contrasting the growth direction of the outer shell labeled ‘A’ and the pillar base labeled ‘B’ of the carbon pillar

Table I. Summary of measured d-spacings for the carbon pillar with comparisons to a bulk graphite sample and calculated values

Graphite Pillar	Bulk Graphite	Graphite Standard	(hkl)
3.41	3.36	3.40	(002)
2.09		2.14	(100)
	2.03	2.04	(101)
		1.81	(102)
1.74		1.70	(004)
		1.55	(103)
		1.33	(104)
1.22		1.24	(110)
	1.16	1.16	(112)
	1.14	1.15	(105)
		1.13	(106)

3. CHARACTERIZATION OF DIAMOND THIN FILMS DEPOSITED BY A CO_2 LASER-ASSISTED COMBUSTION-FLAME METHOD

Travis McKindra[a*], Matthew J. O'Keefe[a], Zhiqiang Xie[b] and Yongfeng Lu[b]

[a]*Department of Materials Science and Engineering, Missouri University of Science and Technology, Rolla, MO 65409, United States*

[b]*Department of Electrical Engineering, University of Nebraska-Lincoln, Lincoln, NE 68588, United States*

*Corresponding Author, Tel: 573-341-4349, Fax: 573-341-2071, Email: mckindra@mst.edu

Abstract

Diamond thin films were deposited by a CO_2 laser-assisted $O_2/C_2H_2/C_2H_4$ combustion-flame process. The effect of the deposition parameters, in particular the laser wavelength and power, on the film surface morphology, microstructure and phases present was the primary focus of the work. The laser power was set at 100, 400 and 800 W while the wavelength was varied and set at 10.591 μm in the untuned condition and set at 10.532 μm to resonantly match the CH_2-wagging vibrational mode of the C_2H_4 molecule when in the tuned condition. When the laser was coupled to the combustion flame during deposition the diamond film growth was enhanced as the lateral grain size increased from 1 μm to greater than 5 μm. The greatest increase in grain size occurred when the wavelength was in the tuned condition. Scanning transmission electron microscopy images from focused-ion beam cross-sectioned samples revealed a sub-layer

of smaller grains less than 1 μm in size near the substrate surface at the lower laser powers and untuned wavelength. X-ray diffraction results showed a more intense Diamond (111) peak as the laser power increased from 100 to 800 W for the films deposited with the tuned laser wavelength. Micro-Raman spectra showed a diamond peak nearly twice as intense from the films with the tuned laser wavelength.

Keywords: diamond thin films; laser-assisted combustion-flame deposition; electron microscopy; X-ray diffraction; Raman spectroscopy

1. Introduction

Diamond thin films find applications in many areas because of a variety of material properties including excellent wear resistance, thermal conductivity and optical transparency [1]. Chemical vapor deposition (CVD) techniques are the preferred method for diamond synthesis [2-6], along with plasma discharge [7,8]. Physical vapor deposition (PVD) using laser ablation has also been reported [9,10]. Common among those techniques is the need for vacuum equipment. The open-atmosphere deposition of diamond films via a combustion-flame method was first reported by Hirose [11]. The process has been studied using different gas precursors, including O_2/C_2H_2 combustion [12,13], O_2/C_2H_4 [14,15] and the O_2/C_3H_6 system [16].

There are a limited number of studies on the use of CO_2 laser irradiation in conjunction with a combustion flame. Han [17,18] and Ling [19] reported the use of a CO_2 laser to enhance diamond nucleation and growth. The O_2/C_2H_2 combustion-flame process was used with CO_2 laser beam incident on the surface of a WC substrate. The

main effect of the laser energy was believed to be localized heating. It was found that the laser power and density were important factors influencing the deposition process. Optimization of those factors improved diamond crystallization and the subsequent quality of the films based on the characteristic diamond peak intensity from visible light Raman spectroscopy. Recent research efforts investigated the effect of the orientation of the incident laser beam from normal to the substrate surface to parallel to the substrate surface [20,21]. The parallel laser arrangement results in interaction of the laser with the combustion flame inner core. Also, the addition of a second hydrocarbon gas, C_2H_4 was studied. Gebre *et.al* [22] showed the effect of the laser irradiation on the combustion flame using the optical emission intensity of the excited species. The researchers proposed an enhancement in the diamond film quality due to an increase in the population of excited species responsible for diamond film growth by the coupling of the laser energy and combustion flame through resonant excitation of the C_2H_4 molecules. The energy coupling is thought to be possible due to CO_2 laser wavelengths of 10.591 and 10.532 μm being sufficiently close to the infrared absorption band associated with the CH_2-wag vibrational mode of the C_2H_4 molecule centered at 10.532 μm [20].

In this study, diamond films deposited on WC substrates by a CO_2 laser-assisted combustion-flame method were investigated. The objective was to characterize the effect of the CO_2 laser irradiation wavelength and power on the microstructure of the deposited films.

2. Experimental

The experimental setup used to deposit the films was similar to those reported in other experiments [17-22]. The diamond films were deposited on tungsten carbide (WC) substrates (BC-6S, Basic Carbide Corp.), with 6% Co binder, placed on a water-cooled hollow brass block. The dimensions of the substrates were 12.7 mm × 12.7 mm × 1.6 mm with an RMS surface roughness of about 1.6 μm. The substrates were cleaned in a supersonic bath of acetone for 30 minutes prior to deposition. A commercial welding torch with a 1.2 mm nozzle diameter was secured normal to the surface of the WC substrate and used to generate an $O_2/C_2H_2/C_2H_4$ combustion flame. The $O_2/C_2H_2/C_2H_4$ gas ratio was held constant at 1200:620:620 sccm by three mass-flow controllers (B7920V, Spec-Air Gases & Technologies). The inner cone of the flame was in direct contact with the substrate surface. A continuous-wave tunable CO_2 laser (PRC Company) was focused, with a ZnSe convex lens, perpendicular to the combustion-flame and parallel to the WC surface approximately 2 mm from the WC substrate. The temperature of the substrate was monitored by a pyrometer (OS3752, Omega Engineering, Inc.) and maintained at approximately 780°C. The deposition time was 15 minutes. The laser power was 100, 400 and 800 W at both 10.591 and 10.532 μm wavelengths.

The surface morphologies and microstructures of the deposited films were characterized by scanning electron microscopy (SEM) with a Hitachi S-4700 field emission scanning electron microscope (FESEM). Phase identification of the films was investigated by X-ray diffraction (XRD) using a Philips X-Pert diffractometer in glancing angle mode. Micro-Raman spectroscopy was conducted with a Horiba ARAMIS system.

The Raman spectra were measured using the 632.8 nm wavelength of a He-Ne laser. The films were prepared for cross-sectional microstructure analysis by scanning transmission electron microscopy (STEM) with a focused-ion beam (FIB) using an FEI Helios NanoLab 600 FIB/FESEM. The film thickness was estimated from the cross-sectional STEM images.

3. Results and discussion

The deposited films covered a circular area, in the center of the WC substrate, approximately 10 mm in diameter (Fig. 1.). The center of the deposited film is labeled as 'A' with an arrow. Plan view SEM of as-deposited films at all laser powers and both laser wavelengths was conducted. The results were similar to previous results [21]. The films were continuous over the deposition area, completely covering the WC substrate, and consisted of overlapping, randomly oriented faceted crystals at all process conditions. Small, white particles were noticeable on the surface of the films and were identified as cobalt through energy dispersive spectroscopy (EDS) conducted during the SEM investigation. Cobalt contamination on the surface of the diamond film is a known complication of depositing on WC(Co) substrates [23-25]. We believe the cobalt is ablated from the substrate surface by the forceful combustion-flame during deposition and then redeposited on top of the diamond film after cessation of the flame. Another possible explanation is that the cobalt diffuses through the growing film, but there was no evidence to that effect, such as cobalt particles detected during the cross-sectional investigation. In general, the films were similar in appearance to the films deposited with the laser wavelength of 10.591 μm in that the surface consisted of randomly orientated, overlapping faceted crystals with cobalt particles present on the top surface. Comparing

the grain sizes of the films deposited at different laser wavelengths revealed significant grain growth in the film deposited with the tuned 10.532 μm laser wavelength, especially at the higher laser powers (400 and 800 W). The SEM results appeared to agree with the studies indicating resonant excitation of the gaseous precursors could increase the population of excited species responsible for diamond formation [20]. If the manifestation of successful energy coupling is larger grains for the same deposition time, then it follows that the 10.532 μm wavelength would produce larger grains since it is closer to the resonant frequency of the CH_2-wagging vibrational mode of the C_2H_4 molecule. The similar grain size at 100 W could be indicative of a critical point in that more power was needed to excite the precursor species and CH_2-wagging vibration that results in enhanced film growth.

The SEM results showed that the deposited films were comprised of faceted crystallites. Crystal structures and phases in the films were investigated using XRD. The X-rays were focused on the area of the substrate covered by the film, a circular region approximately 8 mm in diameter. Figure 2 shows XRD spectra from the as-deposited films and has peaks from the WC substrate as well as two peaks associated with diamond (111) and (220) planes. The spectra from the films deposited with 10.591 and 10.532 μm laser wavelengths are shown in Figs. 2(a) and 2(b), respectively. All the spectra have the same general shape regardless of the laser power. A comparison of the diffraction peak in the 2θ range associated with diamond (111) planes from the films deposited at each laser power and wavelength is presented in Fig. 3. Two comparisons were made between the spectra of films: first, the spectrum from the film deposited without laser irradiation

was compared to the spectra from the films at each laser power, and second, the spectra from the films deposited with the laser irradiation were compared based on laser wavelength for a given power. Specifically, qualitative comparisons were made between diamond (111) peak intensities. At the 10.591 μm laser wavelength, the intensity of the diffraction peak was essentially unchanged with the addition of the laser irradiation and increased laser power. However, at the 10.532 μm laser wavelength, there was a significant increase in the diffraction peak intensity and a sharpening of the peak shape with increased laser power. That result was attributed to the larger grain size exhibited by the films at the higher laser powers. At 100 W, the diffraction peak intensity was virtually identical for the two films. At the higher laser powers of 400 and 800 W, the peak intensity difference was greater than that at 100 W. The fact that enhancement of the diffraction peak was more evident at the higher levels of laser power suggests that a critical laser power was required. The XRD results agreed with the SEM investigation in that there was an increase in the grain size and diffraction peak intensity of the films deposited at the different wavelengths at 400 and 800 W laser power.

Micro-Raman spectroscopy of the center of the as-deposited films was used to investigate the film quality as determined by the shape and intensity of the first order Raman peak. Raman spectra from all of the deposited films were compared (Fig 4). In Fig. 4(a) the Raman spectra for the films deposited with 10.591 μm laser wavelength at 100 , 400 and 800 W are presented along with the spectra for the film deposited without laser irradiation. All of the spectra showed the first order Raman signal characteristic of diamond above a broad band from 1100 to 1650 cm^{-1} that was caused by

photoluminescence. The diamond peak was centered at 1335 cm^{-1} and a broad band associated with graphitic carbon (G-band) centered near 1500 cm^{-1}. The integrated peak intensity of the diamond peak was calculated after 13-point Savitzky-Golay smoothing and background removal and used to make a quantitative comparison between the spectra. With the laser power at 100 W the corresponding Raman spectra showed a more dominant diamond phase compared to the spectra from the film deposited without the laser. The intensity of the diamond peak increased by nearly a factor of two, while the FWHM decreased from 18 to 14 cm^{-1}. The peak intensity of the diamond peak from the film deposited with 400 W was essentially the same as when no laser was used, though the FWHM did decrease to 16 cm^{-1}. When the laser power was increased to 800 W the peak intensity was increased by a factor of 3 and the FWHM was 18 cm^{-1}. The comparison of the Raman spectra from the films deposited with 10.532 μm CO_2 laser wavelength is shown in Fig. 4(b). Similar to the films deposited with 10.591 μm laser irradiation, the 10.532 μm deposited films yielded Raman spectra with a diamond peak near 1335 cm^{-1}. The spectra from the films deposited with the CO_2 laser exhibited a diamond peak that was comparably sharper and more intense than the films deposited without laser irradiation. At the laser powers of 100 and 800 W the diamond peak intensity increased more than 3 times over the no laser case. The spectra from the film deposited with 400 W laser energy had the most intense peak which was more than 4 times as intense compared to the no laser case.

The increase in laser power enhanced the diamond film quality at both wavelengths as evidenced by the increased peak intensity and decreased FWHM. However, the diamond peak intensity was higher and the FWHM less with the 10.532 μm

laser wavelength. Based on that comparison of the spectra from the films deposited at the two different wavelengths it was concluded that the 10.532 μm laser irradiation produced higher quality diamond films.

Cross-sectional scanning transmission electron microscopy (STEM) was utilized to investigate the film microstructure, nucleation and features relevant to film growth. The electron-transparent TEM foils used for the STEM investigation were prepared using the focused-ion beam (FIB) technique. The FIB technique is a very useful tool for site-specific investigations of an area approximately 15 μm x 10 μm [26]. Dark-field (DF) STEM images from films deposited with the untuned 10.591 μm laser wavelength and at all laser powers, including the film deposited without laser irradiation, are shown in Fig. 5. The film deposited without a laser was 3 – 4 μm in thickness with a sharp film/substrate interface as shown in Fig 5(a). The grains near the substrate were approximately 1 μm, compared to the grains near the film surface which were 2-3 μm in size. Columnar grains were observed near the surface with a different morphology than those near the substrate, which were more randomly oriented. The grains near the substrate (sub-layer) had a lamellar, possibly more graphitic, microstructure and were within approximately 2 μm of the substrate surface. Examination of the image suggests that there was competitive growth between the various grains leading to the faceted film surface. As the laser irradiation was added, the overall grain size became larger and the lamellar features became less prevalent as shown in Fig 5(b). When the laser power increased to 400 W a noticeable depression of the WC substrate was seen (Fig 5(c)) that was unique among the cross-sectional specimen presented in this work. The origin of

depression is unclear but there are two plausible explanations. First, given that the feature was not seen in any other samples, the depression could be an aberration borne of a defect in the WC substrate. Second, it was possible that the depression marks the location on the substrate directly beneath the combustion flame and thus Fig 5(c) would represent the initial impact crater. Closer inspection of the microstructure revealed that the lamellar structure was more prevalent in this film than the film deposited with 100 W laser power. Also, the Raman spectra from the film deposited at 400 W showed only a relatively small diamond peak with a larger G-band which suggests that this film was more graphitic over a larger area. At 800 W (Fig 5(d)) the film was 4-5 μm thick with surface grains approximately 2 μm. The columnar growth started nearer to the substrate with grains ~0.5 μm × 1.5 μm in size. The STEM results for the untuned laser films agree with the plan view SEM results in that the addition of the laser resulted in films with large, columnar grains.

For comparison, DF STEM images from the films deposited with the tuned 10.532 μm CO_2 laser as well as the film deposited with no laser irradiation are shown in Fig. 6. At 100 W (Fig 6(b)) the film was approximately 4 μm thick with some grains extending the entire thickness. The sub-layer was less evident at 100 W compared to the untuned laser, but still present. The columnar grains were ~ 1 μm wide. The film deposited with 400 W laser power (Fig 6(c)) also exhibited columnar grains through almost the entire thickness of the film. The grains were slightly wider at this power with some grains greater than 1 μm in width. The film deposited with 800 W (Fig 6(d)) had the largest grain size of approximately 2 – 3 μm near of the surface. The sub-layer was even less evident in the 800 W film. The width of the individual grains was several

micrometers. The STEM results agree with the XRD and Raman as the films deposited with the tuned wavelength of 10.532 μm CO_2 laser irradiation had the largest grains and sharpest peaks.

Comparison of the microstructure of the films deposited with the different laser wavelengths indicated that the films deposited with laser irradiation tuned to match the CH_2-wagging vibrational mode at 10.532 μm had a larger lateral grain size and a significantly different microstructure than the film deposited with the laser irradiation at 10.591 μm. Similarly, the films deposited with the lasers exhibited microstructures significantly different than the films deposited without the laser irradiation. All of the results indicate that the laser energy affected the film nucleation and growth. The sub-layer near the film and substrate interface may be graphitic based on the lamellar microstructure and the fact that the Raman spectra that had an increased non-diamond component. It has been shown that coupling laser energy to the flame increased the population of diamond forming species in the combustion flame [22], specifically CH and C_2 species which have been identified as possible diamond precursors [27, 28]. The results provided here support the idea of increasing the population of diamond forming species in the combustion-flame using a laser focused on the flame and parallel to the substrate, especially a laser tuned to the resonant wavelength of the vibrational modes of the gas precursors. The changing of the laser wavelength and power and subsequent effect on the microstructure of the deposited material suggest that gas phase reactions played a significant role in determining the size, shape and crystallinity of diamond films.

4. Conclusion

Diamond thin films were deposited on WC substrates by a CO_2 laser-assisted combustion-flame method in which the laser was focused on the tip of inner cone of the flame, parallel to the substrate surface. Subsequent characterization of the deposited films determined the effect of the CO_2 laser wavelength and power on the film surface morphology, phase, crystallinity and microstructure. It was determined that for a given wavelength, when the laser power was increased the grain size increased, the diamond X-ray diffraction peak was more intense and the characteristic diamond Raman peak was sharper and more intense. For a given power, comparisons were made between the two different laser wavelengths. In general, the film grain size was twice as large and the diamond diffraction peak intensity increased and sharpened when the films were deposited with 10.532 μm CO_2 laser wavelength tuned to the CH_2-wagging vibrational mode of the C_2H_4 molecule when compared with the films deposited with an untuned 10.591 μm CO_2 laser wavelength. Overall the results indicated the addition of the laser beam parallel to the substrate surface and coupled to the combustion-flame enhanced diamond film growth.

Acknowledgments

This work was financially supported by the U.S. Office of Naval Research (ONR) through the Multidisciplinary University Research Initiative (MURI) program under the advice and guidance of Dr. I. Perez. The assistance of Dr. Eric Bohannon with XRD and Dr. Ming Zhang with FIB/STEM from the Materials Research Center at the Missouri University of Science and Technology is gratefully acknowledged.

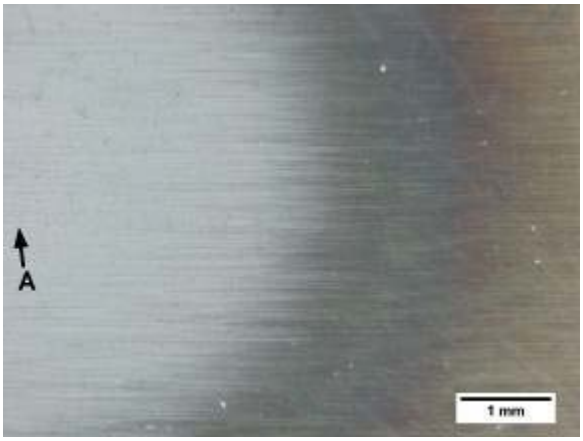

Fig. 1. Optical micrograph of as-deposited film with the center of the deposit labeled ‘A’.

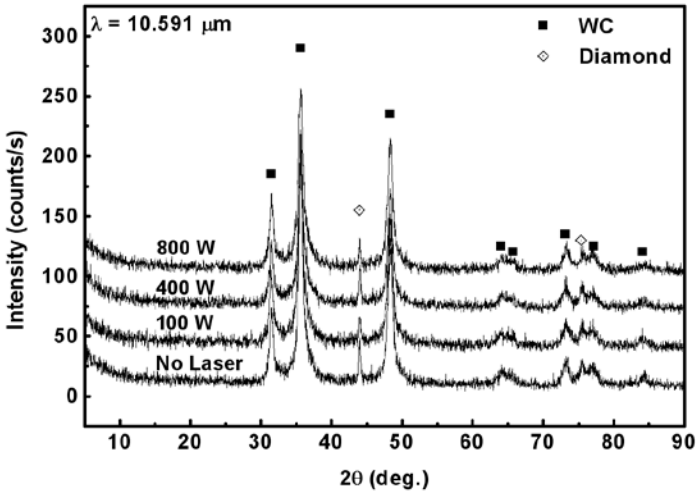

(a)

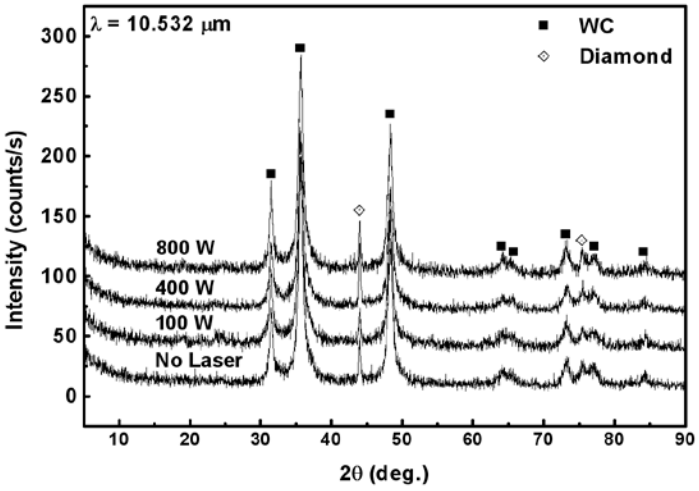

(b)

Fig. 2. XRD spectra from films deposited at CO_2 laser wavelength of (a) 10.591 μm and (b) 10.532 μm.

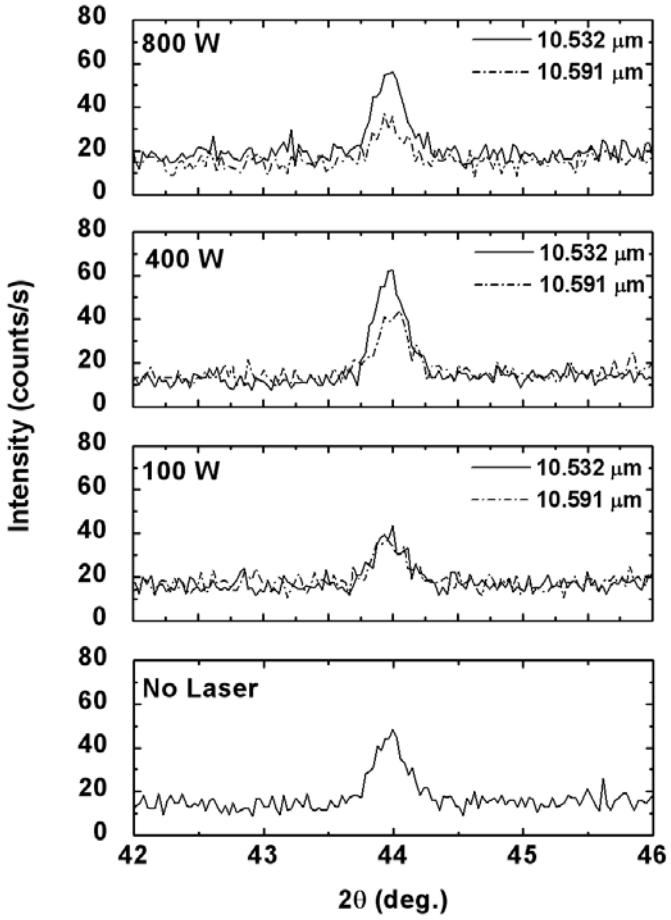

Fig. 3. Comparison laser wavelength effect on X-ray diffraction peak associated with diamond (111) planes from films deposited without laser irradiation and at each laser power.

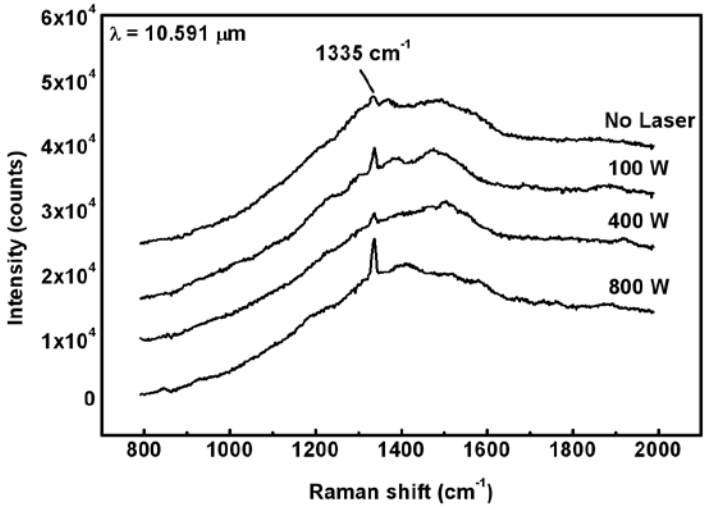

(a)

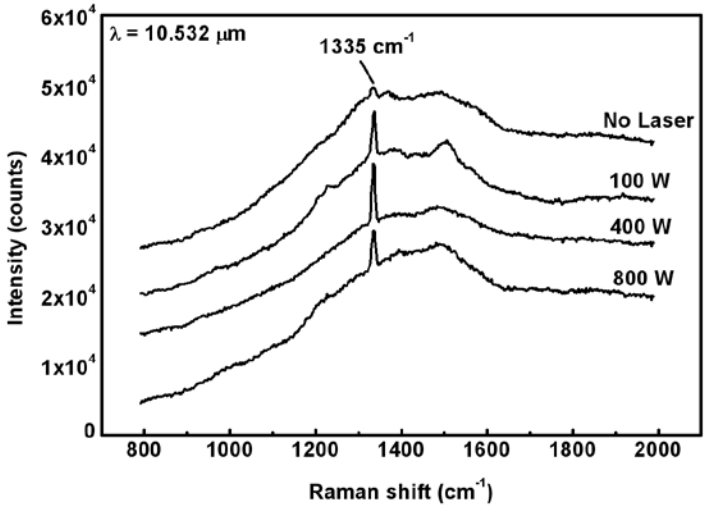

(b)

Fig 4. Comparison of Raman spectra from films deposited with CO_2 laser wavelength of (a) 10.591 μm and (b) 10.532 μm.

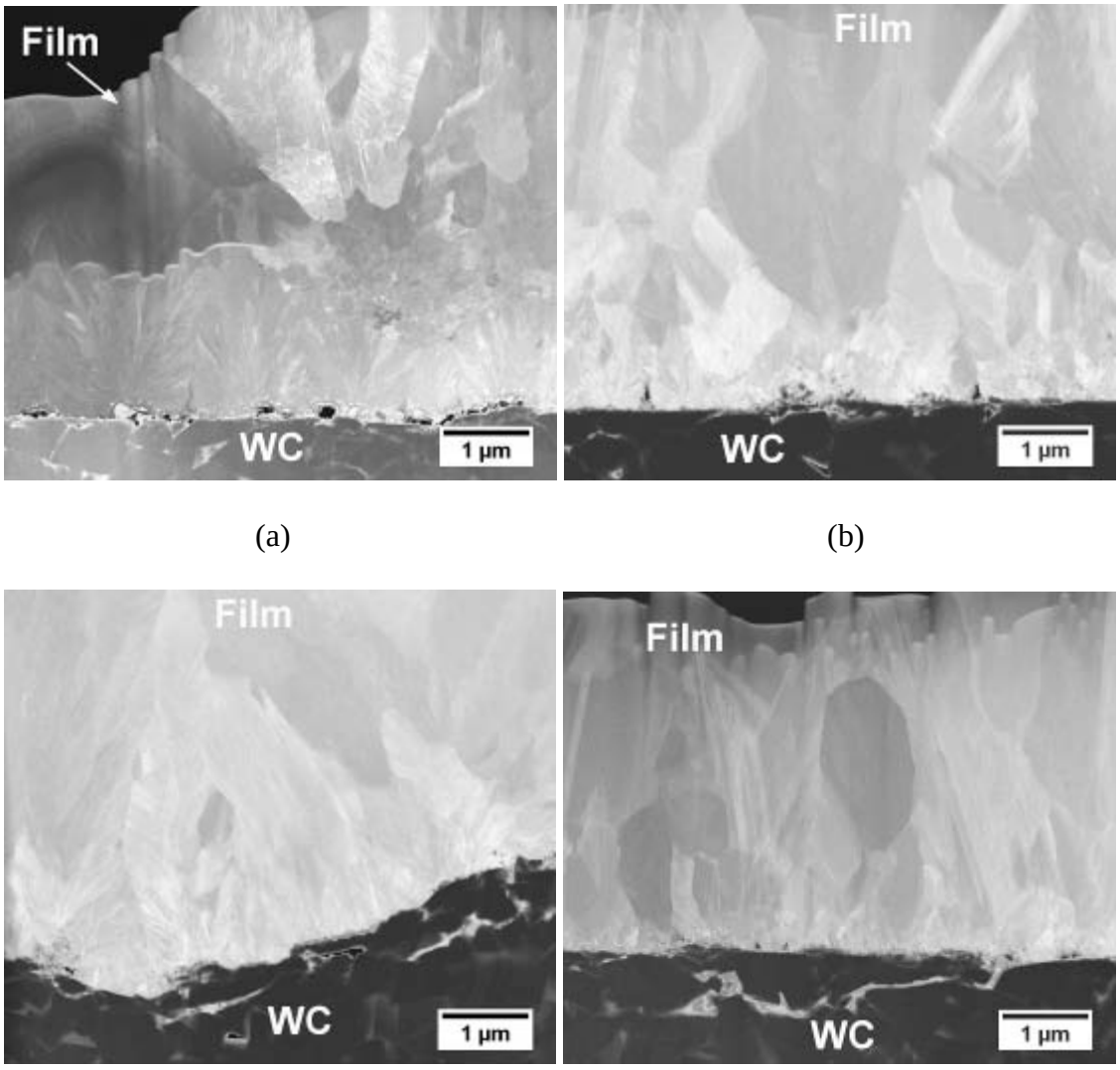

Fig. 5. Dark-field STEM images from diamond films deposited with CO_2 laser wavelength of 10.591 µm and laser power of (a) no laser, (b) 100 W, (c) 400 W and (d) 800 W.

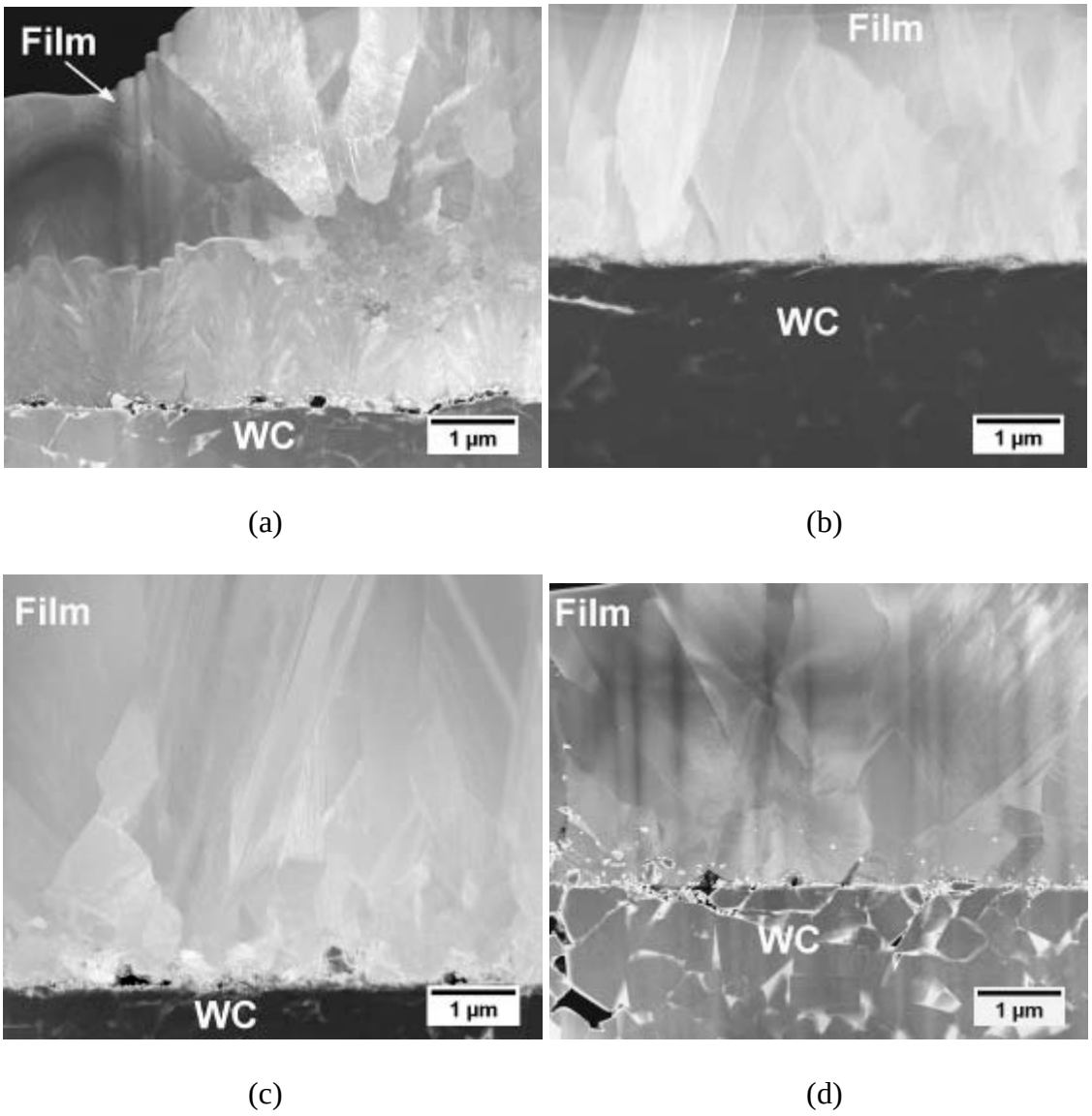

Fig. 6. Dark-field STEM images from diamond films deposited with CO_2 laser wavelength of 10.532 µm and laser power of (a) no laser, (b) 100 W, (c) 400 W and (d) 800 W.

References

[1] D.M. Gruen, Nanocrystalline diamond films, Annu. Rev. Mater. Sci. 29 (1999) 211-259.

[2] K. Kurihara, K. Sasaki, M. Kawarada, and N. Koshino, High rate synthesis of diamond by dc plasma jet chemical vapor deposition, Appl. Phys. Lett. 52(6) (1988) 437-438.

[3] Y. Liou, R. Weimer, D. Knight, and R. Messier, Effect of oxygen in diamond deposition at low substrate temperatures, Appl. Phys. Lett. 56(5) (1990) 437-439.

[4] D. Rats, L. Vandenbulcke, R. Herbin, R. Benoit, R. Erre, V. Serin, and J. Sevely, Characterization of diamond films deposited on titanium and its alloys, Thin Solid Films 270(1-2) (1995) 177-183.

[5] L. Wang, J. Lu, Q. Su, N. Wu, J. Liu, W. Shi, and Y. Xia, [100]-textured growth of polycrystalline diamond films on alumina substrates by microwave plasma chemical vapor deposition, Mater. Lett. 60(19) (2006) 2390-2394.

[6] Q. Yang, C. Xiao, W. Chen, and A. Hirose, Selective growth of diamond and carbon nanostructures by hot filament chemical vapor deposition, Diamond Relat. Mater.13(3) (2004) 433-437.

[7] M. Noda, A. Marui, T. Suzuki, and M. Umeno, Deposition of diamond film on silicon and quartz substrates located near DC plasma, Diamond Relat. Mater.14(11-12) (2005) 1757-1760.

[8] K. Suzuki, A. Sawabe, H. Yasuda, and T. Inuzuka, Growth of diamond thin films by dc plasma chemical vapor deposition, Appl. Phys. Lett. 50(12), (1987) 728-729.

[9] E.B.D. Bourdon, P. Kovarik, and R.H. Prince, Microcrystalline diamond phase by laser ablation of graphite, Diamond Relat. Mater. 2(2-4) (1993) 425-431.

[10] D.K. Mishra, X. Tian, T. Soga, T. Jimbo, and M. Sharon, Diamond synthesized at room temperature by pulsed laser deposition in vacuum, Jpn. J. Appl. Phys. 42(Part 2, No. 10A) (2003) L1164-L1166.

[11] Y. Hirose, S. Amanuma, and K. Komaki, The synthesis of high-quality diamond in combustion flames, J. Appl. Phys.68(12) (1990) 6401-6405.

[12] M.A. Cappelli and P.H. Paul, An investigation of diamond film deposition in a premixed oxyacetylene flame, J. Appl. Phys.67(5) (1990) 2596-2602.

[13] J.B. Donnet, H. Oulanti, T.L. Huu, and M. Schmitt, Synthesis of large single crystal diamond using combustion-flame method, Carbon 44(2) (2006) 374-380.

[14] W. Carrington, L. Hanssen, K. Snail, D. Oakes, and J. Butler, Diamond growth in $O_2 + C_2H_4$ and $O_2 + C_2H_2$ flames, Metall. Mater. Trans. A 20(7) (1989) 1282-1284.

[15] K.A. Snail, D.B. Oakes, J.E. Butler, and L.M. Hanssen, Studies of diamond deposition with 1-D and 2-D combustion flames, New Diam. Sci. Tech. (1991) 503-509.

[16] H.S. Shin and D.G. Goodwin, Diamond growth in premixed propylene-oxygen flames, Appl. Phys. Lett. 66(21) (1995) 2909-2911.

[17] Y.X. Han, H. Ling, J. Sun, M. Zhao, T. Gebre, and Y.F. Lu, Enhanced diamond nucleation on copper substrates by graphite seeding and CO_2 laser irradiation, Appl. Surf. Sci. 254(7) (2008) 2054-2058.

[18] Y.X. Han, M. Zhao, J. Sun, H. Ling, T. Gebre, and Y.F. Lu, Real-time monitoring of diamond nucleation and growth using field-enhanced thermionic emission current, Appl. Surf. Sci. 254(5) (2007) 1423-1426.

[19] H. Ling, Y.X. Han, and Y.F. Lu, CO_2 laser-assisted local deposition of diamond films by combustion-flame method, Proc. SPIE 6459 (2007) 64590Y-1-64590Y-7.

[20] H. Ling, J. Sun, Y.X. Han, T. Gebre, Z.Q. Xie, M. Zhao, and Y.F. Lu, Laser-induced resonant excitation of ethylene molecules in $C_2H_4/C_2H_2/O_2$ reactions to enhance diamond deposition, J. Appl. Phys. 105(1) (2009) 014901-014905.

[21] H. Ling, Z.Q. Xie, Y. Gao, T. Gebre, X.K. Shen, and Y.F. Lu, Enhanced chemical vapor deposition of diamond by wavelength-matched vibrational excitations of ethylene molecules using tunable CO2 laser irradiation, J. Appl. Phys. 105(6) (2009) 064901-064906.

[22] T. Gebre, J. Sun, H. Ling, Y.X. Han, M. Zao, and Y.F. Lu, C_2 and CH rotational temperatures in diamond growth using CO_2 laser-assisted combustion-flames, Proc. SPIE 6880 (2008) 68800O-1-68800O-7.

[23] J.B. Donnet, D. Paulmier, H. Oulanti, and T. Le Huu, Diffusion of cobalt in diamond films synthesized by combustion flame method, Carbon 42(11) (2004) 2215-2221.

[24] G. Cabral, N. Ali, E. Titus, and J. Gracio, Cobalt diffusion in different microstructured WC-Co substrates during diamond chemical vapor deposition, J. Phase Equilib. Diffus. 26(5) (2005) 411-416.

[25] R. Polini, F. Le Normand, G. Marcheselli, and E. Traversa, Early stages of diamond-film formation on cobalt-cemented tungsten carbide, J. Am. Ceram. Soc. 82(6) (1999) 1429-1435.

[26] R. Wirth, Focus ion beam (FIB) combined with SEM and TEM: Advanced analytical tools for sutdies of chemical composition, microstructure and crystal structure in geomaterials on a nanometre scale, Chem. Geol. 261 (2009) 217-229.

[27] R.J.H. Klein-Douwel, J.J.L Spaanjaars, and J.J. ter Meulen, Two-dimensional distributions of C2, CH, and OH in a diamond depositing oxyacetylene flame measured by laser induced fluorescence, J. Appl. Phys. 78(3) (1995) 2086-2096.

[28] Y. Matsui, H. Yabe, and Y. Hirose, The growth mechanism of diamond crystals in acetylene flames, Jpn. J. Appl. Phys. 29(8) (1990) 1552-1560.

4. NUCLEATION AND GROWTH OF DIAMOND THIN FILMS DEPOSITED BY A CO_2 LASER-ASSISTED COMBUSTION-FLAME METHOD

Travis McKindra[a*], Matthew J. O'Keefe[a], Elizabeth Kulp[a], Zhiqiang Xie[b] and Yongfeng Lu[b]

[a]*Department of Materials Science and Engineering, Missouri University of Science and Technology, Rolla, MO 65409, United States*

[b]*Department of Electrical Engineering, University of Nebraska-Lincoln, Lincoln, NE 68588, United States*

*Corresponding Author, Tel: 573-341-4349, Fax: 573-341-2071, Email: mckindra@mst.edu

Abstract

The deposition of diamond thin films using a CO_2 laser-assisted combustion-flame CVD process was investigated using two different CO_2 laser wavelengths for deposition times of less than 5 minutes. The CO_2 laser wavelength was varied based on the resonant absorption of laser energy by gaseous precursors ($O_2/C_2H_2/C_2H_4$), in particular 10.591 μm that did not match a resonant absorption (unturned) and 10.532 μm that matched one of the resonant frequencies of the C_2H_4 molecule (tuned). Deposition without a CO_2 laser was done as a reference. Film morphology and microstructure was characterized by scanning electron microscopy (SEM) and scanning transmission electron microscopy (STEM). After one minute of deposition the films consisted of discrete particles. The amount of faceting and particle size was found to be dependent on the laser wavelength. X-ray diffraction (XRD) and micro-Raman spectroscopy were used for phase identification. The diamond component in the films varied with the deposition time and laser wavelength. The largest diamond component and most faceted grains were

obtained using the tuned CO_2 laser regardless of time. The enhancement of the diamond growth with the tuned laser wavelength was attributed to an increase in the sticking probability of the precursors to adatoms on the substrate surface.

Keywords: diamond thin films; laser-assisted combustion-flame deposition; electron microscopy; X-ray diffraction; Raman spectroscopy

1. Introduction

Diamond thin films have applications in many areas because of material properties including excellent wear resistance, thermal conductivity and optical transparency [1]. Chemical vapor deposition (CVD) techniques are the preferred method for diamond synthesis [2-6], along with plasma discharge [7, 8]. Physical vapor deposition (PVD) using laser ablation has also been reported [9, 10]. The combustion flame method using an O_2/C_2H_2 gaseous precursor and initially reported by Hirose [11] has been proven to deposit diamond in open atmosphere. Variations and investigations on the process include differences in the combustion gasses [12-14], distance of the flame to the substrate surface and the substrate temperature [15]. Recent research has studied the possibility of coupling the combustion-flame with CO_2 laser energies. The energy coupling is possible due to the ability to tune a CO_2 laser to a specific wavelength. The infrared absorption band associated with the CH_2-wagging vibrational mode of the C_2H_4 molecule is centered at 10.532 μm. An OES comparison of the effect of tuning the laser wavelength to match the infrared absorption band and using the standard 10.591 μm CO_2 laser wavelength shows a higher percentage of the laser energy is absorbed using the tuned 10.532 μm wavelength as well an increased deposition rate and better diamond film quality [16].

The nucleation of the films deposited by the CO_2 laser-assisted $O_2/C_2H_2/C2H_4$ combustion-flame method is not fully understood. Research suggests that in CO_2 laser-assisted combustion-flame deposited films greater than 4 μm thick, a sub-layer phase exists near the substrate surface that is microstructurally different than the diamond phase. The structure of the sub-layer phase may contain a graphitic component and is dependent on the CO_2 laser wavelength [17]. The origin of the sub-layer phase is unknown and has not been investigated extensively.

In this study diamond thin films, 1 μm or less in thickness, deposited on WC substrates by a CO_2 laser-assisted combustion-flame method were investigated along with film deposited without a laser. The objective was to use shorter deposition times in order to characterize the effect of the CO_2 laser wavelength on the nucleation and initial growth of diamond thin films.

2. Material and methods

The experimental setup used to deposit the films was similar to those reported elsewhere [16-22]. The diamond films were deposited on tungsten carbide (WC) substrates (BC-6S, Basic Carbide Corp.), with 6% Co binder, placed on a water-cooled hollow brass block. The dimensions of the substrates were 12.7 mm × 12.7 mm × 1.6 mm with an RMS surface roughness of about 1.6 μm. The substrates were cleaned in a supersonic bath of acetone for 30 minutes prior to deposition. A commercial welding torch with a 1.2 mm nozzle diameter was secured normal to the surface of the WC substrate and used to generate an $O_2/C_2H_2/C_2H_4$ combustion flame. The $O_2/C_2H_2/C_2H_4$ gas ratio was held constant at 1200:620:620 sccm by three mass-flow controllers (B7920V, Spec-Air Gases & Technologies). The inner cone of the flame was in direct contact with the substrate

surface. A continuous-wave tunable CO_2 laser (PRC Company) was focused, with a ZnSe convex lens, perpendicular to the combustion-flame and parallel to the WC surface approximately 2 mm from the WC substrate. Using this arrangement the laser interacted only with the flame. The temperature of the substrate was monitored by a pyrometer (OS3752, Omega Engineering, Inc.) and maintained at approximately 780°C. The deposition times were 1, 2 and 5 minutes. The laser power was 800 W at both 10.591 and 10.532 μm wavelengths.

The surface morphologies and microstructures of the deposited films were characterized by scanning electron microscopy (SEM) with a Hitachi S-4700 field emission scanning electron microscope (FESEM). Phase identification of the films was investigated by X-ray diffraction (XRD) using a Philips X-Pert diffractometer in glancing angle mode with a Cu Kα source. Micro-Raman spectroscopy was conducted with a Horiba ARAMIS system. The Raman spectra were measured using the 632.8 nm wavelength of a He-Ne laser. The films were prepared for cross-sectional microstructure analysis by scanning transmission electron microscopy (STEM) with a focused-ion beam (FIB) using an FEI Helios NanoLab 600 FIB/FESEM. The film thickness was estimated from the cross-sectional STEM images.

3. Results and discussion

Optically the films appeared very similar to the bare WC substrates. There were areas of discontinuous particles and discoloration due to oxidation caused by heat from the combustion-flame. The as-deposited films were investigated by XRD to determine what phases were present. The XRD spectra from the center of the substrate at each laser condition and deposition time are shown in Fig 1. The spectra from the films deposited

for 1 and 2 minutes are shown in Figs 1(a) and (b), respectively. There were several peaks from the WC substrate as well as peaks attributed to WO_3 and $CoWO_4$, but none associated with diamond. Diamond (111) peaks were visible in the spectra from the films deposited for 5 minutes as shown in Fig 1(c). The diamond peak intensity was highest for the film deposited with the tuned CO_2 laser (Fig 1(d)) possibly indicating a thicker film or structurally more complete diamond phase. That result would agree with previous findings concerning the use of the tuned CO_2 laser [17]. From the XRD results it is apparent that diamond is not detectable during the early stages of deposition and that there is a critical amount of time required for the diamond to nucleate into a film of sufficient quality or thickness to be detected. The nucleation time appears to be dependent on, or at least influenced by, the laser wavelength. Previous studies found that using the tuned wavelength affected the growth of the diamond films where the main improvement was in the grain size, but there was little indication that the film nucleation would also be affected [17, 21].

Micro-Raman spectroscopy was used to further characterize the deposited films. The Raman spectra from the as-deposited films are shown in Fig 2. After 1 minute of deposition the Raman spectra (Fig 2(a)) varied with the laser condition. The spectra from the film deposited without the laser and with the tuned laser were typical of a material with a small grain size (~10 nm) [23]. There were pronounced G-bands located near 1600 cm^{-1} associated with a significant amount of amorphous, graphitic carbon phase in the films. In the spectra from the film deposited with the standard 10.591 μm CO_2 laser wavelength, there were pronounced D and G peaks located at 1326 and 1585 cm^{-1}, respectively. The spectrum closely resembles that of nanocrystalline graphite which has

D and G peaks at 1350 and 1582 cm^{-1}, respectively [24], but the D peak was shifted to a lower wavenumber closer compared to that of diamond (1332 cm^{-1}). For that reason the films likely have graphitic and diamond components. There was also an upshift in the location of the D peak depending on the laser condition. Specifically, the D peak increased from 1323 cm^{-1} from the film when no laser was used to 1329 cm^{-1} from the film when the tuned laser was used. The shift in the D peak may indicate that the film deposited with the tuned laser was of a higher quality compared to the other films or that the particles sampled by the Raman laser were in a different stress state [25]. There was a squared-shoulder at approximately 1100 cm^{-1} in the spectra from the film deposited with the tuned laser that has been attributed to nanocrystalline diamond [26]. The Raman spectra for the films deposited for 2 minutes are shown in Fig 2(b). The first-order Raman peak from diamond was much more apparent, though still relatively broad and the G band from the graphitic species was reduced but still observable. Similar to the films deposited for 1 minute, the D peak location increased from 1322 to 1329 to 1332 cm^{-1} when the laser condition was changed from no laser to untuned to the tuned laser condition. When the deposition time was increased to 5 minutes the Raman spectra (Fig 2(c)) appeared similar to the spectra from the films deposited for 2 minutes though the diamond Raman signal was relatively sharper. The peak shift trend seen in the other deposition times was not apparent at 5 minutes. As with the 2 minute deposition times, the 10.532 μm tuned laser condition produced the sharpest and most intense diamond peak. The Raman results provided more evidence that the addition of the tuned laser irradiation reduced the film nucleation time.

The surface morphology of each film was examined using SEM. Representative images from the films deposited for 1, 2 and 5 minutes are shown in Fig 3, 4 and 5, respectively. Each figure contains an image from a film deposited without the laser irradiation and in the untuned and tuned laser condition. The films deposited for 1 minute consisted of discrete, faceted particles (crystallites) surrounded by a cobalt-rich phase, which was confirmed by energy dispersive spectroscopy (EDS). The crystallite shape was consistent despite the changing deposition parameters and exhibited {111} facets. The size of the crystallites was less than 100 nm when no laser was used (Fig 3(a)); approximately 100 nm in the untuned laser condition (Fig 3(b)); and nearly 300 nm in the tuned laser condition (Fig 3(c)). The crystallite size increase was in agreement with previous findings [17, 21]. The cobalt-rich phase has been previously shown to occur during the initial growth stages [27]. When the deposition time was increased to 2 minutes the films were more continuous. The images from the films deposited without laser irradiation (Fig 4(a)) and in the untuned condition (Fig 4(b)) show some faceted particles on top of or surrounded by rounded non-faceted material. The image of the film deposited in the tuned laser condition (Fig 4(c)) shows overgrown, faceted crystals. It should be noted that the amount of faceted material as well as the grain size increased when the deposition conditions transitioned from using no laser (~100 nm) to the untuned laser (250 nm) to the tuned laser (1000 nm). The evolution of the cobalt binder particles (the smaller, lighter and rounded particles) on the faceted particles is a known byproduct from usage of the cemented carbide substrate [27-29]. The films deposited for 5 minutes were the most continuous and diamond-like in appearance. The film deposited without the laser had grain sizes of 0.5-1 μm (Fig 5(a)). The grain size increased to 1 μm with

the use of the untuned laser (Fig 5(b)) and further increased to more than 2 μm when in the tuned laser condition (Fig 5(c)). The SEM results suggested that the addition of the laser irradiation to the flame, but not the substrate, decreased the nucleation time and lead to predominantly grain growth as opposed to nucleation.

A cross-sectional investigation of the film microstructure was conducted using STEM. Details of the sample preparation were previously reported [17, 30]. Dark-field (DF) STEM images from the films deposited for 1 and 5 minutes are shown in Fig 6 and 7. The cross-section of the film deposited without laser irradiation shown in Fig 6(a) was consistent with the plan view SEM images in that discrete, faceted particles were evident. The particles ranged from 100 to 250 nm in diameter. The somewhat rounded edges of the crystallites are believed to be caused by the ion milling required to thin the sample to electron transparency. When the laser was added in the untuned condition the microstructure consisted of slightly larger (~300 nm) and more faceted discrete particles (Fig 6(b)). The crystallite size of the film deposited with the tuned laser shown in Fig 6(c) was larger (400 to 500 nm) than the films deposited in the other laser conditions. When the deposition time was increased to 5 minutes the crystallite size increased regardless of the laser condition. When no laser was used (Fig 7(a)) discrete particles nearly 1.5 μm could be seen. The grains showed a lamellar structure, only seen previously in much thicker films [31]. The film deposited with the untuned laser, shown in Fig 7(b), was thicker than the film deposited without the laser. The microstructure appeared to also have the lamellar features though the grains were more columnar in shape. When the tuned laser was used the film did not appear substantially thicker (Fig 7(c)) though the microstructure exhibited more columnar grains. The lamellar features

present in the other films were not as prevalent in this film. The STEM investigation revealed a transition from irregular to columnar grain growth with the addition of the untuned laser and the tuned laser, respectively.

An explanation of the nucleation and initial growth stages of the diamond thin films can be discussed using work from Kajikawa and Noda [32]. First consider the probabilities of the following processes that affect the nucleation time: the film growth species adsorbing directly onto the substrate, onto already deposited material, or desorbing from the substrate. The XRD and Raman investigations suggested that the nucleation time decreased for the film deposited with the tuned laser wavelength. The SEM and STEM images show that there are larger crystallites with the tuned laser, but it is difficult to discern the effects on the film nucleation. However, the differences in the grain size can be explained by examining the relative sticking probabilities of the growth species. The relative sticking probability is the ratio of growth species adsorbing to the substrate surface versus those sticking directly to adatoms (direct impingement). It was possible that the CH-wagging vibrational mode caused by the tuned laser resulted in species that were orientated such that the sticking probability for direct impingement was increased. The increase in direct impingement then results in larger grain sizes.

Ling *et.al* have shown that the absorbed energy from the 10.532 μm tuned CO_2 laser wavelength could be directed to C-H bonds [21] causing the generation of CH and C_2 species active in diamond deposition [16]. It follows that the probability of the CH and C_2 species adsorbing to the growing carbon film is higher than the probability of the specie nucleating on the WC substrate surface.

4. Conclusion

Nucleation and the initial growth stages of diamond thin films deposited by a CO_2 laser-assisted combustion-flame method were characterized. The investigation focused on the effect of the CO_2 laser wavelength and deposition time on the film surface morphology, the as-deposited chemical species and film microstructure. It was determined that regardless of the laser condition (no laser, untuned or tuned) as the deposition time increased the films transitioned from discrete and faceted crystallites to continuous films. The grain size increased from as small as 100 nm at 1 minute to as large as 2 μm at 5 minutes. X-ray diffraction and Raman spectroscopy revealed that the diamond phase was only significant after 2 minutes of deposition. At each deposition time comparisons were made between the two different laser wavelengths. When the films were deposited with the laser wavelength tuned to match the CH_2-wagging vibrational mode of the C_2H_4 molecule, the grain size was generally twice as large, the diamond (111) x-ray diffraction peak intensity increased and the diamond Raman peak was sharper and more intense. The increased grain size was attributed to tuned laser increasing the sticking probability of growth species onto adatoms on the substrate surface. There was a noticeable change in growth mechanism of the films which was dependent on the laser condition. When no laser irradiation was used during deposition there was nucleation of a sub-layer of smaller grains followed by irregular grain growth. The use of the untuned laser wavelength yielded nucleation of a sub-layer followed by columnar grain growth. The tuned laser wavelength appeared to induce nucleation and growth of columnar grains directly from the substrate surface. The transition of the growth mode was attributed to the changing the orientation of gaseous precursors such

that the sticking probability was increased. Overall the results confirmed previous findings that diamond growth can be enhanced with the use of laser energy coupling.

Acknowledgments

This work was financially supported by the U.S. Office of Naval Research (ONR) through the Multidisciplinary University Research Initiative (MURI) program under the advice and guidance of Dr. I. Perez. The assistance of Dr. Eric Bohannon with XRD and Dr. Ming Zhang with FIB/STEM from the Materials Research Center at Missouri University of Science and Technology is gratefully acknowledged.

References

[1] D.M. Gruen, Annu. Rev. Mater. Sci. 29 (1999) 211-259.

[2] K. Kurihara, K. Sasaki, M. Kawarada, N. Koshino, Appl. Phys. Lett. 52(6) (1988) 437-438.

[3] Y. Liou, R. Weimer, D. Knight, R. Messier, Appl. Phys. Lett. 56(5) (1990) 437-439.

[4] D. Rats, L. Vandenbulcke, R. Herbin, R. Benoit, R. Erre, V. Serin, J. Sevely, Thin Solid Films 270(1-2) (1995) 177-183.

[5] L. Wang, J. Lu, Q. Su, N. Wu, J. Liu, W. Shi, Y. Xia, Mater. Lett. 60(19) (2006) 2390-2394.

[6] Q. Yang, C. Xiao, W. Chen, A. Hirose, Diam. Relat. Mater. 13(3) (2004) 433-437.

[7] M. Noda, A. Marui, T. Suzuki, M. Umeno, Diam. Relat. Mater. 14(11-12) (2005) 1757-1760.

[8] K. Suzuki, A. Sawabe, H. Yasuda, T. Inuzuka, Appl. Phys. Lett. 50(12), (1987) 728-729.

[9] E.B.D. Bourdon, P. Kovarik, R.H. Prince, Diam. Relat. Mater. 2(2-4) (1993) 425-431.

[10] D.K. Mishra, X. Tian, T. Soga, T. Jimbo, M. Sharon, Jpn. J. Appl. Phys. 42(Part 2, No. 10A) (2003) L1164-L1166.

[11] Y. Hirose, S. Amanuma, K. Komaki, J. Appl. Phys. 68(12) (1990) 6401-6405.

[12] M.A. Cappelli, P.H. Paul, J. Appl. Phys. 67(5) (1990) 2596-2602.

[13] W. Carrington, L. Hanssen, K. Snail, D. Oakes, J. Butler, Metall. Mater. Trans. A 20(7) (1989) 1282-1284.

[14] H.S. Shin, D.G. Goodwin, Appl. Phys. Lett. 66(21) (1995) 2909-2911.

[15] T. Le Huu, H. Zaidi, D. Paulmier, Thin Solid Films 308-309 (1997) 147-153.

[16] H. Ling, J. Sun, Y.X. Han, T. Gebre, Z.Q. Xie, M. Zhao, Y.F. Lu, J. Appl. Phys. 105(1) (2009) 014901-014905.

[17] T. McKindra, M.J. O'Keefe, Z.Q. Xie, Y.F. Lu, Mater. Charac. 61 (2010) 661-667.

[18] Y.X. Han, H. Ling, J. Sun, M. Zhao, T. Gebre, Y.F. Lu, Appl. Surf. Sci. 254(7) (2008) 2054-2058.

[19] Y.X. Han, M. Zhao, J. Sun, H. Ling, T. Gebre, Y.F. Lu, Appl. Surf. Sci. 254(5) (2007) 1423-1426.

[20] H. Ling, Y.X. Han, Y.F. Lu, Proc. SPIE 6459 (2007) 64590Y-1-64590Y-7.

[21] H. Ling, Z.Q. Xie, Y. Gao, T. Gebre, X.K. Shen, Y.F. Lu, J. Appl. Phys. 105(6) (2009) 064901-064906.

[22] T. Gebre, J. Sun, H. Ling, Y.X. Han, M. Zao, Y.F. Lu, Proc. SPIE 6880 (2008) 68800O-1-68800O-7.

[23] S.M. Huang, Z. Sun, Y.F. Lu, M.H. Hong, Surf. Coat. Technol. 151-152 (2002) 263-267.

[24] G. Irmer, A. Dorner-Reisel, Adv. Eng. Mater. 7(8) (2005) 694-705.

[25] N.G. Ferreira, E. Abramof, N.F. Leite, E.J. Corat, V.J. Trava-Airoldi, J. Appl. Phys. 91(4) (2002) 2466-2472.

[26] A. Kromka, J. Breza, M. Kadlečíková, J. Janík, F. Balon, Carbon 43 (2005) 425-429.

[27] R. Polini, F. Le Normand, G. Marcheselli, E. Traversa, J. Am. Ceram. Soc. 82(6) (1999) 1429-1435.

[28] J.B. Donnet, D. Paulmier, H. Oulanti, T. Le Huu, Carbon 42(11) (2004) 2215-2221.

[29] G. Cabral, N. Ali, E. Titus, J. Gracio, J. Phase Equilib. Diffus. 26(5) (2005) 411-416.

[30] R. Wirth, Chem. Geol. 261 (2009) 217-229.

[31] L. Vandenbulcke, M.I. De Barros, Surf. Coat. Technol. 146-147 (2001) 417-424.

[32] Y. Kajikawa, S. Noda, Appl. Surf. Sci. 245 (2005) 281-289.

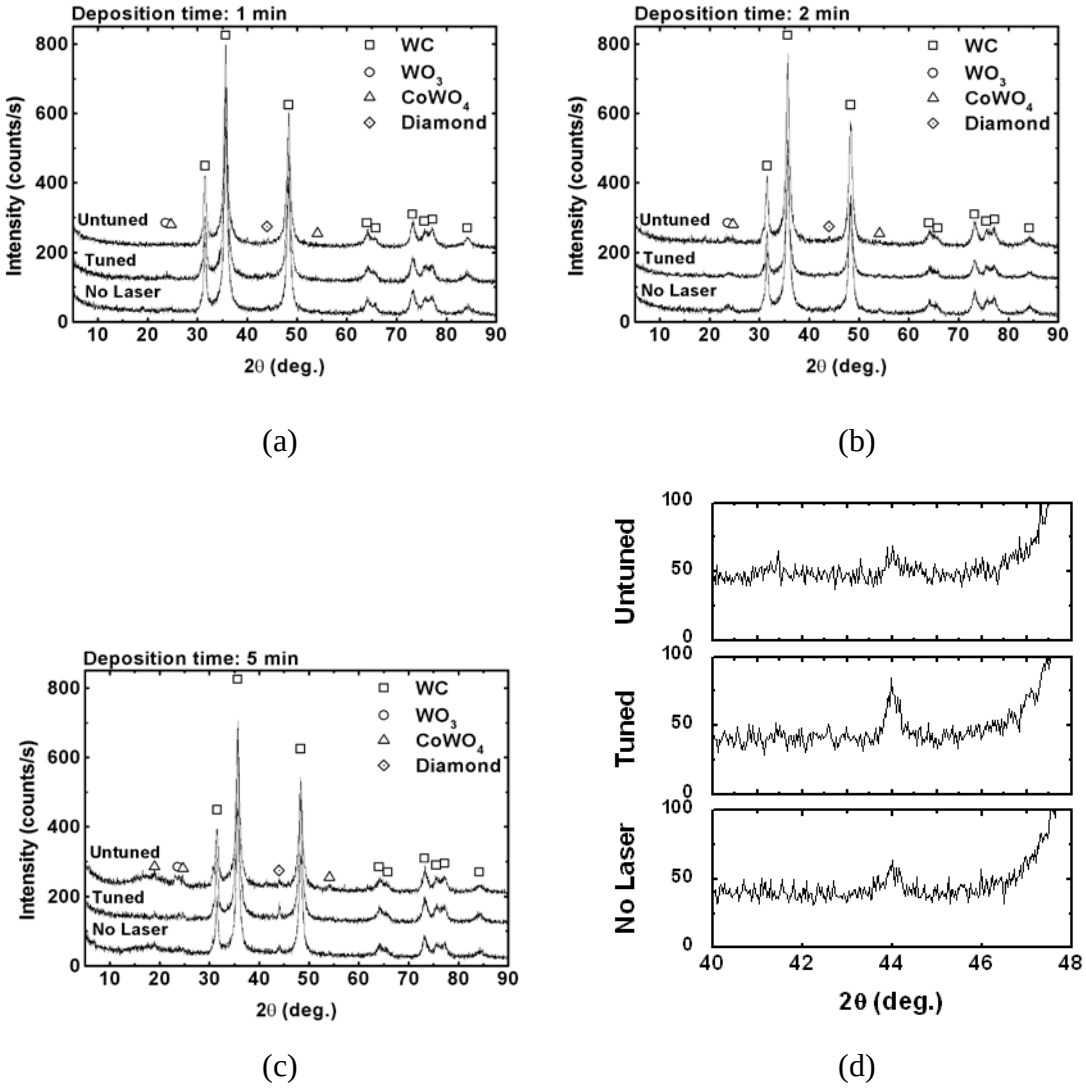

Fig. 1. XRD spectra from films deposited for (a) 1, (b) 2, (c) 5 minutes with (d) 2θ range associated with diamond (111) planes from films deposited for 5 minutes.

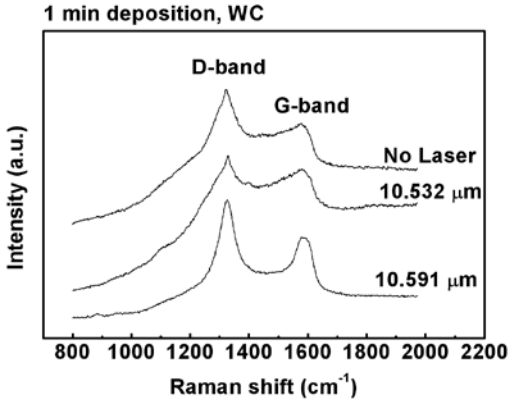

(a)

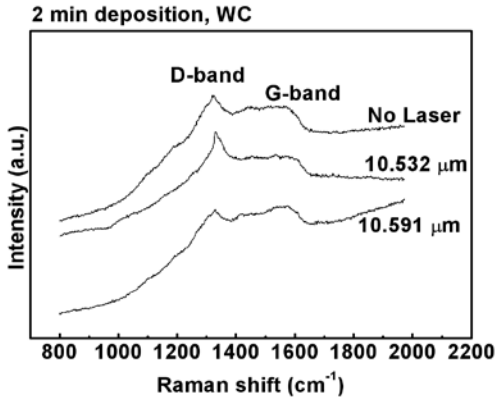

(b)

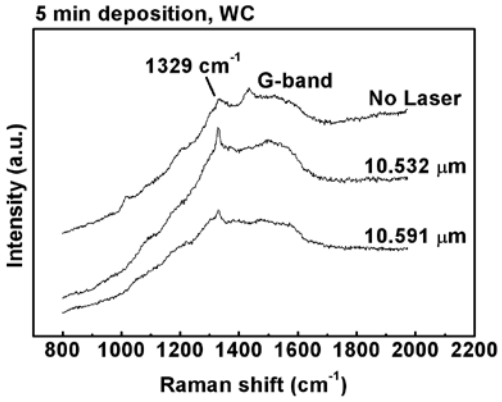

(c)

Fig 2. Comparison of Raman spectra from films deposited (a) 1, (b) 2 and (c) 5 minutes.

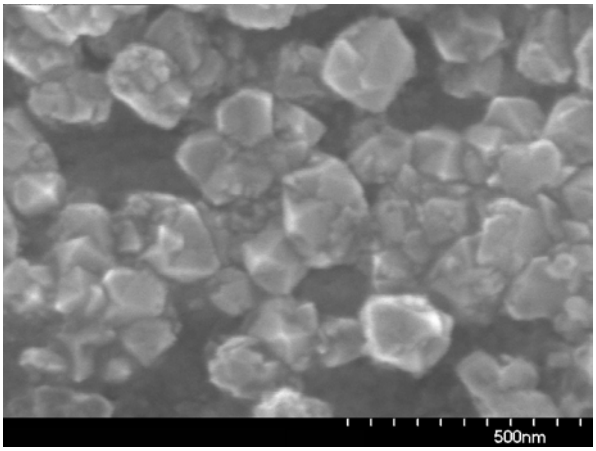

(a)

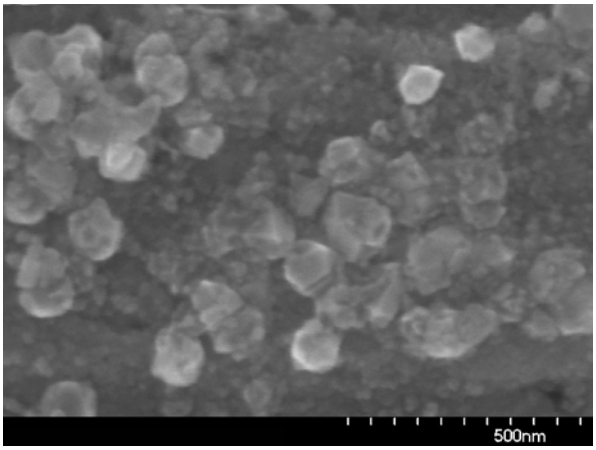

(b)

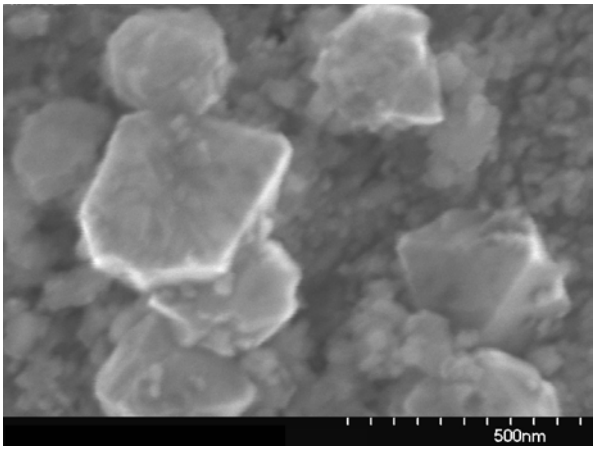

(c)

Fig 3. SEM micrographs from the center of films deposited for 1 minute with (a) no laser irradiation, (b) untuned laser irradiation and (c) tuned laser irradiation.

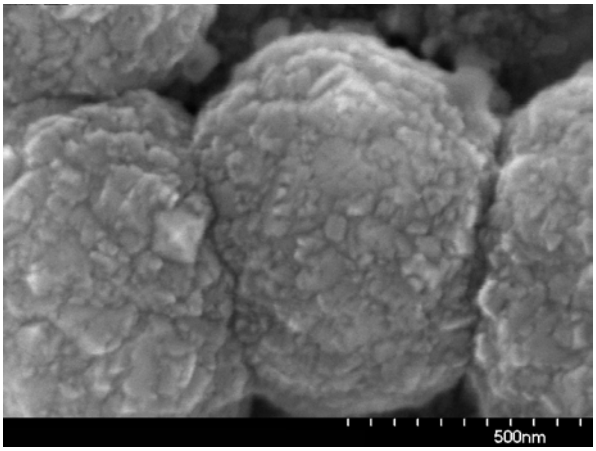

(a)

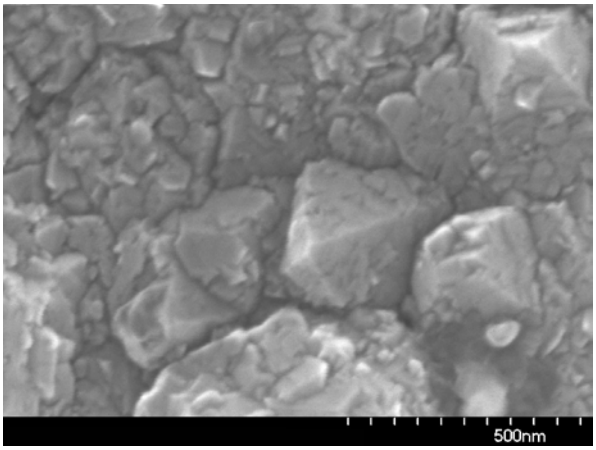

(b)

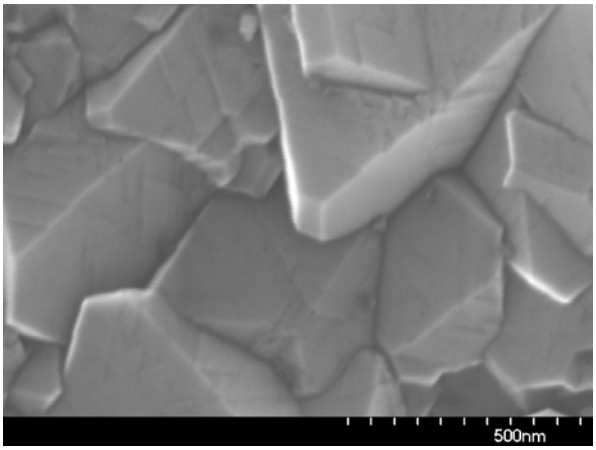

(c)

Fig 4. SEM micrographs from the center of films deposited for 2 minutes with (a) no laser irradiation, (b) untuned laser irradiation and (c) tuned laser irradiation.

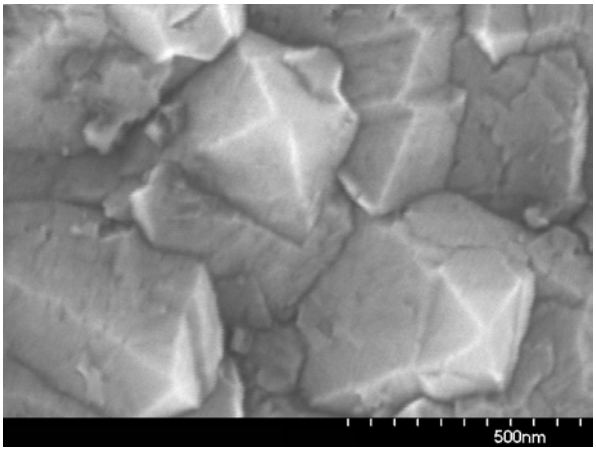

(a)

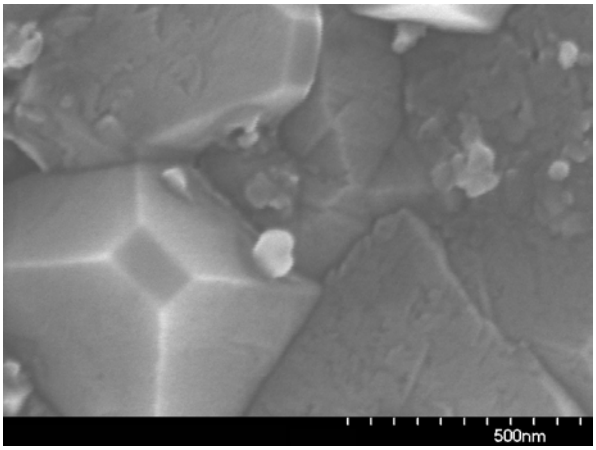

(b)

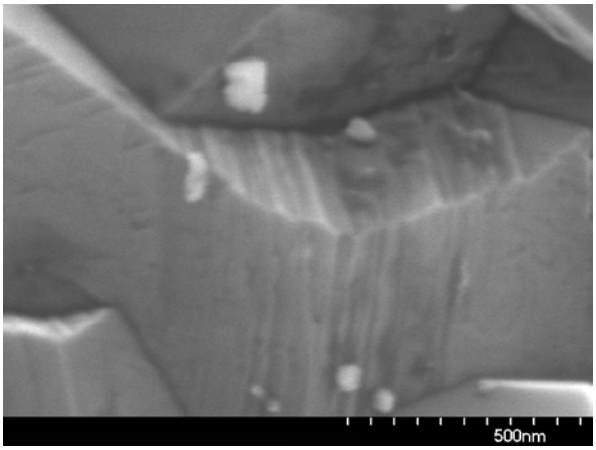

(c)

Fig 5. SEM micrographs from the center of films deposited for 5 minutes with (a) no laser irradiation, (b) untuned laser irradiation and (c) tuned laser irradiation.

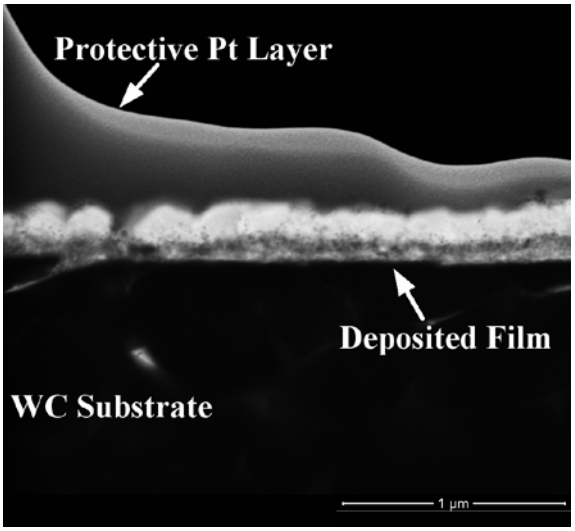

(a)

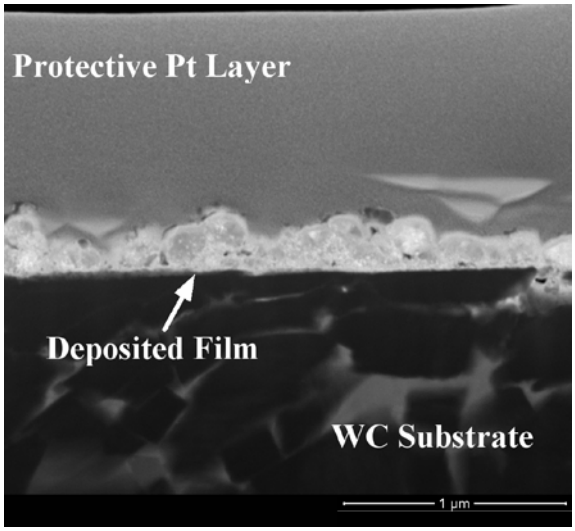

(b)

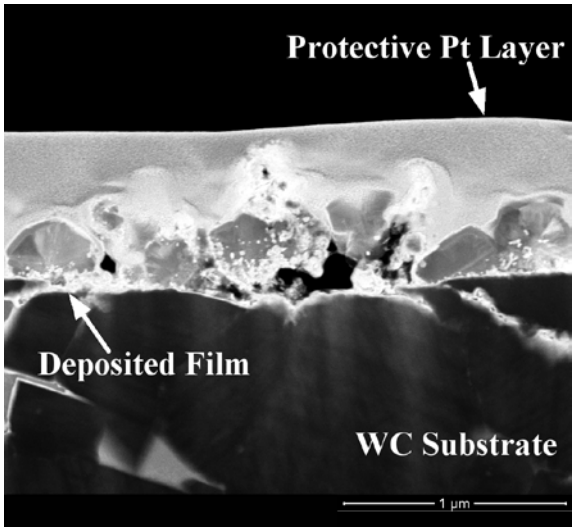

(c)

Fig 6. Dark-field STEM images from cross-sections of diamond films deposited for 1 minute with (a) no laser, (b) untuned and (c) tuned laser irradiation

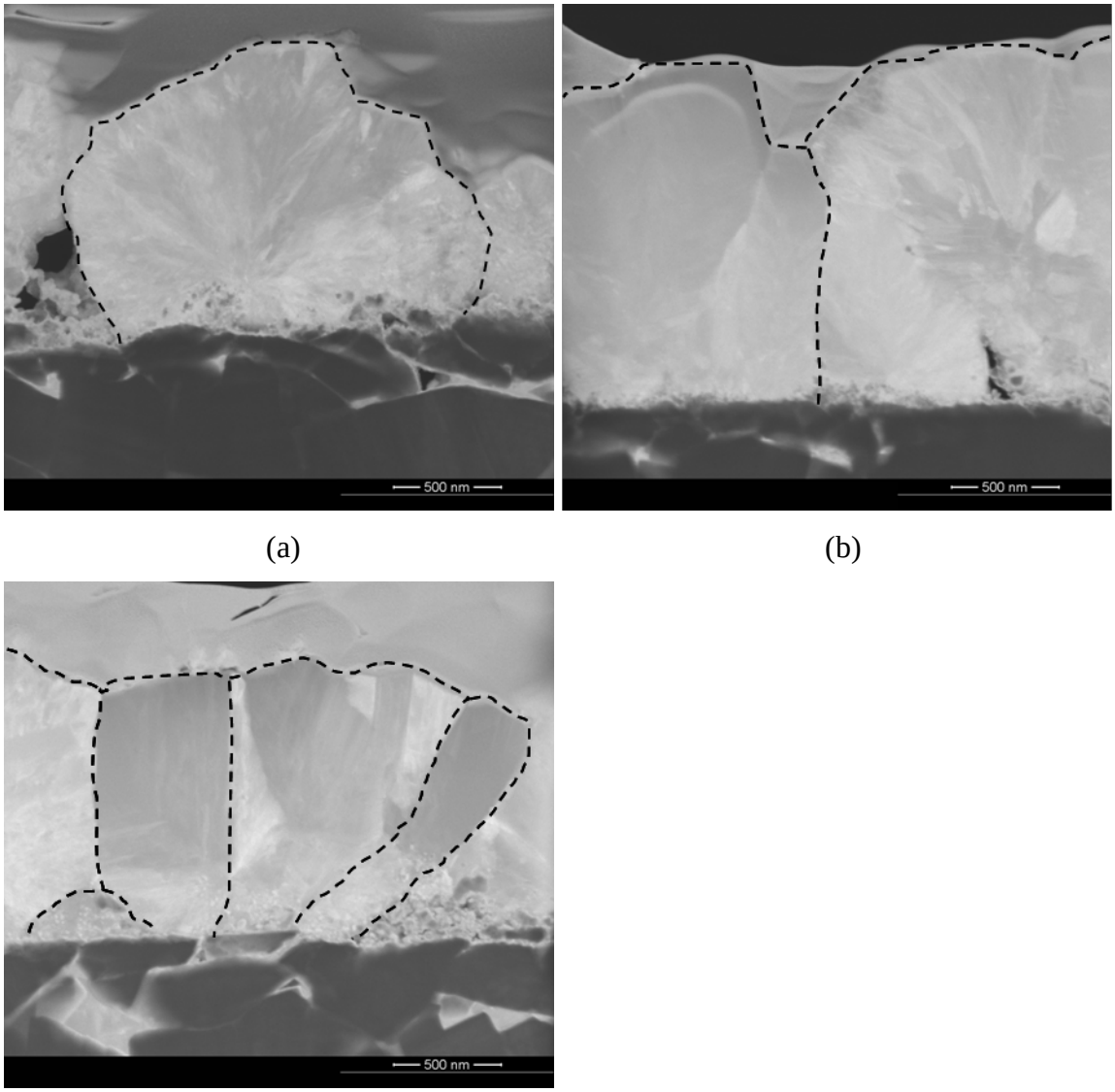

(a) (b)

(c)

Fig 7. Dark-field STEM images from cross-sections of diamond films deposited for 5 minutes with (a) no laser, (b) untuned and (c) tuned laser irradiation. Some individual grains have been outlined for clarity.

2. SUMMARY AND CONCLUSIONS

The addition of a CO_2 gas in the sputter-deposition process of amorphous carbon has not been previously reported and was found to affect the crystallinity surface morphology and bonding arrangement of the thin films. A comparison of the reactive gases of O_2 and CO_2 showed many similarities, but also some differences. In general, the deposition rate decreased with an increase in the partial pressure of either reactive gas. The decrease was attributed to the reaction of oxygen or carbon dioxide with the sputtered graphite while still in the vapor phase or even after deposition on the substrate surface. The deposition rate was higher when CO_2 was used, most likely due to O_2 being the more reactive species. The surface chemistry results showed that indeed a reaction between the graphite species and the reactive gas did occur as oxygen was detected on the surface of the films. As the partial pressure of reactive gas in the plasma increased, the amount of oxygen detected in the films increased up to a point and then the amount detected decreased. The trend suggested that there was a saturation limit for the amount of oxygen in the graphite films. The characterization results revealed that the oxygen affected the deposition and growth of the amorphous carbon thin films. Sputtered carbon films from a graphite target using a noble gas were amorphous when deposited at room temperature. There was a consistent trend with the films with CO2 or O2 in the sputtering gas that the increasing oxygen content enhanced the long-range order in the films while suppressing the more amorphous species.

Samples produced at UNL were characterized and analyzed. The samples included films deposited by the CO_2 laser-assisted combustion-flame chemical vapor deposition (CVD) process in open atmosphere. The concept of multi-energy processing was investigated by coupling the energy from CO_2 laser irradiation with the combustion flame.

For example, the graphite pillars deposited on WC substrates in open atmosphere used a novel deposition technique utilizing a C_2H_2/O_2 combustion-flame combined with CO_2 laser irradiation perpendicular to the substrate surface. The deposition rate, 750 μm/minute, was very high for a crystalline material deposited under ambient conditions. The microstructure was unaffected by the amount of laser power. Increased laser power

caused a shape change in the pillar, producing a depression near the nucleation site. Additional efforts to investigate the laser effect on substrate and thus the nucleation of the films leading to the high deposition rate would be beneficial. An understanding of the growth mechanism may allow for the application of this process to other materials systems.

Diamond thin films were deposited on WC substrates by a CO_2 laser-assisted $O_2/C_2H_2/C_2H_4$ combustion-flame method in which the laser was focused on the tip of inner cone of the flame, parallel to the substrate surface. With a tunable CO_2 laser, the laser wavelength could be tailored to affect specific species in the combustion-flame. Subsequent characterization of the deposited films determined the effect of the CO_2 laser wavelength and power on the film surface morphology, phase, crystallinity and microstructure. It was determined that for a given wavelength, when the laser power was increased the grain size increased, the diamond X-ray diffraction peak was more intense and the characteristic diamond Raman peak was sharper and more intense. In general, the film grain size was twice as large and the diamond diffraction peak intensity increased and sharpened when the films were deposited with 10.532 μm CO_2 laser wavelength tuned to the CH_2-wagging vibrational mode of the C_2H_4 molecule when compared with the films deposited with an untuned 10.591 μm CO_2 laser wavelength. Overall the results indicated the addition of the laser beam parallel to the substrate surface and coupled to the combustion-flame enhanced diamond film growth, a result not previously reported.

Knowing that the effect of using the tunable CO_2 laser on the growth of the diamond films was very significant, the next issue was to determine how the laser affected the deposition process. It was difficult to determine whether the laser only affected the growth or if there was an effect on the nucleation of the diamond films. Nucleation and the initial growth stages of diamond thin films deposited by a CO_2 laser-assisted combustion-flame method were characterized. The investigation focused on the effect of the CO_2 laser wavelength and deposition time on the film surface morphology, the as-deposited chemical species and film microstructure. The diamond phase was measurable only after 2 minutes of deposition. At each deposition time comparisons were made between the two different laser wavelengths. When the films were deposited

with the laser wavelength tuned to match the CH_2-wagging vibrational mode of the C_2H_4 molecule, the grain size was generally twice as large as the untuned case. The increased grain size was attributed to tuned laser increasing the sticking probability of growth species onto adatoms on the substrate surface. There was a noticeable change in growth mechanism of the films which was dependent on the laser condition. When no laser irradiation was used during deposition there was nucleation of a sub-layer of smaller grains followed by irregular grain growth. The use of the untuned laser wavelength yielded nucleation of a sub-layer followed by columnar grain growth. The tuned laser wavelength appeared to induce nucleation and growth of columnar grains directly from the substrate surface. The transition of the growth mode was attributed to the changing the orientation of gaseous precursors such that the sticking probability was increased. Overall the results confirmed previous findings that diamond growth can be enhanced with the use of laser energy coupling directly into the flame.

Initially, the laser energy and the combustion flame were combined at the substrate which would have involved more of the substrate material in the deposition process. In subsequent experiments the laser was positioned parallel to the substrate surface meaning it only came in content with the combustion-flame. It stood to reason that a laser beam focused on the substrate surface would affect the nucleation and growth of a film, but it seemed less plausible that the laser interacting only with the combustion-flame would have a positive effect. That is one of the most significant findings of this work.

3. FUTURE WORK

Given the various applications of amorphous carbon and diamond-like carbon films, determining the properties of the oxygenated carbon thin films would be would be of interest. The studies on the reactive sputtering of oxygenated carbon thin films did not include any mechanical or optical properties. Qualitatively, the films were scratch resistant and very adherent to the silicon substrates, but quantitative values would be more telling. Determining the process by which the oxygen is retained in the carbon films may be essential in understanding how the microstructure is affected. Auger electron spectroscopy (AES) may be helpful in determining if the oxygen detected is as prevalent in the bulk of the film compared to the film surface. It was shown that the oxygen affected the bonding in the films, but films were all less than a 500 nm in thickness. An interesting study would be to determine if there is film thickness dependence on the phenomena seen thus far. The XRD results suggested that the films had a very small grain size, but were not completely amorphous. Using TEM would allow for a better determination of the crystallinity of the films.

The diamond films were deposited on WC and Si and the film microstructure was slightly different. It would be interesting to investigate the films on a wider range of substrates to determine the effect of the substrate on the nucleation and growth of the films. The studies on the films deposited for shorter times showed predominantly carbonaceous crystallites, but the Raman results were inconclusive. Further characterization is required and would include TEM for the purpose of electron diffraction to determine the exact nature of the initial nuclei. It may yield answers to the nature of the sub-layer grains seen in some of the diamond films as well as to whether the laser energy affects the location of the film nucleation. One question that remains to be answered: Are the precursor species combining in the gas phase and adsorbing on the substrate surface as diamond or are there initial non-diamond growth species adsorbing and acting as nuclei for diamond growth? The effect of the excitation of the C_2H_4 molecules has undoubtedly enhanced the diamond deposition, but the reasons for the enhancement could be explored more fully. For example, the issue of the flame temperature during the deposition is of some concern. While the rotational flame

temperatures showed no temperature increase, the fact that the flame burns brighter seems an indicator of an increase in temperature. Additionally, some of the microstructural changes such as the larger grain size and faster nucleation time seem to indicate that the reaction kinetics are faster with the tuned CO2 laser wavelength which may be temperature related. The researchers at UNL have studied various CO_2 laser wavelengths that match other vibrational modes and it would be interesting to view those films in cross-section and compare the results with the previous studies. In general, the mode-selective excitations of the gaseous precursors (C_2H_4, also C_3H_6) may yield many investigations. It would also be beneficial to determine the mechanical and optical properties of the diamond films.

APPENDIX A

DEPOSITION OF CARBON THIN FILMS IN Ar/CO_2

Sputter deposition of oxygenated carbon thin films in Ar/CO_2

Travis McKindra, Matthew J. O'Keefe

Department of Materials Science and Engineering, Missouri University of Science and Technology, Rolla, MO 65409, United States

Abstract

Carbon thin films were deposited by RF magnetron reactive sputtering of a graphite target in Ar/CO_2 plasmas. A variety of process conditions were used to investigate the effect of the CO_2 partial pressure on the film deposition. Film properties were characterized by glancing angle X-ray diffraction (XRD), X-ray photoelectron spectroscopy (XPS) and scanning electron microscopy (SEM). The deposition rate decreased steadily with an increasing partial pressure of CO_2 in the plasma. Increasing amounts of oxygen was retained in the films as the CO_2 partial pressure increased and evidence of C-O and C=O bonding was found. A nanocrystalline phase was apparent at certain partial pressures of CO_2 compared to films deposited without any CO_2 in the plasma. The film morphology transitioned from a typically amorphous topography to a granular topography similar to sputtered metallic films. The addition of oxygen via the Ar/CO_2 reactive sputtering gas enhanced the crystallinity of sputtered carbon thin films.

Experimental

The effect of CO_2 gas during reactive sputter deposition of carbon thin films was investigated. A full factorial experiment was designed where carbon films were deposited onto Si substrates (1 x 1 cm^2) by rf-sputtering of a graphite target using Ar plus 1, 3, 10, and 25% CO_2 gases at working pressures of 2, 5, and 10 mTorr. The depositions were run for approximately 2 hours at 300 W RF power. The CO_2 content was determined using the N_2-normalized flow rate of Ar to CO_2. The film thickness was measured with a Tencor Alpha-step 100 profilometer. The O_2 content referred to the percentage of the working pressure that was not Ar gas. Selected films were characterized by X-ray diffraction (XRD), X-ray photoelectron spectroscopy (XPS), and scanning electron microscopy (SEM). The deposition rate results were analyzed with MINITAB 14 Statistical Software.

Results and Discussion

Statistical analysis of the mean deposition rate of the films determined that both the working pressure and percentage of CO_2 in the sputtering gas had a significant effect. A contour plot from the statistical software (MINITAB) is presented in Figure 1. In general, the trend was that as the percentage of CO_2 and working pressure increased, the deposition rate decreased. The effect of the percentage of CO_2 on the deposition rate for a given working pressure is shown graphically in Figure 2. Films deposited at 2 mTorr showed the least amount of change in the deposition rate with increased CO_2 in the sputtering gas. The mean deposition rates of the films with 1% and 3% CO_2 at 2 mTorr were not statistically different as determined by analysis with MINITAB. Alternatively,

the films with 10% and 25% CO_2 were statistically different and showed a decrease in deposition rate with increased CO_2 in the sputtering gas. At 5 mTorr the mean deposition rate decreased as the amount of CO_2 increased to the point (>10% CO_2) where little to no film was measured in the predetermined two hour deposition time. The deposition rate of films deposited at 10 mTorr showed a similar trend in that no measurable deposition occurred with more than 3% CO_2 in the sputtering gas. The inability to deposit a film was indicative of a very slow sputter rate. The slow rate was attributed to poisoning of the target surface and the difficulty of ionizing the CO_2 in the plasma of the sputter deposition system. This caused problems during replications of the depositions at lower CO_2 percentages and required cleaning of the graphite target in pure Ar prior to reactive sputtering with the CO_2. From these results, it was determined that the absolute amount of CO_2 in the sputtering gas was the critical parameter in affecting the deposition rate.

X-ray photoelectron spectroscopy was used to determine the binding state of the atoms in and the chemical make up of the deposited films. It has been reported that the sp^3 and sp^2 components can be delineated from the spectra of amorphous carbon films [1]. The binding energy of the sp^3 species is shifted to approximately one eV higher binding energy with respect to the sp^2 content [2]. Figure 3 shows the comparison between the C 1s spectra for the selected samples as well as the spectra for graphite sputtered in pure argon. Table 1 summarizes the peak values for the components of each spectrum. The XPS spectra for all of the samples exhibited a major peak centered at 285 eV indicative of graphite or sp^2 bonding, as well as definitive minor peaks at higher binding energies. The C 1s spectra from the films deposited with 1% and 25% CO_2 at 2 mTorr exhibited only two peaks. The C 1s spectra from films deposited with 3% CO_2 at

10 mTorr and 10% CO_2 at 5 mTorr were fitted with three peaks. The highest peak for both samples, 288.6 eV and 288.7 eV respectively, was attributed to the C=O bond [3, 4]. The second peak for both samples, 286.8 eV and 286.9 eV, was attributed to the C-O bond [3-5]. It was expected that the C=O bond would produce an C 1s electron with a higher binding energy since atoms with a higher positive oxidation state exhibit higher binding energy due to the extra coulombic interaction between the photo-emitted electron and the ion core. However, it was unexpected that C=O was found. The C=O bonding found in the XPS spectra was attributed to non-dissociated CO_2 in the plasma that caused C=O species to embed in the film.

Table I: Summary of peaks for selected samples.

Sample	Species	Peak Location (eV)	Half Width Half Max (eV)	% Total Area
Ar only	C-C	285	0.7	81.3
	C-O	286.2	0.6	18.7
1% CO_2, 2 mTorr	C-C	285	0.8	84.18
	C-O	286.7	0.7	15.82
3% CO_2, 10 mTorr	C-C	285	0.9	63.3
	C-O	286.8	0.8	19.78
	C=O	288.6	1.0	16.92
10% CO_2, 5 mTorr	C-C	285	0.9	64.95
	C-O	286.9	0.9	21.78
	C=O	288.7	0.9	13.27
25% CO_2, 2 mTorr	C-C	285	0.8	87.75
	C-O	286.3	0.6	12.25

Given the unexpected C=O species detected by XPS, x-ray diffraction (XRD) at a glancing angle was used to determine the crystallinity and phase identification of the selected films. XRD samples were deposited concurrently with the samples used to determine the deposition rate and XPS samples. Figure 4 shows the summary of the

XRD results. The films were predominantly amorphous though there were some broad peaks, highlighted by arrows, which suggested there might have been some crystallinity. The peaks most closely matched graphite, though shifted to higher 2θ values from the standard for graphite (JCPDF # 75-1621). The spectrum from the sample deposited at 2 mTorr and 1% CO_2 showed only one broad peak at approximately 28° near the graphite (002) peak. The remaining samples did not have the low angle peak, but a broad peak at approximately 48° close to the graphite (101) peak. The XRD results suggest that the addition of the oxygen, via the CO_2 gas, to the plasma enhanced the crystallinity of the films and this was in agreement with the literature [6, 7].

The scanning electron microscope (SEM) was used to investigate the morphology of the sputtered films to explain the features from the XRD spectra. The features from the spectra could have been interpreted as broad amorphous humps or nanocrystalline and, as such, it was expected that the films would show minimal surface features, but that was not the case. The surface morphology changed with the change in CO_2 content. As the CO_2 content in the sputtering gas increased there was an increase in the observed grain structure of the films. The SEM images are shown in Figure 5. Figure 5(a) shows the film deposited at 2 mTorr with 1% CO_2 had the fewest surface features (least granular). Figures 5(b), 5(c) and 5(d) show the films deposited with increasing amount of CO_2 respectively and a more crystalline grain structure. A correlation was drawn between the XRD and SEM results in that the broad peaks (crystalline features) in the XRD spectra were more prevalent when more CO_2 was added to the sputtering gas. It was theorized that the increased granular structure was due to etching of the amorphous carbon species by the free oxygen in the plasma.

Conclusions

Carbon thin films were reactively sputtered in an Ar/CO_2 gas mixture. The deposition rate decreased as the partial pressure of CO_2 increased due to target poisoning. X-ray photoelectron spectroscopy results showed variations in the C 1s spectra with respect to the amount of CO_2 in the process gas took the form of chemical states at higher binding energies than that of graphite. X-ray diffraction spectra of selected films exhibited predominantly amorphous features, though crystalline features, such as broad peaks slightly shifted to higher 2θ values, became evident with increased CO_2 used in the deposition. Scanning electron microscopy images of the films revealed an increasingly granular microstructure with the addition of CO_2 caused by etching of the amorphous species.

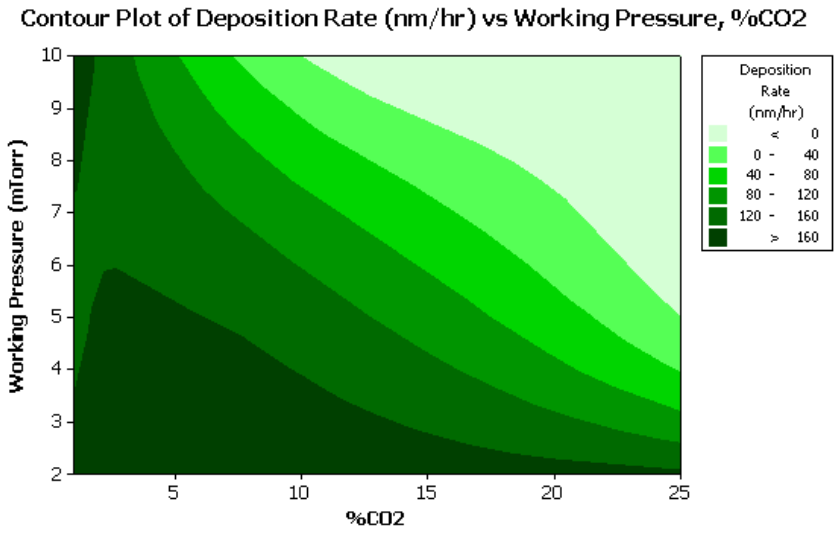

Figure 1: Contour plot of showing deposition rate (nm/hr) for a given working pressure and percentage of CO_2 gas.

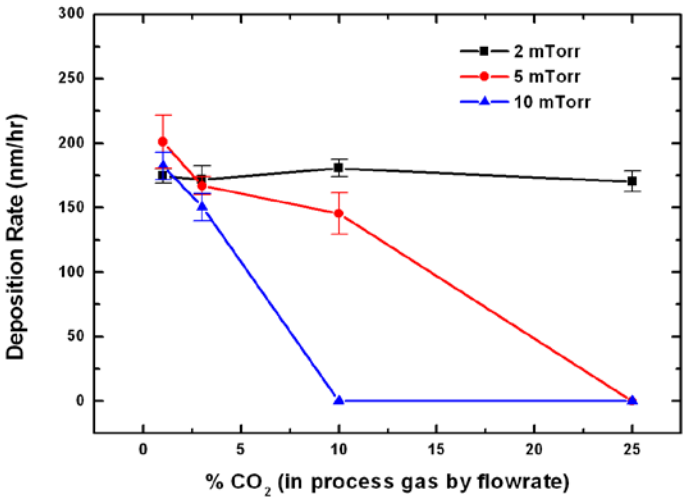

Figure 2: Plot of deposition rate versus percentage of CO_2 for a given working pressure.

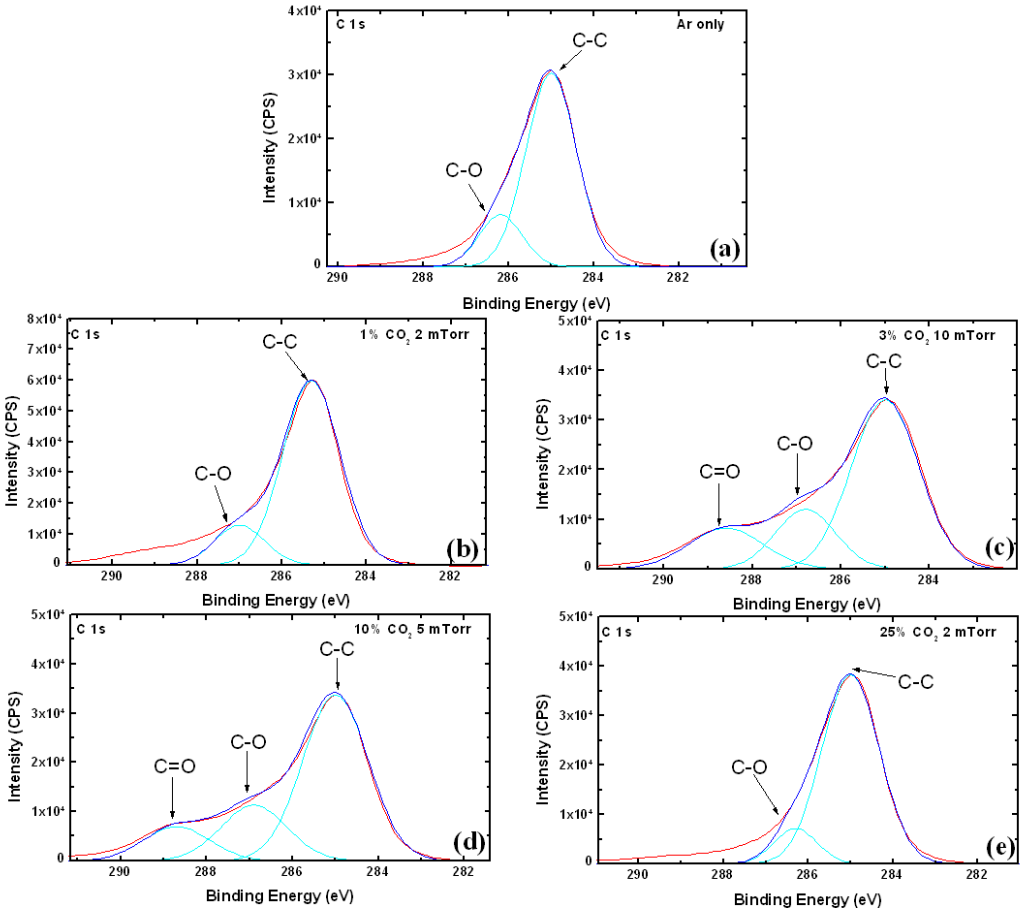

Figure 3: XPS spectra of selected samples sputter with (a) Ar only at 2 mTorr, (b) 1% CO_2 at 2 mTorr, (c) 3% CO_2 at 10 mTorr, (d) 10% CO_2 at 5 mTorr, and (e) 25% CO_2 at 2 mTorr.

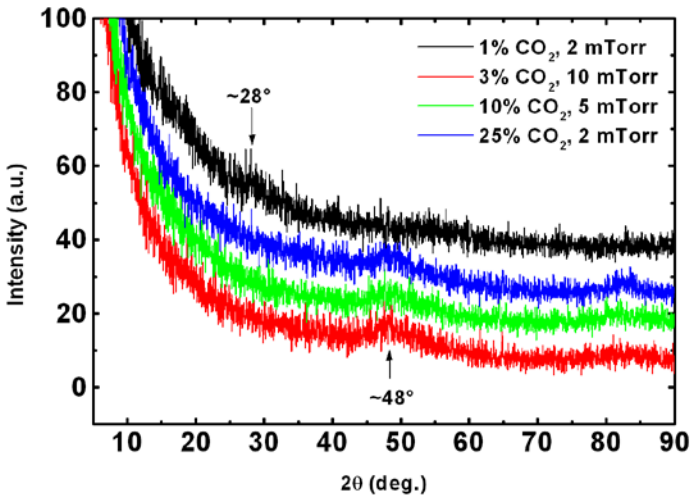

Figure 4: Comparison of XRD results for selected samples, which shows a predominantly amorphous structure. The crystalline features of the spectra are highlighted by arrows.

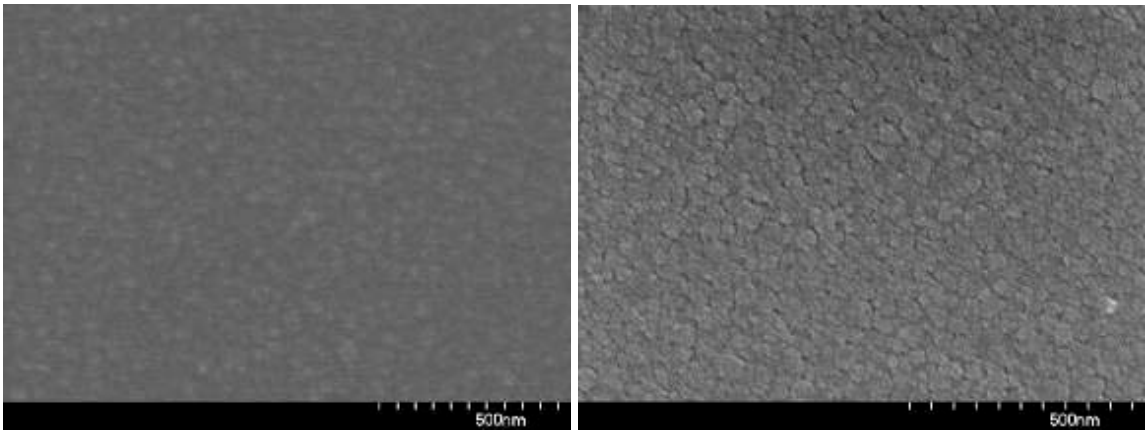

(a) (b)

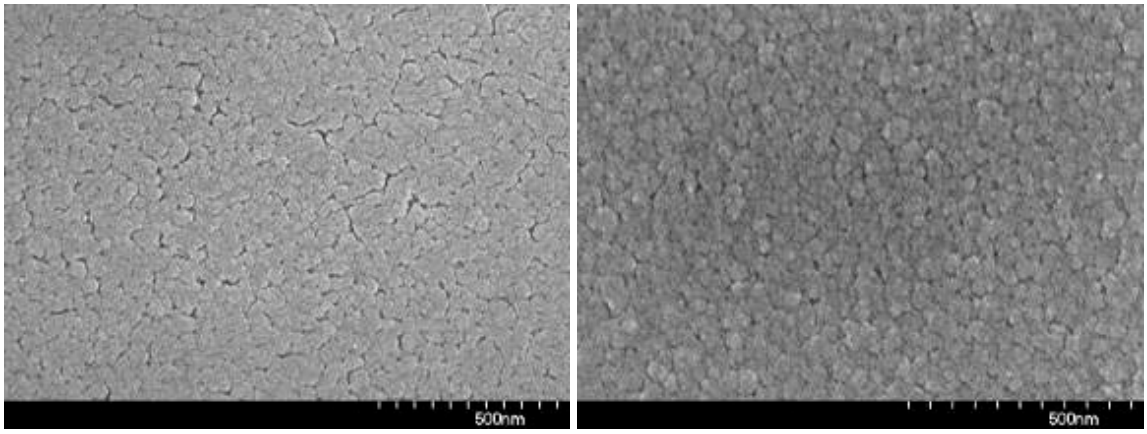

(c) (d)

Figure 5: Secondary electron SEM images for the selected samples (a) 1% CO_2-2 mTorr, (b) 3% CO_2-10 mTorr, (c) 10% CO_2-5 mTorr, and (d) 25% CO_2-2 mTorr.

References

[1] Díaz, J., G. Paolicelli, S. Ferrer, and F. Comin, Physical Review B, (1996) 54(11) 8064-8069.

[2] Mérel, P., M. Tabbal, M. Chaker, S. Moisa, and J. Margot, Applied Surface Science, (1998) 136(1-2) 105-110.

[3] Kowbel, W. and C.H. Shan, Carbon, (1990) 28(2-3) 287-299.

[4] Rats, D., L. Vandenbulcke, R. Herbin, R. Benoit, R. Erre, V. Serin, and J. Sevely, Thin Solid Films, (1995) 270(1-2) 177-183.

[5] Sumant, A.V., P.U.P.A. Gilbert, D.S. Grierson, A.R. Konicek, M. Abrecht, J.E. Butler, T. Feygelson, S.S. Rotter, and R.W. Carpick, Diamond and related materials, (2007) 16(4-7) 718-724.

[6] Ono, T., Y. Suda, M. Akazawa, Y. Sakai, and K. Suzuki, Japanese Journal of Applied Physics, (2002) 41 4651-4654.

[7] Chen, Z.Y., J.P. Zhao, T. Yano, and J. Sakakibara, Physical Review B, (2000) 62(11) 7581.

APPENDIX B

NUCLEATION AND INITIAL GROWTH OF DIAMOND THIN FILMS ON SILICON

Initial growth of diamond thin films deposited by a CO_2 laser-assisted combustion-flame method on silicon substrates

Travis McKindra[a], Matthew J. O'Keefe[a], Elizabeth Kulp[a], Zhiqiang Xie[b] and Yongfeng Lu[b]

[a]*Department of Materials Science and Engineering, Missouri University of Science and Technology, Rolla, MO 65409, United States*

[b]*Department of Electrical Engineering, University of Nebraska-Lincoln, Lincoln, NE 68588, United States*

Abstract

The deposition of diamond thin films on Si substrates using a CO_2 laser-assisted combustion-flame CVD process was investigated by comparing no laser and two different wavelengths for deposition times of less than 5 minutes. The CO_2 laser wavelength was varied based on the resonant absorption of laser energy by gaseous precursors ($O_2/C_2H_2/C_2H_4$), in particular 10.591 μm that did not match a resonant absorption (unturned) and 10.532 μm that matched one of the resonant frequencies of the C_2H_4 molecule (tuned). The film morphology and microstructure was characterized by scanning electron microscopy (SEM) and scanning transmission electron microscopy (STEM). After one minute of deposition the films consisted of discrete particles. The amount of faceting and particle size was found to be dependent on the laser wavelength. X-ray diffraction (XRD) and micro-Raman spectroscopy were used for phase identification. The diamond component in the films varied with the deposition time and laser wavelength. The largest diamond component and most faceted grains were

obtained using the tuned CO_2 laser regardless of time. The enhancement of the diamond growth with the tuned laser wavelength was attributed to an increase in the sticking probability of the precursors to adatoms on the substrate surface.

Introduction

The nucleation of the films deposited by the CO_2 laser-assisted $O_2/C_2H_2/C_2H_4$ combustion-flame method is not fully understood. Research suggests that in CO_2 laser-assisted combustion-flame deposited films greater than 4 μm thick, a sub-layer phase exists near the substrate surface that is microstructurally different than the diamond phase. The structure of the sub-layer phase may contain a graphitic component and is dependent on the CO_2 laser wavelength [17]. The origin of the sub-layer phase is unknown and has not been studied extensively, though it may be related to the substrate.

In this study diamond thin films 1 μm or less in thickness were deposited on Si substrates by a CO_2 laser-assisted combustion-flame method. Similarly to previous work [18], the objective was to use shorter deposition times in order to characterize the effect of the CO_2 laser wavelength on the nucleation and initial growth of diamond thin films. The substrate effects were also investigated.

Experimental

The experimental setup used to deposit the films was similar to those reported elsewhere [16-23]. The diamond films were deposited on silicon (100) substrates and placed on a water-cooled hollow brass block. The dimensions of the substrates were approximately 1 x 1 cm^2. The substrates were cleaned in a supersonic bath of acetone for 30 minutes prior to deposition, and then seeded with diamond powders with an average size of 0.25 μm. A commercial welding torch with a 1.2 mm nozzle diameter was secured normal to the surface of the WC substrate and used to generate an $O_2/C_2H_2/C_2H_4$ combustion flame. The $O_2/C_2H_2/C_2H_4$ gas ratio was held constant at 1200:620:620 sccm

by three mass-flow controllers (B7920V, Spec-Air Gases & Technologies). The inner cone of the flame was maintained at approximately 0.5 mm from the substrate surface. A continuous-wave tunable CO_2 laser (PRC Company) was focused, with a ZnSe convex lens, perpendicular to the combustion-flame and parallel to the Si surface approximately 2 mm from the Si substrate. Using this arrangement the laser interacted only with the flame. The temperature of the substrate was monitored by a pyrometer (OS3752, Omega Engineering, Inc.) and maintained at approximately 780°C. The deposition times were 1 and 5 minutes. The laser power was 800 W at both 10.591 and 10.532 μm wavelengths.

The surface morphologies and microstructures of the deposited films were characterized by scanning electron microscopy (SEM) with a Hitachi S-4700 field emission scanning electron microscope (FESEM). Phase identification of the films was investigated by X-ray diffraction (XRD) using a Philips X-Pert diffractometer in glancing angle mode with a Cu Kα source. Micro-Raman spectroscopy was conducted with a Horiba ARAMIS system. The Raman spectra were measured using the 632.8 nm wavelength of a He-Ne laser. The films were prepared for cross-sectional microstructure analysis by scanning transmission electron microscopy (STEM) with a focused-ion beam (FIB) using an FEI Helios NanoLab 600 FIB/FESEM. The film thickness was estimated from the cross-sectional STEM images.

Results and Discussion

After 1 minute of deposition the films appeared as dispersed particles on the Si substrate surface. There was not an appreciable difference in the size or dispersion of the particles depending on the laser condition. After 5 minutes there was a distinct circular

area of deposited material surrounded by an area of dispersed particles. Even though the substrates were seeded with diamond powder it is not clear how much of the powder remained on the substrate during the deposition due to the force of the combustion flame. X-ray diffraction (XRD) was used to determine what phases were present. The XRD pattern from the films deposited for 1 and 5 minutes are shown in Fig 1(a) and Fig 1(b), respectively. The inset shows the pattern in the diamond (111) 2θ range. After 1 minute of deposition there were visible diamond diffraction peaks from each laser condition that were equally intense. The patterns from the films deposited for 5 minutes had diamond (111) and (220) diffraction peaks. The peak intensity for the film deposited with the 10.591 μm laser wavelength was higher than that from the film deposited without any laser. The peak intensity was the highest for the film deposited with the 10.532 μm tuned laser wavelength. Unlike the films deposited on WC [18] the nucleation time did not appear to be affected by the laser wavelength. It may be due to the silicon substrate, though it is more likely due to the diamond seeding surface pretreatment.

The Raman spectra from the films are shown in Fig 2. The characteristic diamond peak at 1332 cm^{-1} was apparent in all of the spectra from the films deposited for 1 minute (Fig 2(a)). The spectrum from the film deposited without the CO_2 laser was similar to that of crystalline graphite due to the presence of the G-band [24]. No graphite was detected in the XRD, so it was possible that the film just had a significant graphitic component. The spectra from the laser-assisted films showed G-bands, though not as intense as when no laser was used. After Savitzky-Golay smoothing and background removal, further analysis of the spectra revealed that the FWHM of the diamond peak decreased from 80 to 60 to 14 cm^{-1} when the laser condition was changed from the no

laser to 10.591 μm tuned to 10.532 μm tuned, respectively. The decrease in the FWHM was an indication that the quality of the diamond sampled was better with the tuned laser wavelength. The Raman spectra from the films deposited for 5 minutes are shown in Fig 2(b). The characteristic diamond peak was present in all of the spectra and located near 1334 cm^{-1}. There was also a broad G-band in each spectrum resulting from graphitic components in the deposited films. Further analysis showed that the intensity increased while the FWHM decreased for the characteristic diamond peak with the addition of the 10.532 μm tuned laser wavelength. The graphitic component also decreased as the G-band became less intense.

Representative plan view SEM images from the films deposited for 1 minute are shown in Fig 3. Every attempt was made to image the films in the area in the center of the deposition area for ease of comparison. The film deposited without laser irradiation consisted of overlapping faceted crystals with some voids where the Si substrate was visible (Fig 3(a)). The lateral grain size varied as there appeared to be more grains closer to 0.25 to 0.50 μm, though some grains were as large as 1 μm. The film deposited with the 10.591 μm untuned laser wavelength also consisted of overlapping faceted crystals (Fig 3(b)). There are no voids shown in the figure. However, some voids were visible during the SEM investigation, but not as many as in the film deposited without the laser. Again, the grain size was variable, though in this film the range was between 0.5 and 1.0 μm. The grain size increase trend appeared to hold true with the short deposition times as with longer deposition times [17, 22]. The film deposited with the 10.532 μm tuned laser wavelength had the largest grain size (Fig 3(c)). The size range was roughly the same as the films deposited with the untuned laser, but there were grains closer to 1 μm in size.

The tuned film also appeared to be the most continuous of the three films. The SEM images from the films deposited for 5 minutes are shown in Fig 4. There was a distinct change in the film morphology in the center of the deposition area. Both the film deposited without the CO_2 laser (Fig 4(a)) and the film deposited with the untuned laser (Fig 4(b)) show isolated crystal faces amongst less faceted material. The grain size did appear larger in the film deposited with the untuned laser. The film deposited with the tuned laser (Fig 4(c)) was completely faceted with grains in excess of 2 μm in size. The SEM images from the films deposited for 5 minutes correlated with the XRD and Raman results in that the film deposited with the 10.532 μm tuned laser wavelength had the largest amount of faceted diamond.

The cross-sectional STEM images were produced in a manner similar to those previously reported [17]. Dark-field STEM images from the films deposited for 1 minute are shown in Fig 5. The film/substrate interface was very clearly defined in all of the films. The film deposited without the CO_2 laser and the film deposited with the 10.591 μm untuned laser exhibited some overlapping and discrete crystals as shown in Fig 5(a) and Fig 5(b), respectively. The grain size was roughly the same and the film thickness was approximately 0.5 μm in both films. The morphology was that of irregularly shaped, randomly oriented grains. The film deposited with the 10.532 μm tuned laser was more continuous with a film thickness of approximately 1 μm (Fig 5(c)). The grains were predominantly columnar in shape. The STEM images from the films deposited for 5 minutes are shown in Fig 6(a) (no laser), Fig 6(b) (10.591 μm untuned laser) and Fig 6(c) (10.532 μm tuned laser), respectively. The films were all continuous and noticeably thicker. The film deposited without the laser was approximately 1.5 μm in thickness.

There were some columnar grains visible, but the microstructure consisted of predominantly equiaxed grains. There was also evidence of competitive grain growth. The use of the untuned laser caused an increase in the film thickness to approximately 3 μm. The grains were also noticeably larger in the lateral direction. The competitive growth was not apparent as the grains nucleated on the substrate surface and grew in columns. The film deposited with the tuned laser was columnar with a thickness of approximately 4.5 μm. The lateral grain size also increased. The microstructural investigation showed the change in the growth mechanism was dependent on the laser wavelength.

The change in film microstructure, when grown on WC, was shown previously [17, 18] and was generally consistent with the trend shown for the films deposited on Si. One noticeable difference was that the grain sizes seen in the films deposited on Si substrates were larger. It is possible that the diamond seeding decreased the nucleation time. It has been proposed that when the 10.532 μm tuned laser interacts with the combustion-flame that new gaseous species were produced that were more likely to condense on the substrate and form diamond [18]. If that is the case then, adding the nuclei by way of the surface pretreatment and using the tuned laser could explain the much larger grain sizes.

Conclusions

The initial growth stages of diamond thin films deposited by a CO_2 laser-assisted combustion-flame method were characterized. The investigation focused on the effect of the silicon substrate, deposition time and the CO_2 laser wavelength on the film

morphology and microstructure. When the films were deposited with the laser wavelength tuned to match the CH_2-wagging vibrational mode of the C_2H_4 molecule, the grain size was generally twice as large, the diamond (111) diffraction peak was more intense and the characteristic Raman peak was more intense. The increase in grain size was attributed to the 10.532 μm tuned laser creating new growth species more likely to grow onto the diamond seeds rather than nucleate on the substrate surface.

References

[1] H. Ling, J. Sun, Y.X. Han, T. Gebre, Z.Q. Xie, M. Zhao, and Y.F. Lu, Laser-induced resonant excitation of ethylene molecules in C2H4/C2H2/O2 reactions to enhance diamond deposition, J. Appl. Phys. 105(1) (2009) 014901-014905.

[2] T. McKindra, M.J. O'Keefe, Z.Q. Xie, and Y.F. Lu, Characterization of diamond thin films deposited by a CO2 laser-assisted combustion-flame method, Mater. Charac. 61 (2010) 661-667.

[3] T. McKindra, M.J. O'Keefe, E. Kulp, Z.Q. Xie and Y.F. Lu, Nucleation and growth of diamond thin films deposited by a CO2 laser-assisted combustion-flame method, Surf. Coat. Technol. Submitted.

[4] Y.X. Han, H. Ling, J. Sun, M. Zhao, T. Gebre, and Y.F. Lu, Enhanced diamond nucleation on copper substrates by graphite seeding and CO2 laser irradiation, Appl. Surf. Sci. 254(7) (2008) 2054-2058.

[5] Y.X. Han, M. Zhao, J. Sun, H. Ling, T. Gebre, and Y.F. Lu, Real-time monitoring of diamond nucleation and growth using field-enhanced thermionic emission current, Appl. Surf. Sci. 254(5) (2007) 1423-1426.

[6] H. Ling, Y.X. Han, and Y.F. Lu, CO2 laser-assisted local deposition of diamond films by combustion-flame method, Proc. SPIE 6459 (2007) 64590Y-1-64590Y-7.

[7] H. Ling, Z.Q. Xie, Y. Gao, T. Gebre, X.K. Shen, and Y.F. Lu, Enhanced chemical vapor deposition of diamond by wavelength-matched vibrational excitations of ethylene molecules using tunable CO2 laser irradiation, J. Appl. Phys. 105(6) (2009) 064901-064906.

[8] T. Gebre, J. Sun, H. Ling, Y.X. Han, M. Zao, and Y.F. Lu, C2 and CH rotational temperatures in diamond growth using CO2 laser-assisted combustion-flames, Proc. SPIE 6880 (2008) 68800O-1-68800O-7.

[9] S.M. Huang, Z. Sun, Y.F. Lu, M.H. Hong, Ultraviolet and visible Raman spectroscopy characterization of chemical vapor deposition diamond films, Surf. Coat. Technol. 151-152 (2002) 263-267.

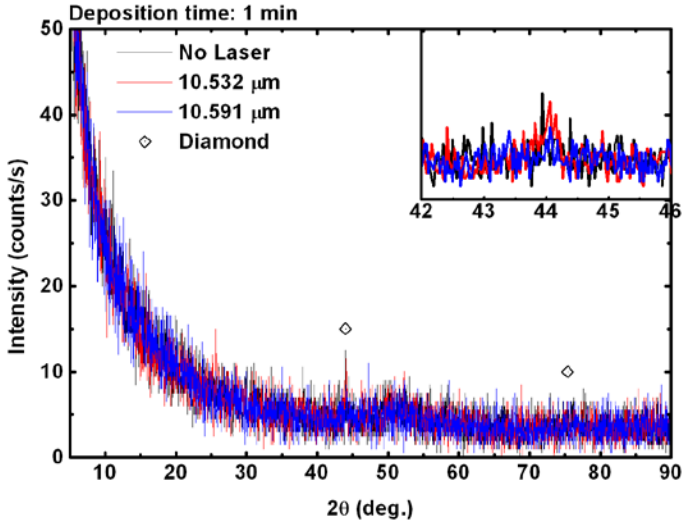

(a)

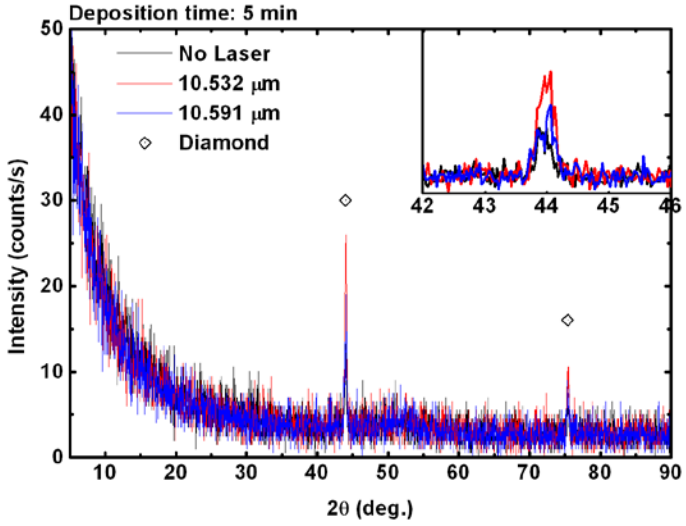

(b)

Fig 1. XRD spectra from films deposited for (a) 1 and (b) 5 minutes with 2θ range associated with diamond (111) planes inset.

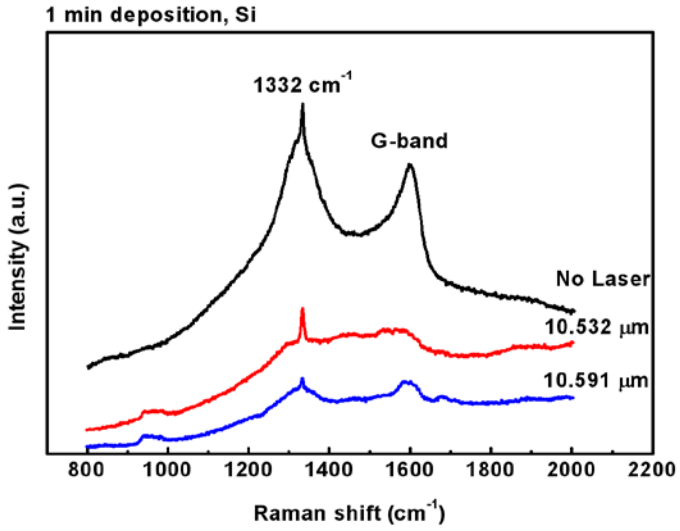

(a)

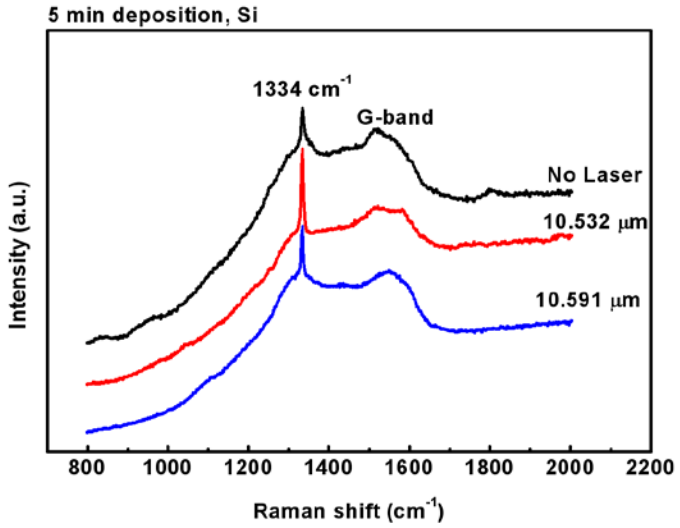

(c)

Fig 2. Raman spectra from films deposited for (a) 1 and (b) 5 minutes.

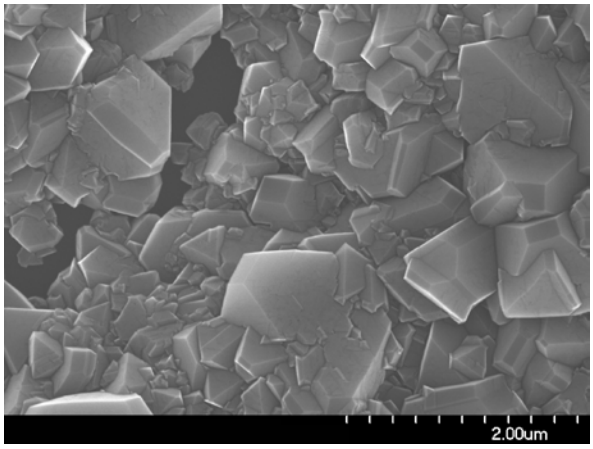

(a)

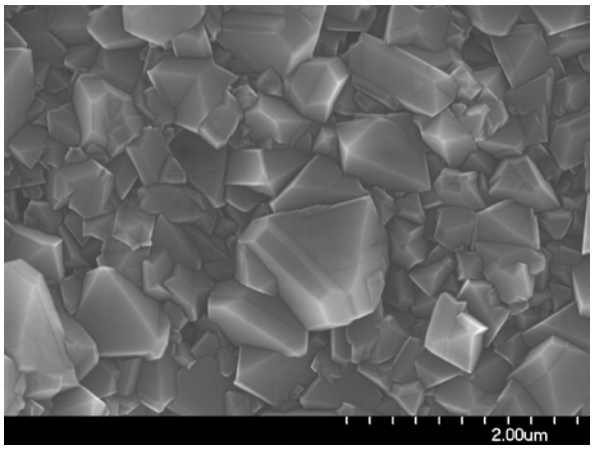

(b)

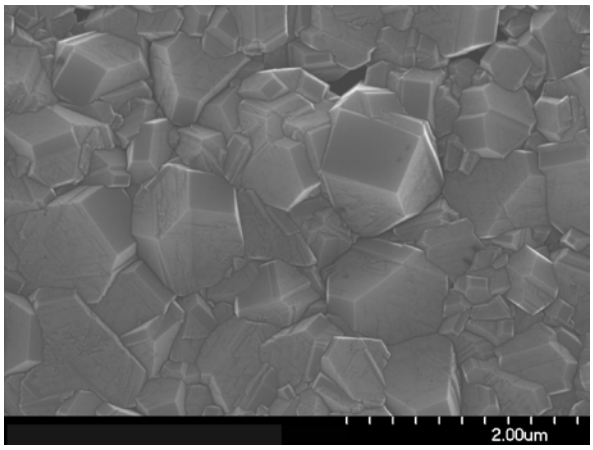

(c)

Fig 3. SEM micrographs from the center of films deposited for 1 minute with (a) no laser, (b) untuned laser wavelength and (c) tuned laser wavelength.

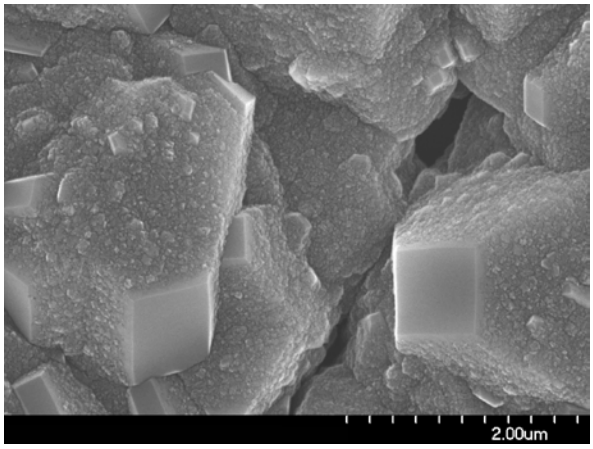

(a)

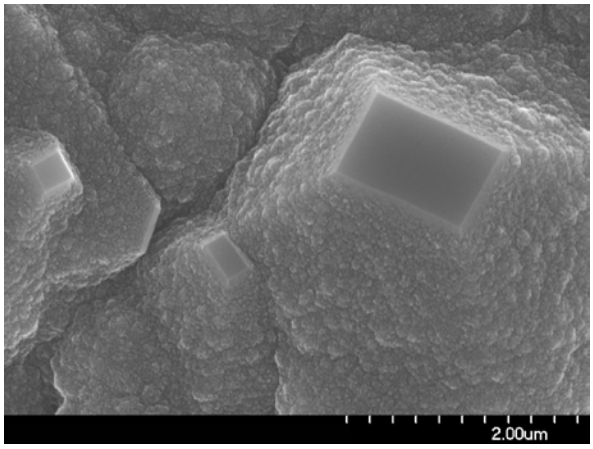

(b)

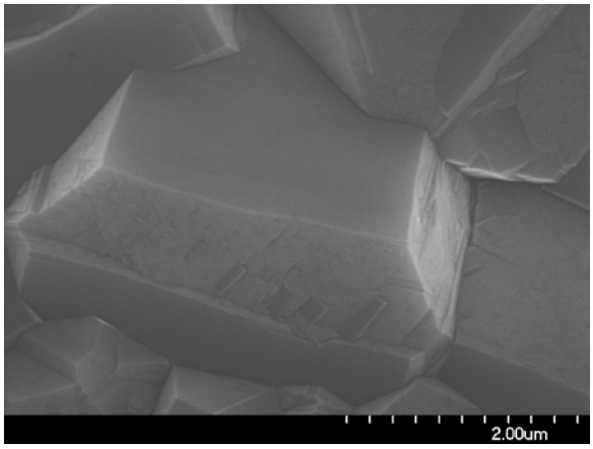

(c)

Fig 4. SEM micrographs from the center of films deposited for 5 minute with (a) no laser, (b) untuned and (c) tuned laser irradiation.

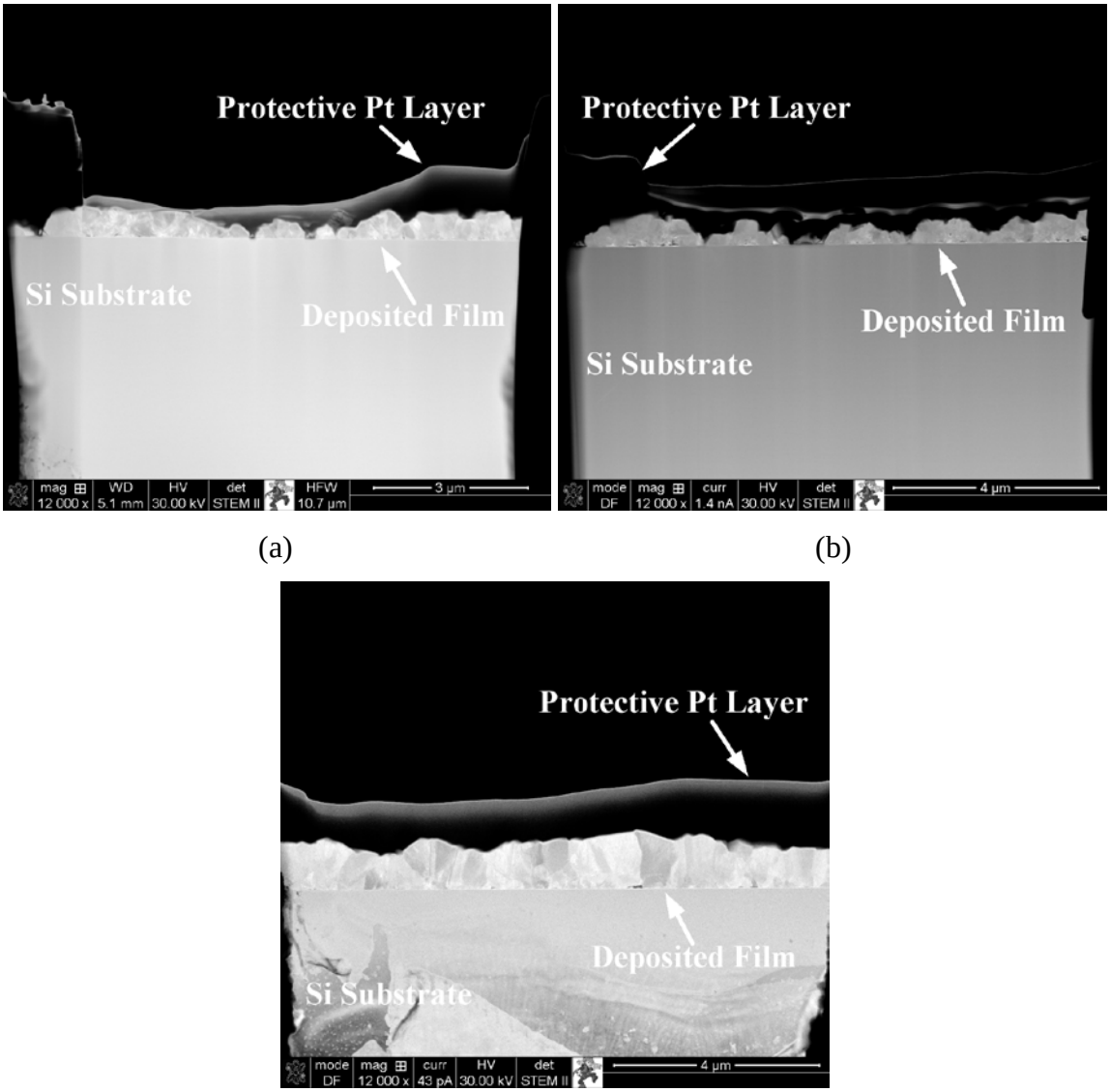

Fig 5. Dark-field STEM images from cross-sections of diamond films deposited for 1 minute with (a) no laser, (b) untuned and (c) tuned laser irradiation.

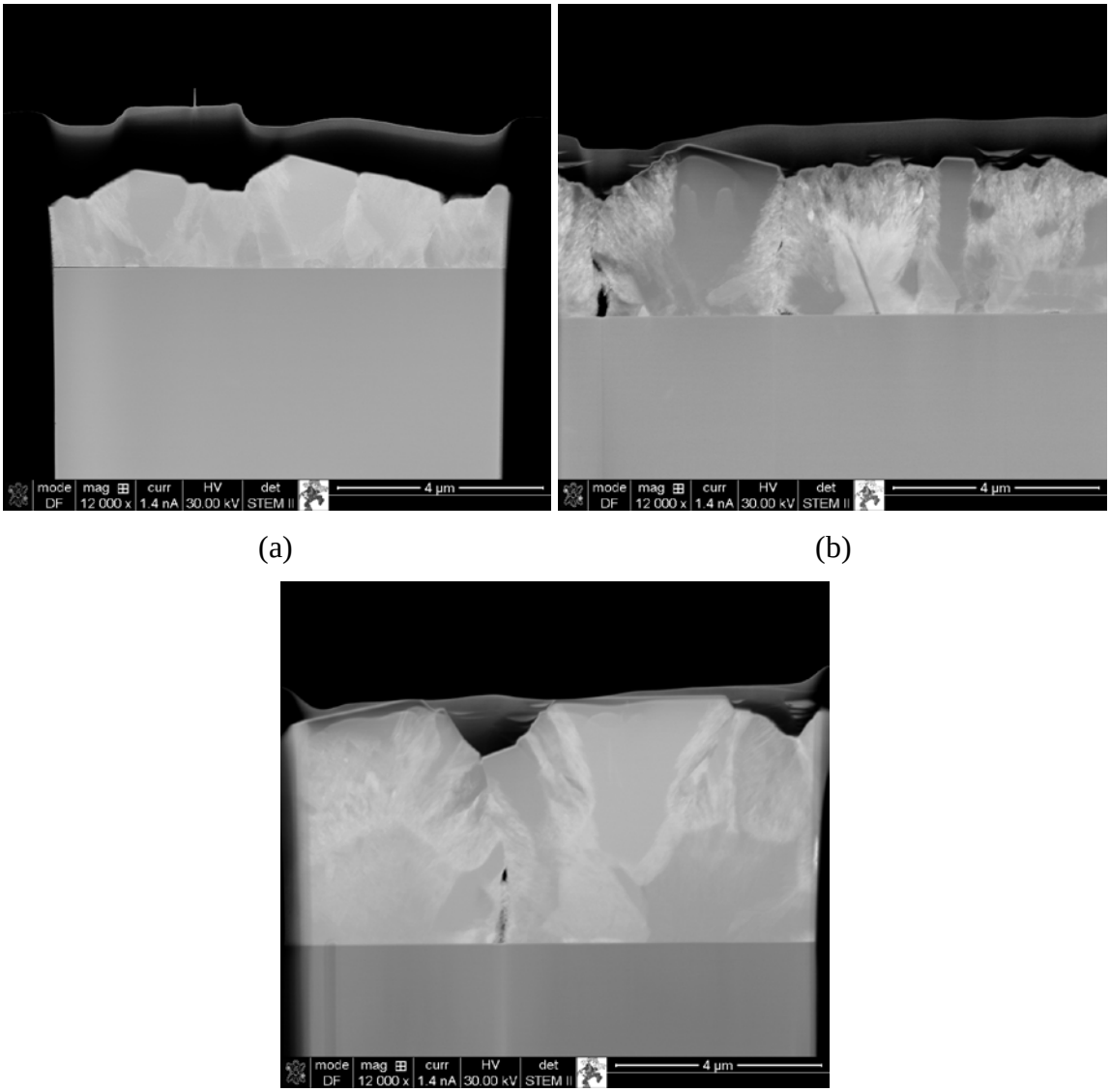

Fig 6. Dark-field STEM images from cross-sections of diamond films deposited for 5 minute with (a) no laser, (b) untuned and (c) tuned laser irradiation.

APPENDIX C
UNPUBLISHED RESULTS

MURI Annual Review 2007

Materials Characterization

Samples processed at UNL were characterized and analyzed throughout the year. The samples were separated into the categories of ultra-fast deposited (carbon pillars) and low deposition rate discrete particles.

Ultra-fast deposition

Shown in Fig. 1 are samples processed by CO_2 laser assisted combustion-flame (LACF) with 300 W and 600 W for 3 minutes at an O_2:C_2H_2 of 250:320 sccm were characterized by scanning electron microscopy (SEM) and energy dispersive spectrometry (EDS). The EDS results shown in Figure 2, revealed that the pillars consisted almost entirely carbon. There was some tungsten and oxygen contamination present most likely from handling of the samples.

X-ray diffraction (XRD) methods were used to determine the crystal structure of the 300/600W pillars. As shown in Figure 3, the pillars had very crystalline diffraction peaks that most closely matched graphite while no diamond peaks were detected.

The samples were also characterized by x-ray photoelectron spectroscopy (XPS). The peak intensity of the 600 W sample was higher and its location shifted to a higher binding energy. As a result, Figure 4 shows the 300 W sample spectrum was resolved by only one peak centered at 285 eV while the 600W sample was resolved by two peaks at 285 eV and 286.2 eV.

Previously, a technique for producing cross-sectional TEM samples was developed. Another technique for producing plan-view TEM samples was also developed whereby portions of the pillars were removed with a razor blade and deposited onto a TEM grid in order to image any electron transparent particles. During sample preparation it was observed that the pillars exhibited brittle fracture during the shaving. Particles in the size range of 200-1000 nm were imaged in the TEM and electron diffraction patterns were obtained. Figure 5 shows representative bright-field TEM images with the selected area electron diffraction (SAED) pattern inset for both samples. The electron diffraction patterns from the particles yielded ring patterns indicative of a

polycrystalline material. Some particles displayed single-crystal spot patterns. Some of the d-spacings measured from the diffraction patterns matched graphite.

The effect of laser power on the ultra-fast depositions occurred through an SEM and XPS investigation. The pillars were deposited for 3 minutes at laser powers varied from 300 W to 800 W with an O_2:C_2H_2 ratio of 250:340. The SEM images showed a similar microstructure to previously analyzed samples. Figure 6 shows representative SEM images. The amount of laser power affected the shape of the pillar. Lower laser powers produced pillars more cylindrical in shape while higher laser powers deposited pillars that were "flatter" and a noticeable depression directly beneath the laser beam. Also, as the laser power increased, the amount of "base" material on the substrate increased.

Attempts were made to analyze the different portions of the pillar cross-section by XPS. The results for the shell showed a more pronounced shoulder at a higher binding energy compared to the core, but the signal intensity was much less intense. Spectra for both locations were resolved by two peaks, but the higher binding energy peak area for the core comprised a larger percentage of the area (~17% to 11%). The overall signal intensity was relatively low for both areas which was attributed to sample geometry. Also, the spatial resolution in the XPS system limited the data analysis. Figure 7 shows the comparison of XPS spectra based on location on the pillar.

The effect of the C_2H_2 content in the combustion flame was investigated in a manner similar to the previous samples. Pillars were deposited at 600 W with O_2:C_2H_2 ratios of 250:320/340/360 sccm for 3 min. The samples were labeled by their C2H2 flowrate and were referred to as such during examination. The SEM characterization revealed the microstructure of the pillars to consist of two definitive portions. It appeared the pillars grew vertically as well as radially and included an inner "core" and an outer "shell". The core appeared to be very dense and lie parallel to the substrate surface while deposited conformally. The shell was "lamellar-like" and appeared to grow perpendicular to the substrate and towards the combustion flame. Figure 6 shows an SEM image of the 360 pillar.

The XRD analysis focused on the material left on the WC substrate after removal of the pillar. The results showed that the "base" material initially deposited on the

substrate was crystalline with similar characteristics to that of the pillar itself. Figure 9 shows the XRD results which detected the WC substrate and several graphite peaks. SEM analysis on these samples revealed a similar morphology to that of the pillars. Figure 10 shows a representative secondary electron image of the "base" material. Some samples were mounted in epoxy and polished with various SiC grinding pads and diamond slurry in order to investigate any subsurface artifacts and the interface between the substrate and deposit. There was a very abrupt interface with no apparent transition zone from the substrate to the "base" material determined by the SEM analysis and optical images obtained after polishing. There was some indication that there may be a transition zone in the deposit itself which is shown in Figure 11. Some samples were mounted in epoxy in order to observe the pillar while still attached to the substrate. After polishing, a possible interaction zone became apparent in the WC substrate directly beneath the deposited material. The microstructure of the pillar structure was visible. The base consisted of layers of material parallel to the substrate surface and it appeared that some layers turned or folded vertically which created the "shell". Some of the layers remained parallel to the substrate and were stacked vertically in the direction of the combustion flame which formed the "core". Figure 12 is an optical micrograph of one such sample after polishing.

The effect of C_2H_2 in the combustion flame was also investigated via TEM. The TEM samples were prepared similarly to those previously discussed. Samples were also created from a graphite sputtering target for comparison. All of the samples (320/340/360) exhibited speckled ring patterns indicative of diffraction from a polycrystalline material. The 340 sample also produced a hexagonal spot pattern. The d-spacings determined from the ring patterns were compared to calculated spacings for graphite and diamond as well as the spacings from the graphite sputtering target. There were no exact matches for diamond or graphite. Figure 13 and 14 display bright-field TEM images with SAED patterns from the 320 pillar sample. Table 1 lists the d-spacings compared during the experiment.

Low deposition rate discrete particles

Certain parameters used resulted in the high deposition rates observed with the laser-assisted combustion-flame process previously discussed. Other parameters, namely

combustion-flame content, caused slower deposition of discrete particles. The direction of the laser focus, vertically normal to the substrate or perpendicular to the combustion-flame also had an effect. Some of these particles were identified as diamond through Raman spectroscopy and TEM analysis. SEM analysis discovered several faceted crystal faces. Figure 15 shows some representative SEM images of the discrete particles in each investigated condition. In general, the vertically focused laser produced a discontinuous film area with discrete particles. The horizontally focused laser produced a larger, more continuous film with faceted crystals observed in the center of the deposited area. It should be noted that the combustion-flame used in the horizontally focused laser experiments contained an additional gas (C_2H_4) and was positioned perpendicular to the WC substrate.

XRD was used to determine the crystal structure of the films. The experimental films, including a film deposited without laser assistance, were compared to commercially available diamond powder and diamond films deposited by CVD. The flame-only sample produced comparable peak intensity to the CVD diamond with a good peak location match to the natural diamond powder. The vertical laser samples (200/300 W) showed nearly identical spectra, but no diamond peaks were observed. When compared to the vertical laser samples, the horizontal laser sample showed higher signal intensity as well as a diamond peak. Compared to the flame-only sample, the horizontal laser sample had a more intense diamond peak. This result needs verification as only one sample was analyzed. Figure 16 shows the XRD comparison for the flame only sample, the horizontal laser sample, and the natural diamond powder in the range of the 43.965° diamond peak. The peak shift noticeable in the flame-only and horizontal laser samples was attributed to uneven topography of the deposited material.

Cross-sectional TEM analysis of the vertical laser samples utilized the sample preparation technique developed in the previous year. The samples were identified by the laser power used during processing. Some diamond component was identified in the electron diffraction pattern for the 200 W samples. The speckled ring pattern was indicative of a polycrystalline material. Some diffuse rings were also identified as graphite (possibly lignite). Some diamond and graphite components were identified in the speckled ring diffraction pattern from the sample processed at 300 W. Figures 17 and

18 show bright-field TEM images with accompanying diffraction patterns for samples processed at 200 W. Figure 19 displays the bright-field TEM image and diffraction pattern for the 300 W sample.

Figure 1: Optical micrographs of pillars processed with CO_2 laser at 300 W (left) and 600 W (right) showing the deposits are millimeters in height.

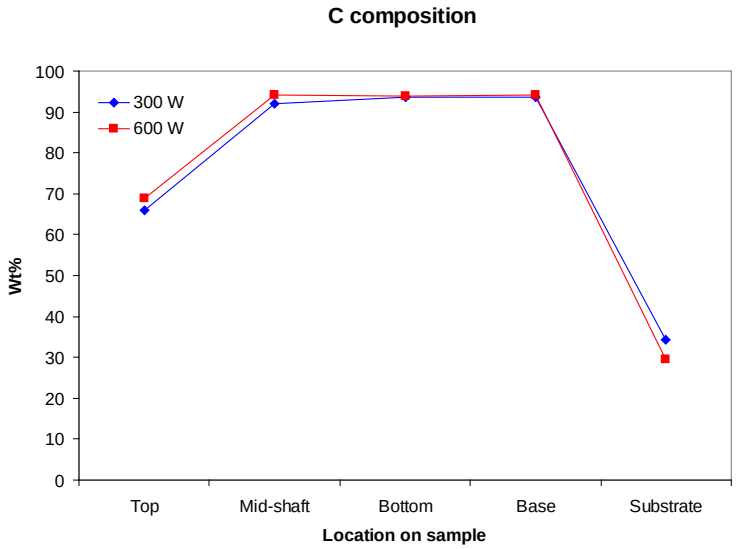

Figure 2: Comparison of carbon composition (wt %) based on the location on the sample for the samples processed with CO_2 laser at 300 W and 600 W.

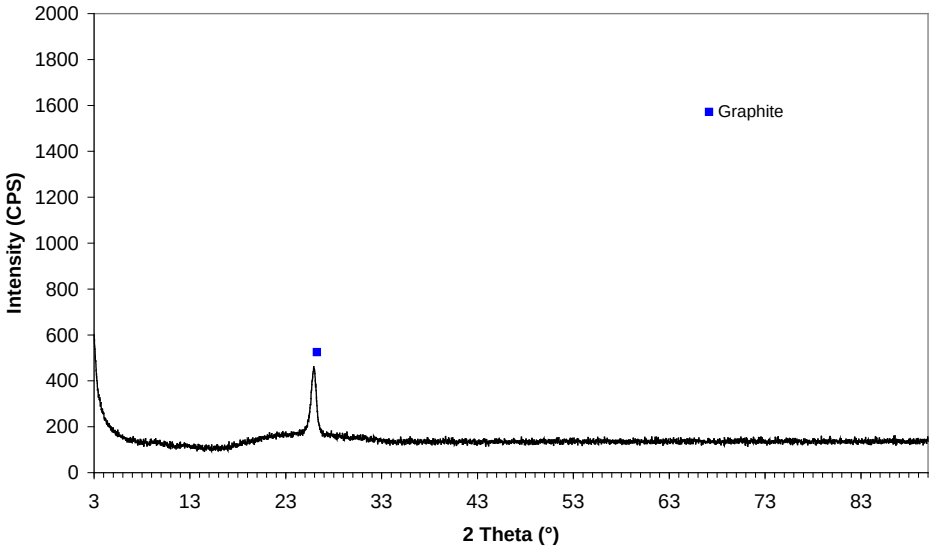

(a)

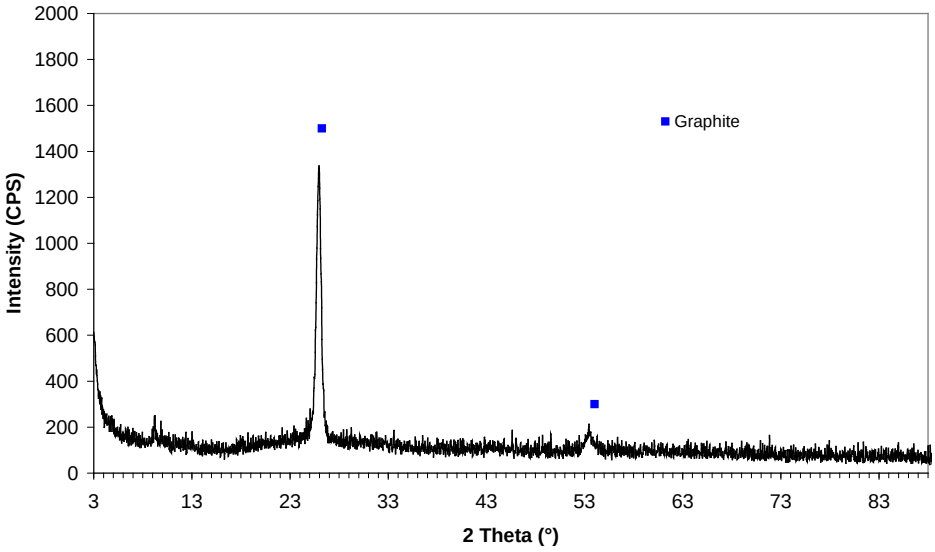

(b)

Figure 3: XRD of LACF ultra-fast deposited pillars processed with CO_2 laser at (a) 300 W and (b) 600 W.

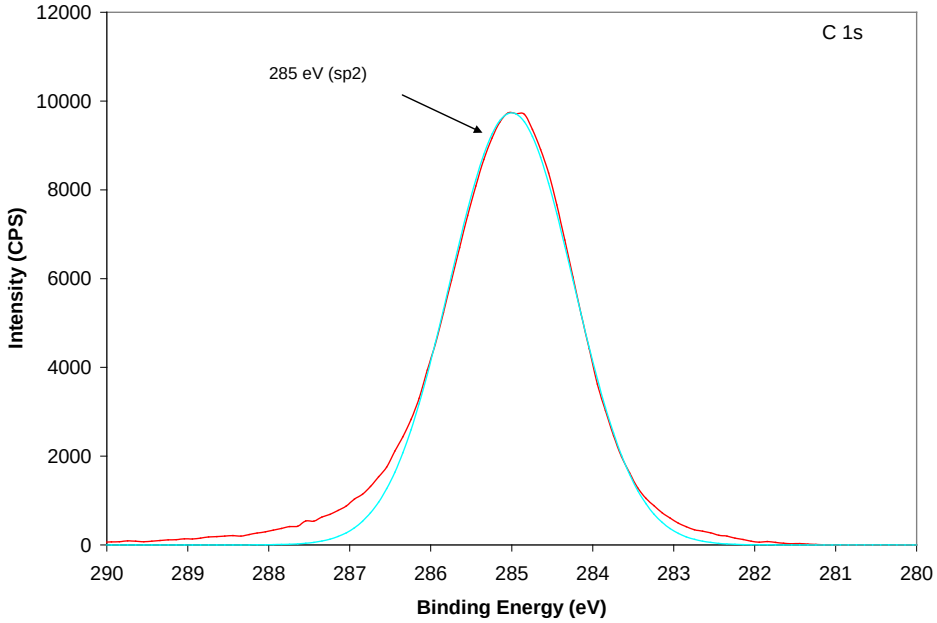

(a)

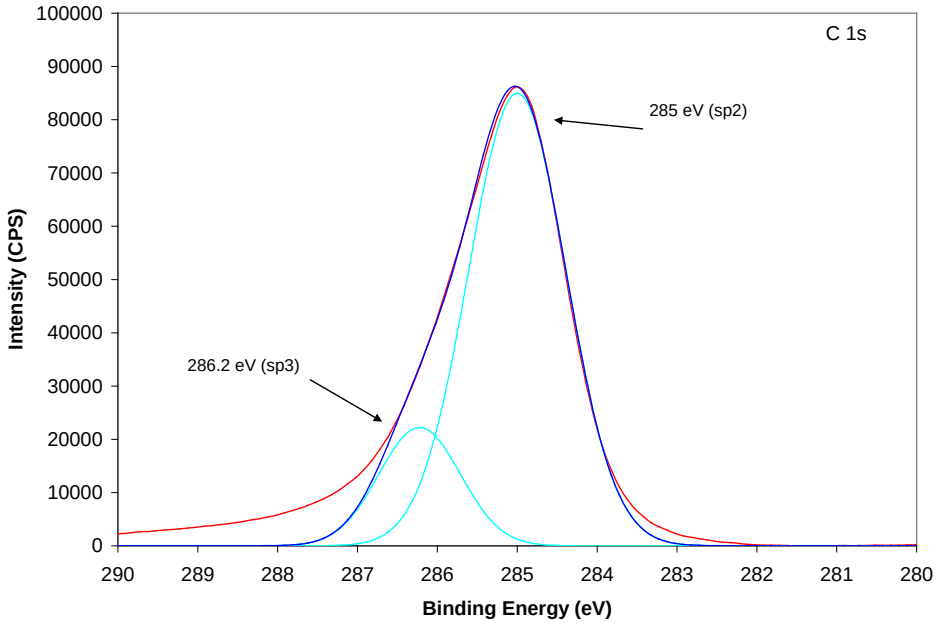

(b)

Figure 4: XPS of LACF ultra-fast deposited pillars processed with CO2 laser at (a) 300 W and (b) 600 W.

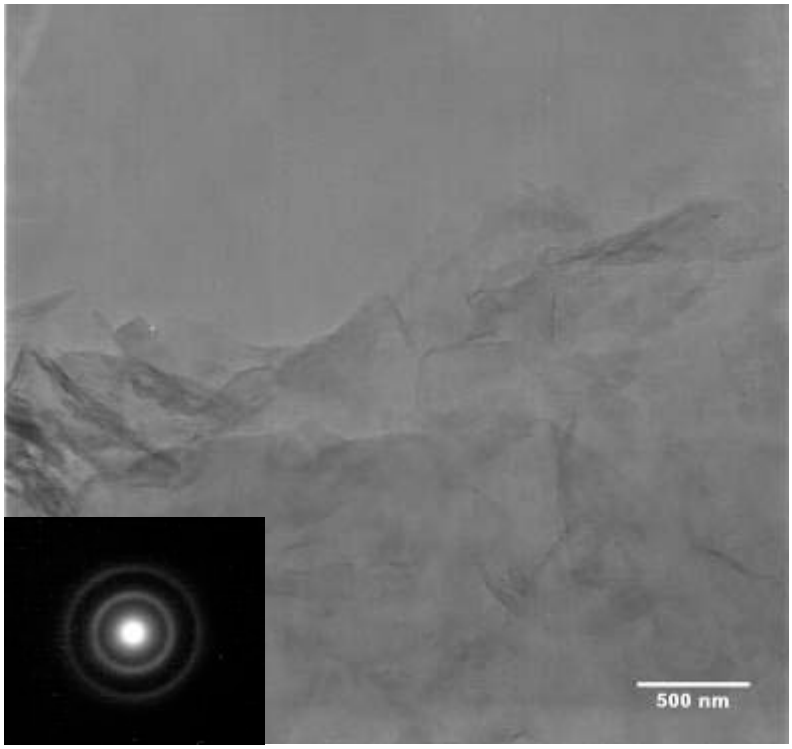

(a)

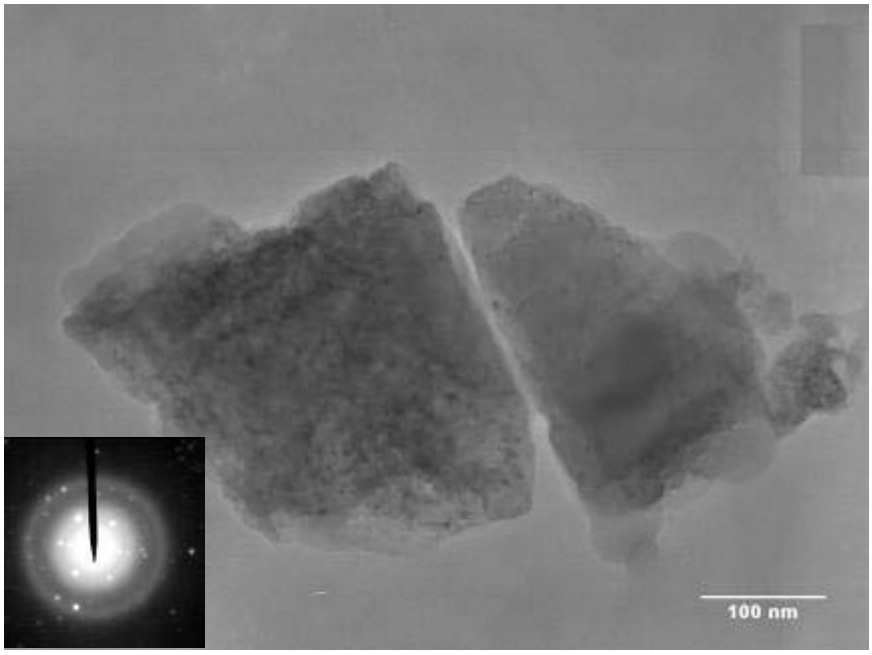

(b)

Figure 5: Bright-field TEM image with SAED pattern inset for particles from LACF ultra-fast deposited pillars processed with CO_2 laser at (a) 300 W and (b) 600 W.

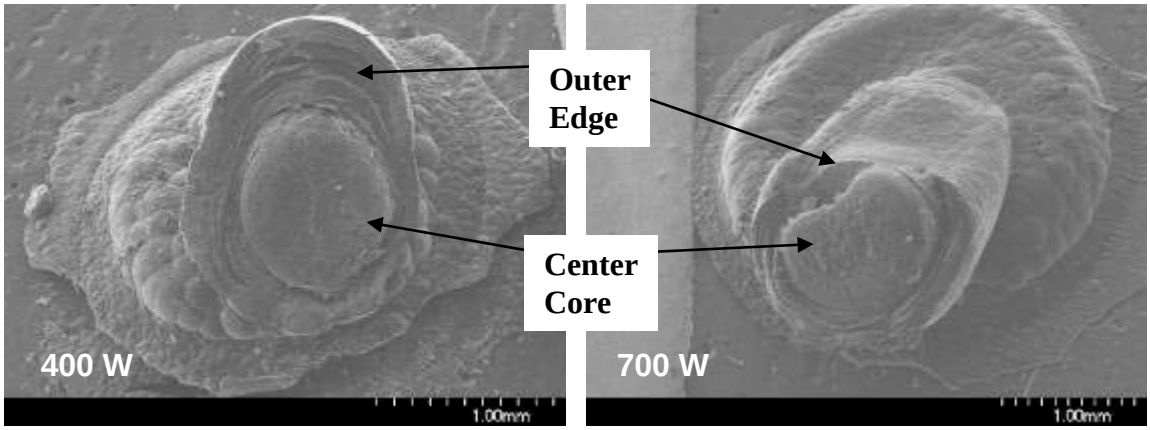

Figure 6: SEM image of LACF ultra-fast deposited pillars processed with CO_2 laser at 400 W and 700 W laser powers.

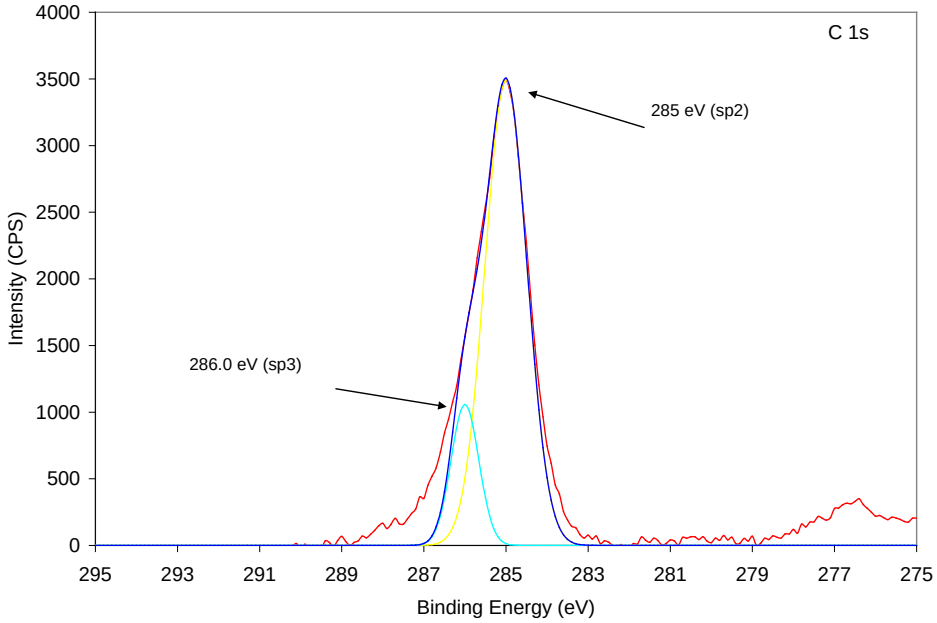

(a)

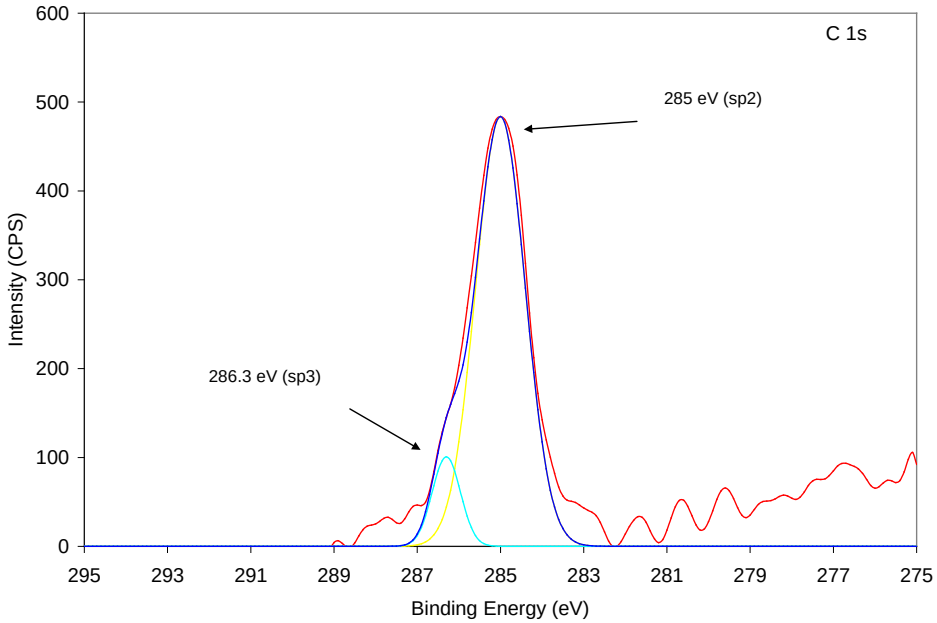

(b)

Figure 7: XPS of LACF ultra-fast deposited pillar processed with CO_2 laser at 400 W which compares the results from (a) the inner “core” and (b) outer “shell” of the pillar.

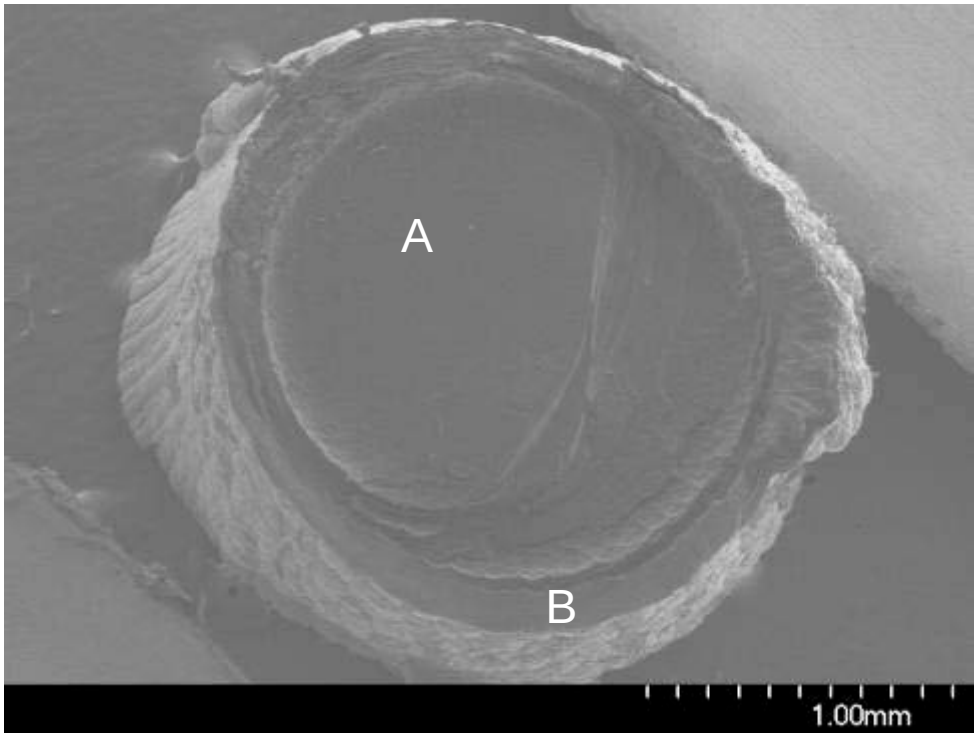

(a)

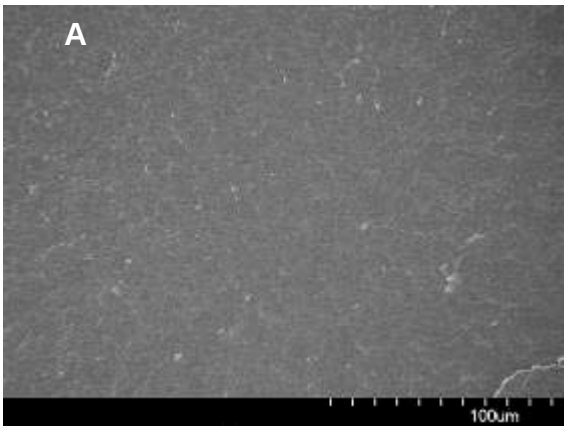

(b)

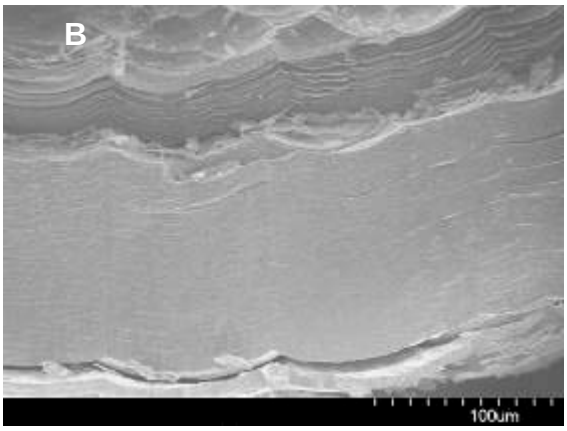

(c)

Figure 8: SEM images of LACF ultra-fast deposited pillar processed with CO_2 laser with O_2:C_2H_2 ratio of 250:320 showing (a) the entire cross-section showing inner "core" labeled "A" and outer "shell" labeled "B", (b) higher magnification image of dense core, and (c) higher magnification of outer shell.

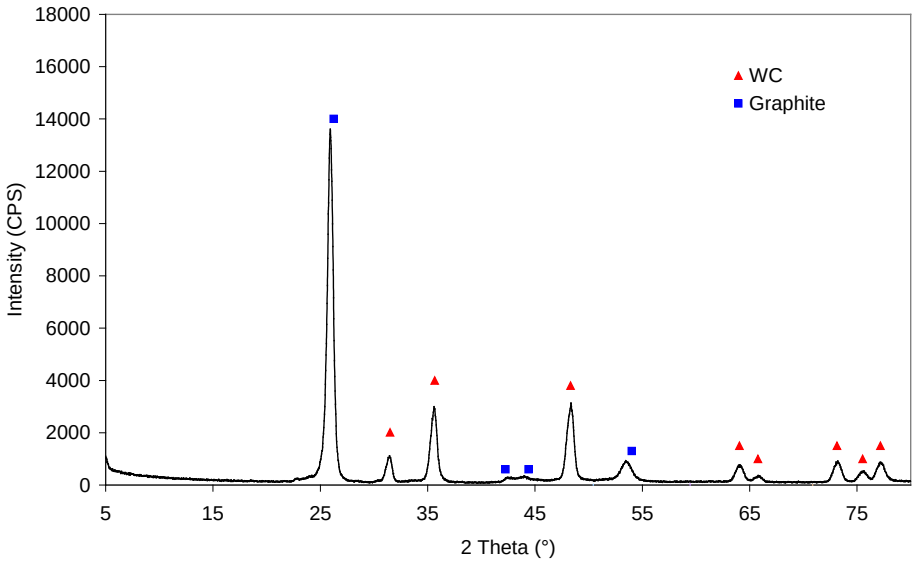

Figure 9: XRD of WC substrate with base material of LACF ultra-fast deposition at C_2H_2 flowrate 320 sccm.

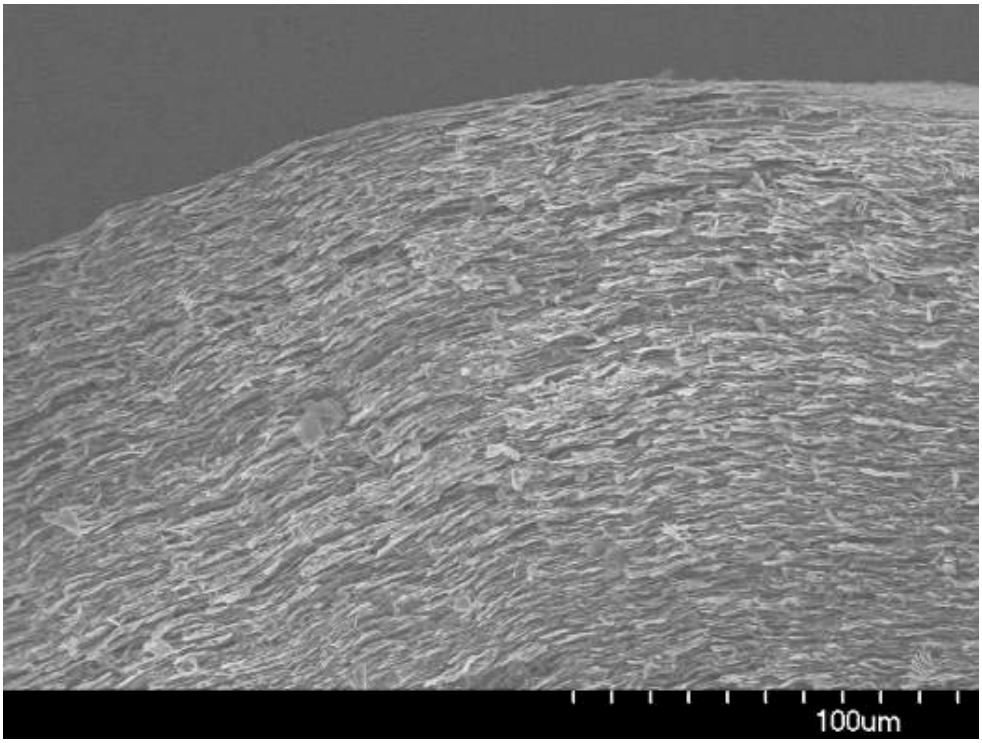

Figure 10: SEM image of the “base” material remaining on the 340 WC substrate showing horizontally layered material.

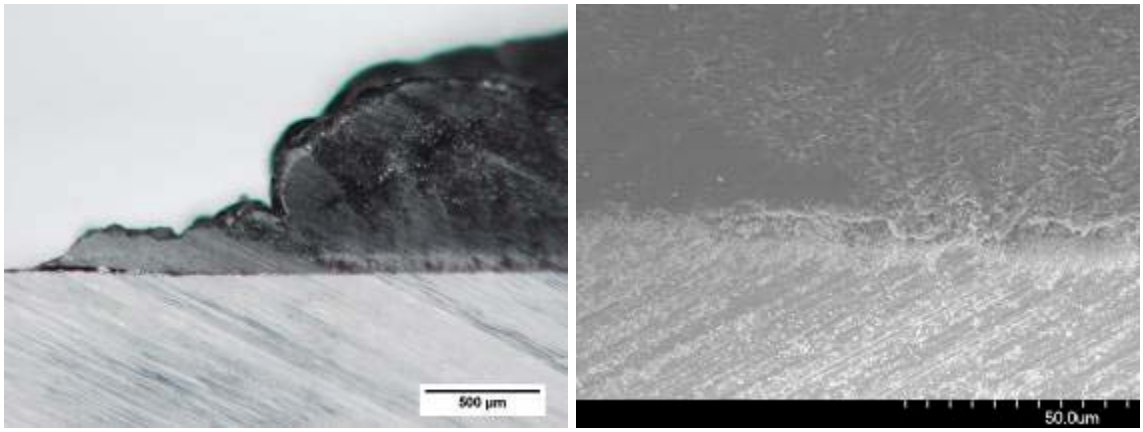

Figure 11: Optical image (left) and SEM image (right) of sectioned 340 substrate showing possible transition zone in the “base” material.

Figure 12: Composite optical images detailing the microstructure of the pillar after sectioning (left) and after polishing (right).

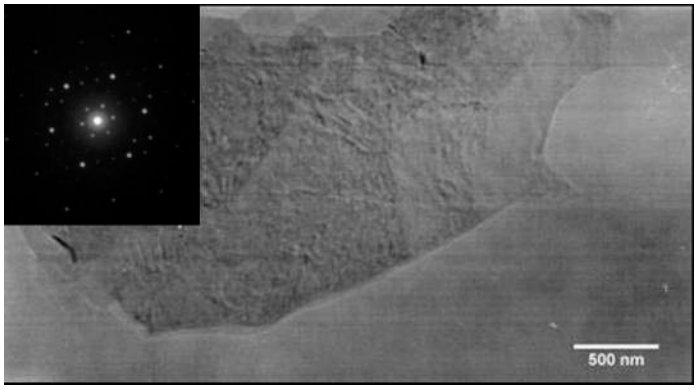

Figure 13: Bright-field TEM image with inset SAED pattern showing hexagonal structure.

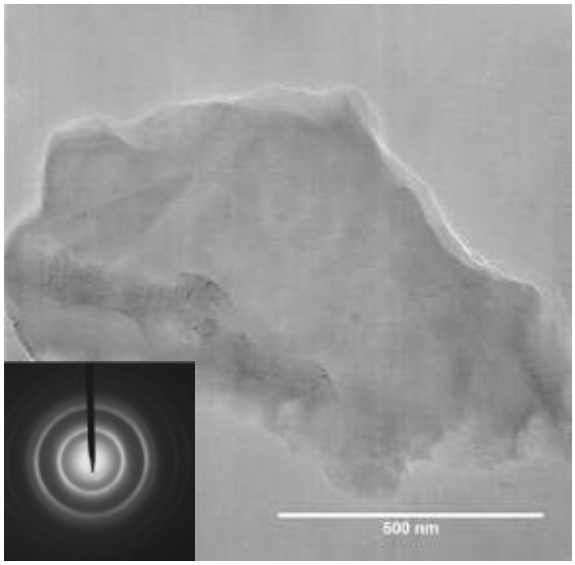

Figure 14: Bright-field TEM image with inset SAED pattern showing definitive ring structure.

Table I: D-spacing comparison

Graphite Calculated	Graphite Measured	320 sccm	340 sccm	360 sccm	Diamond Calculated
3.391	3.23	3.29	3.41	3.43	
2.137					
2.038			2.09	2.05	2.058
1.808	1.93	1.92			
1.695	1.59		1.74	1.67	
1.553					
1.328					
1.234			1.22		1.259
1.159				1.18	
1.145	1.14	1.12			
1.130					
	1.08		1.04		1.074
		0.97	0.8		0.891
		0.73	0.71		0.817

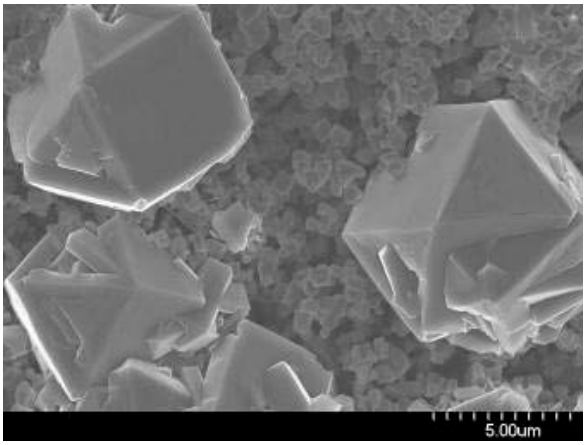

(a)

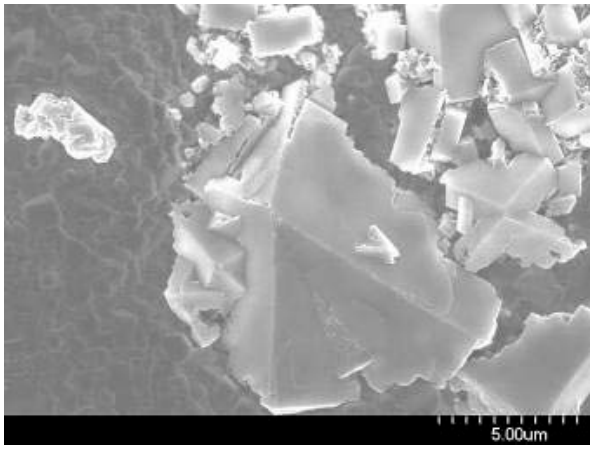

(b)

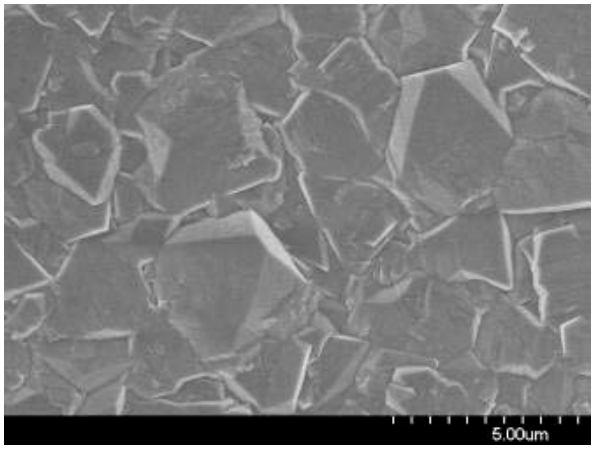

(c)

Figure 15: SEM images from (a) vertically focused CO_2 laser at 200 W, (b) at 300 W, and (c) horizontally focused CO_2 laser at 500 W.

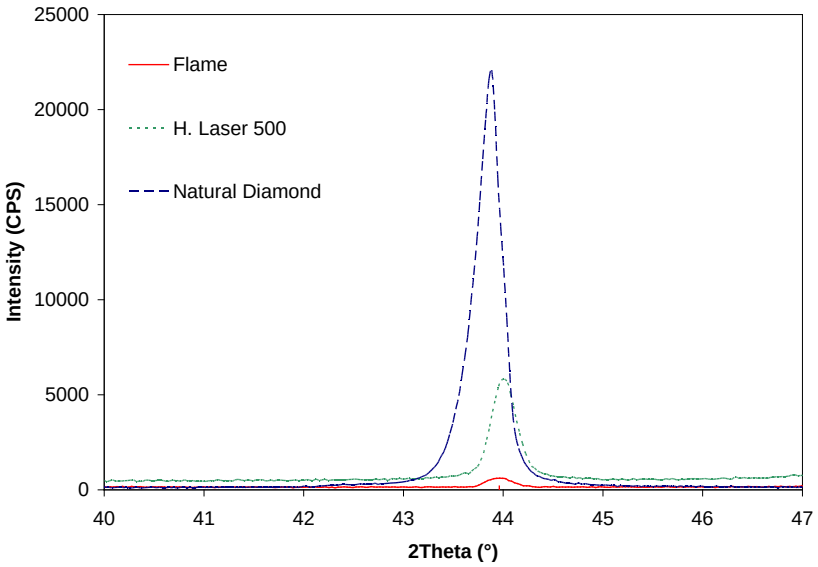

Figure 16: XRD comparison of selected samples of discrete particle deposition with natural diamond powder.

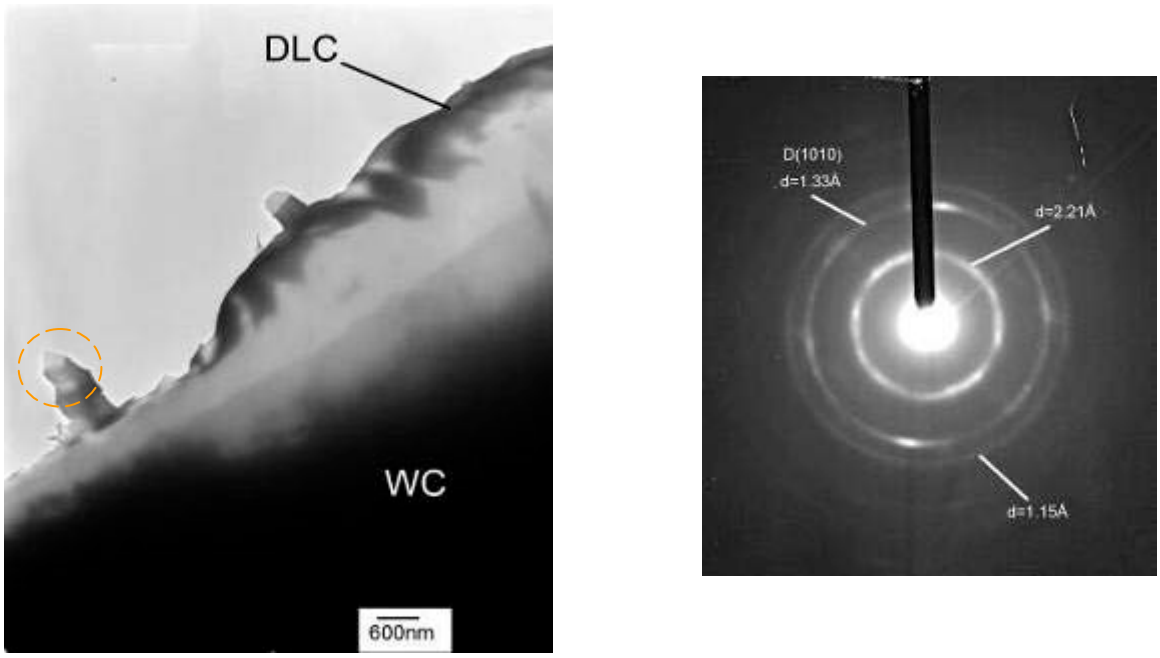

Figure 17: Bright field TEM image of cross-section of discrete particle deposition on WC with CO_2 laser processing at 200 W. The accompanying speckled ring SAED pattern comes from the circled area. D-spacings matched diamond and graphite.

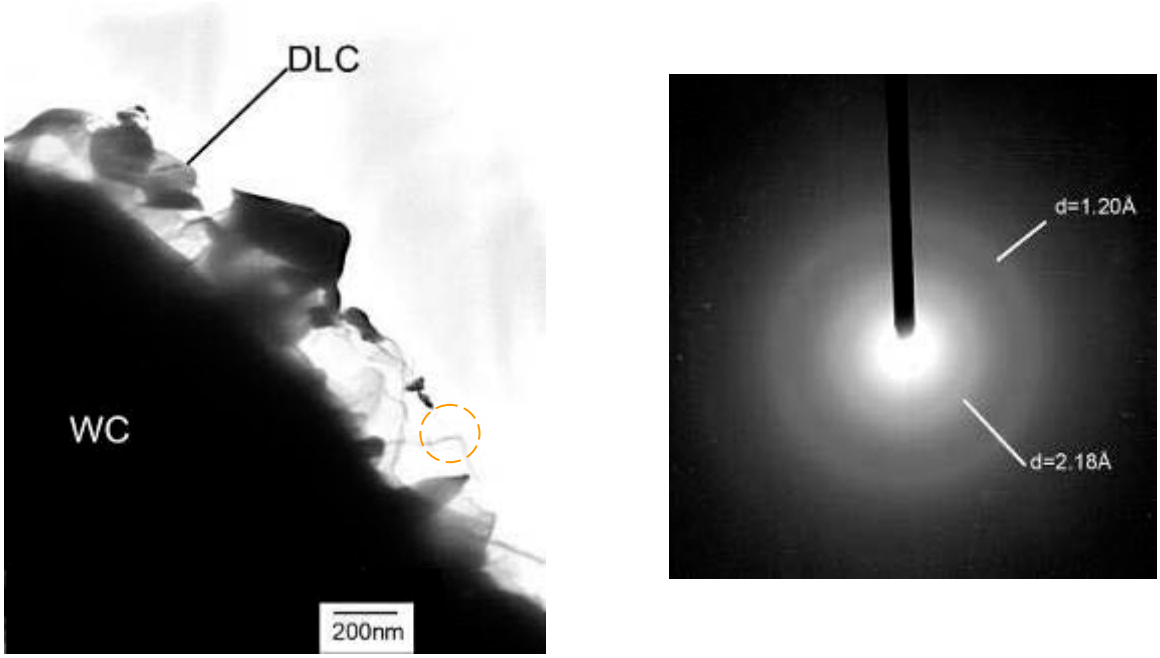

Figure 18: Bright field TEM image of cross-section of discrete particle deposition on WC with CO_2 laser processing at 200 W. The accompanying diffuse ring SAED pattern comes from the circled area. D-spacings matched graphite.

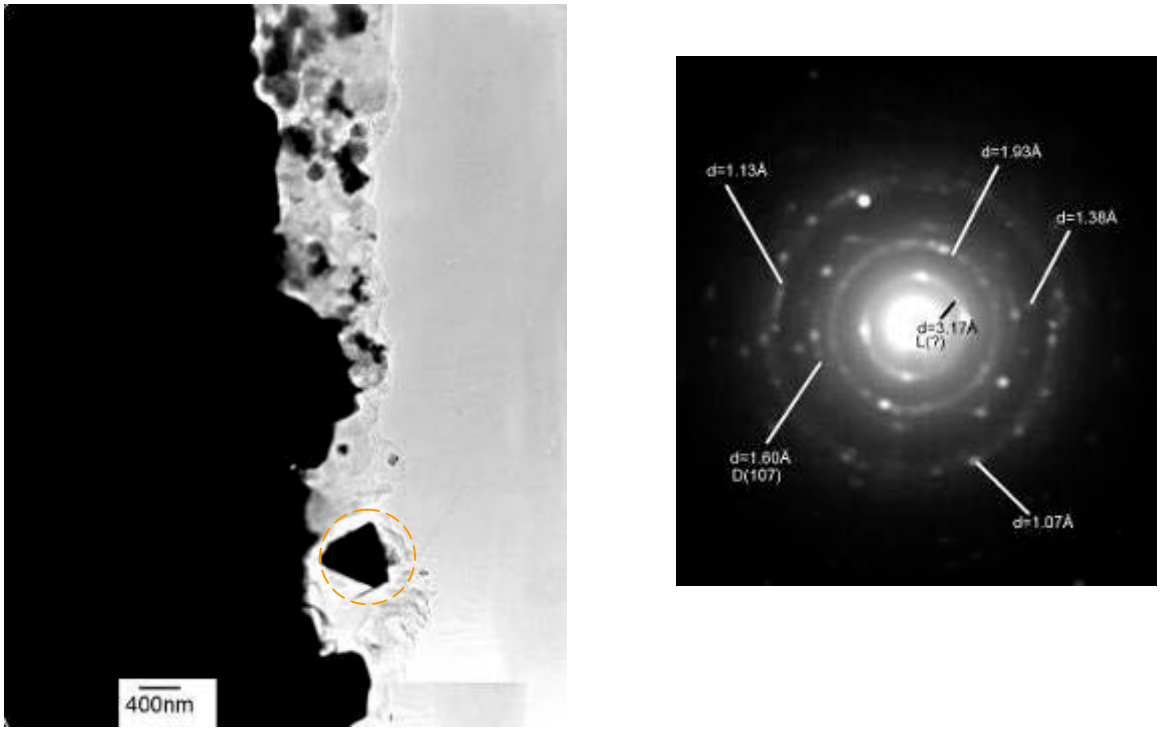

Figure 19: Bright-field TEM image of cross-section of discrete particle deposition on WC with laser processing at 300 W. The accompanying speckled ring SAED pattern comes from the circled area. Some d-spacings matched to diamond and graphite.

Materials Characterization

Samples produced at UNL were characterized and the results were analyzed throughout the year. The samples consisted of continuous thin films deposited by the CO_2 laser-assisted combustion-flame process. The results were separated by combustion gas composition ($O_2 + C_2H_2 + C_2H_4$ and $O_2 + C_3H_6$). Also, carbon pillars deposited with the assistance of the CO_2 laser were characterized.

Depositions with O_2+C_2H_2+C_2H_4

The samples were horizontally focused CO_2 laser-assisted combustion-flame (LACF) deposited films on WC substrates. Various parameters were varied which included the combustion gas ratio (O_2:C_2H_2:C_2H_4), the flame inner cone to substrate distance (0.5mm – 1.0mm), and with and without the laser (600W). Optically, the films appeared continuous, covering a circular area roughly 1 cm in diameter in the center of the WC substrate. The samples were characterized by scanning electron microscopy (SEM), x-ray diffraction (XRD) and x-ray photoelectron spectroscopy (XPS). Several studies were conducted including the effect of the CO_2 laser irradiation; the effect of the flame inner cone to substrate distance; and the effect of the combustion gas composition.

The effect of CO_2 laser irradiation on the deposited films was investigated by SEM and XRD. SEM images from the center of the substrate revealed continuous films of overlapping crystallites. Regardless of the deposition conditions, the film morphology changed radially outward from the center of the deposit, from larger grains with crystalline features toward the center to smaller grains and particles with amorphous-like features toward the perimeter. Figure 1 shows representative SEM images of the center of the deposited area. In both cases, the grain size was 1-2 μm. The films deposited with the assistance of the CO_2 laser had a generally larger grain size (Figure 1(a)) when compared to the film without laser irradiation (Figure 1(b)).

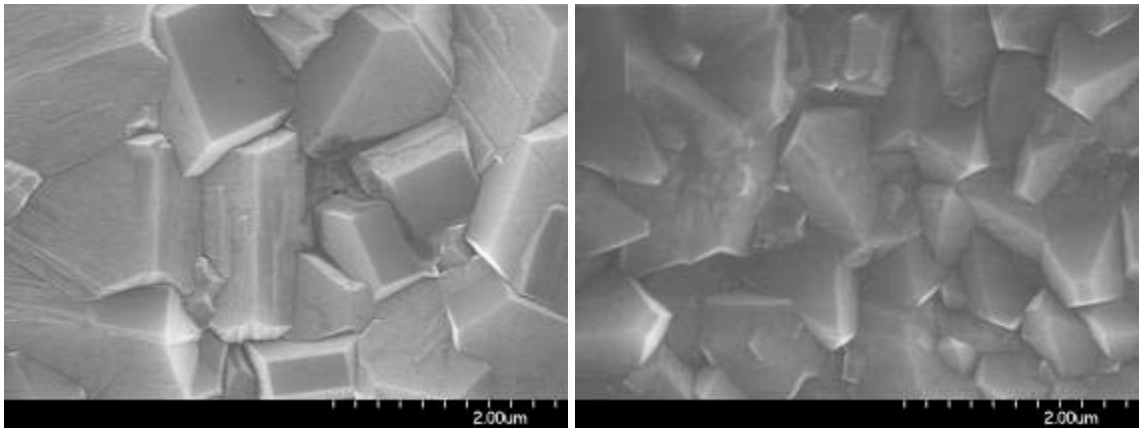

(a) (b)

Figure 1: SEM images of LACF films deposited (a) with horizontally focused CO2 laser at 600 W, and (b) without laser irradiation.

From the SEM images alone it was difficult to determine the effect of the parameter changes; therefore XRD analysis was conducted. The XRD contained the WC diffraction peaks along with at least two crystalline, cubic diamond peaks (Figure 2(a)). The calculated peak for diamond at 43.965° was used for comparison as it was the largest identifiable peak that was clearly not associated with the WC substrate. As with previous samples, there was a slight peak shift which was attributed to difficulties with positioning the sample flat. The WC peaks had the same relative intensity for all the samples which made straightforward comparisons of the diamond peak possible. For all cases investigated, the diamond peak intensity increased with the use of the laser. Figure 2(b) shows the associated XRD spectra within the 2θ range associated with the cubic diamond (111) planes.

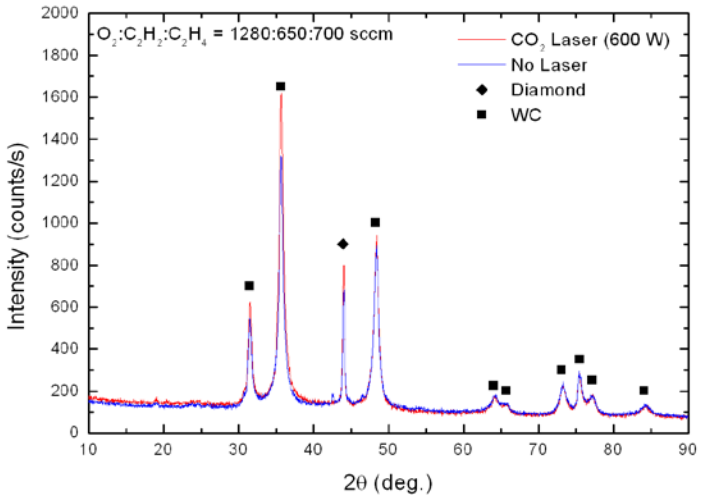

(a)

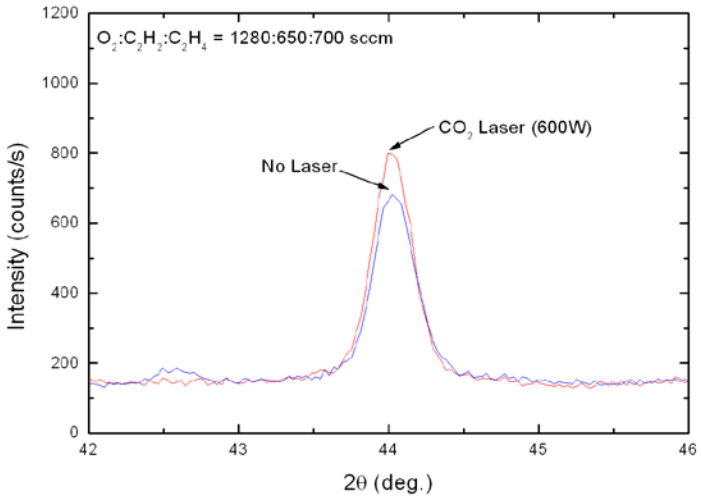

(b)

Figure 2: XRD spectra showing the effect of CO_2 laser irradiation on LACF deposited diamond thin films (a) over the entire 2θ range and (b) range associated with cubic diamond (111).

In addition to investigating the effect of the laser, the effect of the distance between the WC substrate and the combustion flame's inner cone was studied. XRD and XPS were used to characterize the effect. Figure 3 shows XRD spectra from samples

deposited with a flame inner cone to substrate distances of 0.5 and 1.0 mm, respectively. The combustion gas was held constant at O_2:C_2H_2:C_2H_4 = 1280:650:700 sccm. At both distances the diffraction peak intensity increased with the addition of the CO_2 laser. However, the change in the diffraction peak intensity with the change in distance was minimal. Figure 4 presents the XPS spectra of the C 1s electron for each condition. The spectra exhibited shoulders at higher binding energies and were resolved by two curves. The lower binding energy peak was located at 285 eV and identified as C-C bonding associated with sp^2 bonding. The higher binding energy peak, at ~286.1 eV was identified as C-C bonding associated with the sp^3 bonding found in diamond. Comparison of the data revealed little difference in the samples from a chemical bonding stand point. This was evidenced by the fact that the shape and intensity of the spectra were very similar.

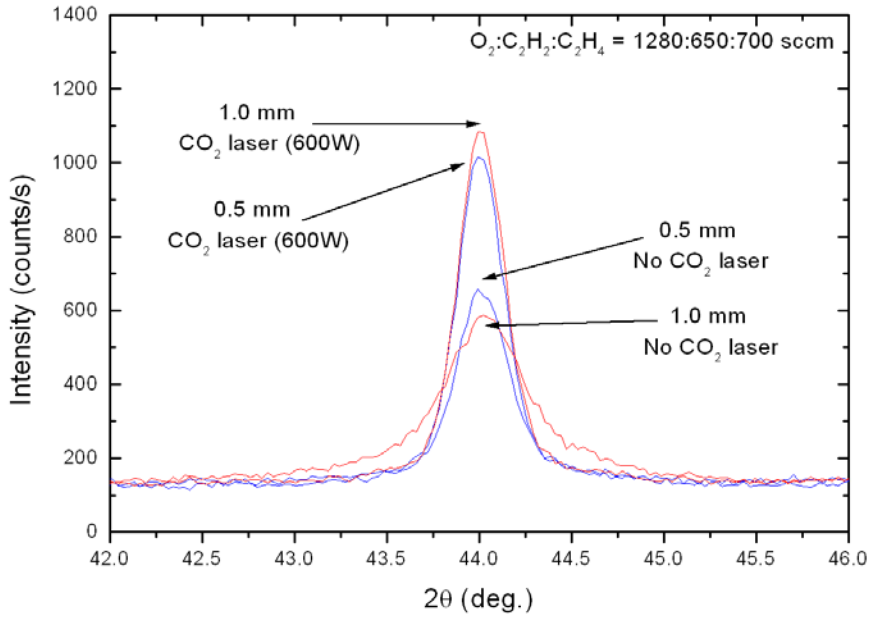

Figure 3: XRD spectra from LACF films deposited at varying flame inner cone to substrate distances.

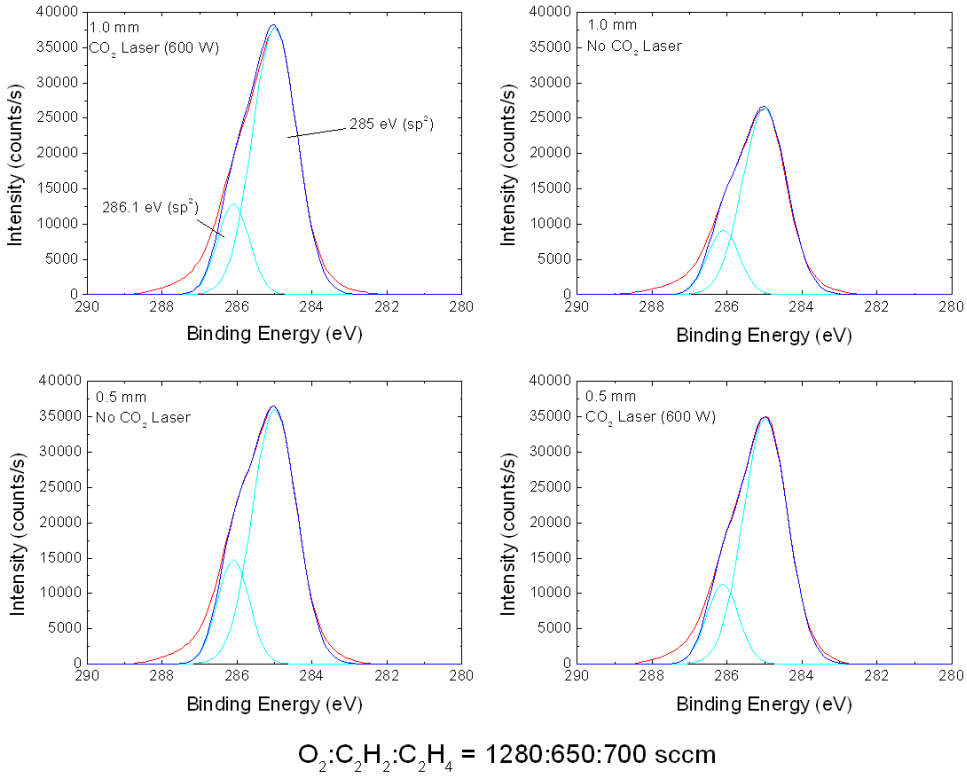

Figure 4: XPS spectra from samples with varied flame inner cone to substrate distances.

The effect of the combustion gas composition was investigated by XRD and XPS. Specifically, the effect of changing the partial pressures of C_2H_4 and O_2 in the combustion gas was studied. The O_2:C_2H_2 ratio was held constant at 1280:650 sccm and the C_2H_4 flow rate was varied between 650 and 700 sccm. Figure 5 shows the comparison of the XRD spectra for the cubic diamond (111) diffraction peak. Regardless of C_2H_4 flowrate, the inclusion of the CO_2 laser irradiation increased the diffraction peak intensity. These results were in agreement with the film morphology results from the SEM images as the film deposited with the laser had a larger grain size which results in a sharper, more intense peak. The increase in the C_2H_4 flowrate increased the intensity of the cubic diamond diffraction peak regardless of whether the laser was included.

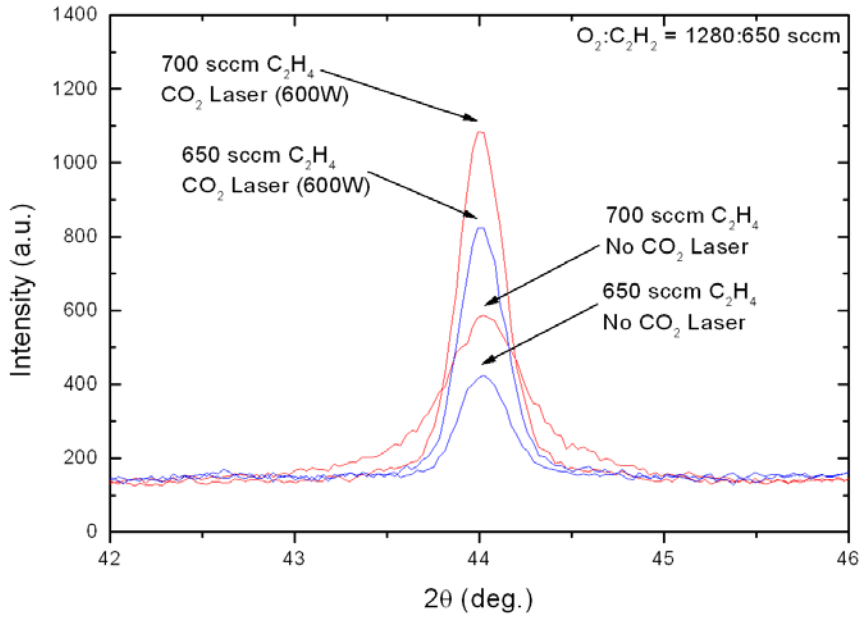

Figure 5: XRD spectra of LACF deposited diamond thin films at varying C_2H_4 flowrates.

The study of the effect of the oxygen partial pressure utilized XRD and XPS. The C_2H_2:C_2H_4 ratio was held constant at 650:700 sccm and the O_2 flowrate was at two levels, 1280 and 1320 sccm. The effect of changing the O_2 partial pressure in the combustion gas, with and without the laser, was evident in XRD spectra from the appropriate samples (Figure 6). With the laser, a lower partial pressure of oxygen resulted in a more intense diamond diffraction peak. Without the laser, a higher partial pressure of oxygen produced a more intense diamond peak. The XPS results (Figure 7) confirmed that the film had a significant amount of diamond in that the C 1s spectra for all the samples exhibited a noticeable shoulder at a higher binding energy. As such, each spectrum was again resolved by two curves, 285.0 eV (sp^2) and 286.1 eV (sp^3). The 1.1 eV difference corresponds to the generally accepted difference from the literature. A comparison of the percentage of the area under the fitted curve attributed to sp^2 and sp^3 components revealed each sample (laser and no laser) to have essentially the same values.

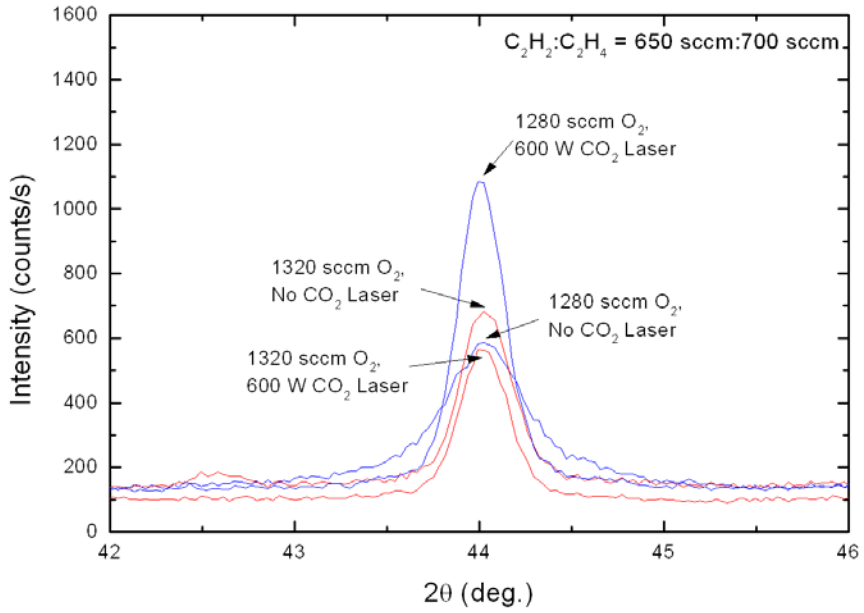

Figure 6: XRD spectra of LACF deposited diamond thin films at varying O_2 flowrates.

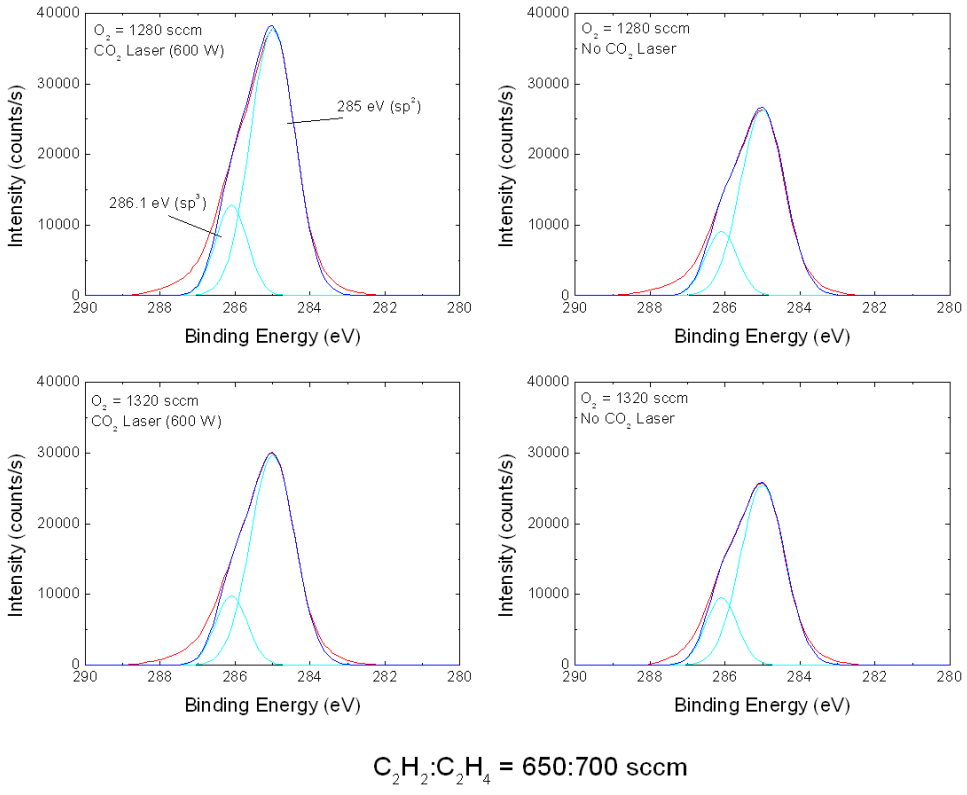

Figure 7: XPS spectra from films deposited at different oxygen flowrates.

A diamond film deposited at UNL was masked with kapton tape and exposed to Ar and O_2 plasmas in the reactive ion etcher (RIE) at different etch conditions to determine what, if any, morphological effects would result. The diamond film was deposited for 21 minutes by the LACF process with a horizontally focused CO_2 laser at 500 W and process gas mixture of O_2:C_2H_2:C_2H_4 = 1250:1000:400 sccm. After exposure to the plasma in the RIE there were four separate areas of the film which were observable through light microscopy and corresponded to the four etch conditions. Figure 8 below, shows the four areas labeled with the etch condition (UE = un-etched, AO = Argon only, ATO = Argon then oxygen, and O_2O = Oxygen only).

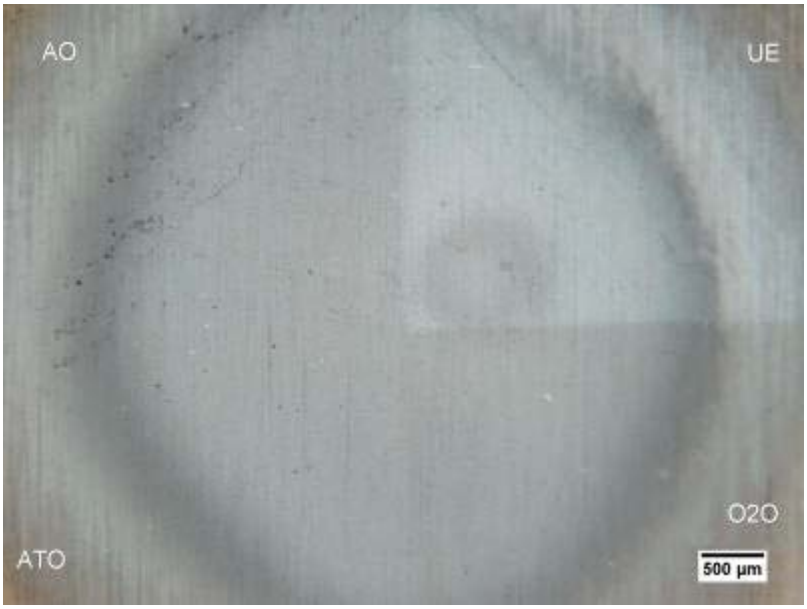

Figure 8: Digital micrograph of CO_2 laser-assisted combustion-flame deposited diamond film after exposure to Ar and O_2 plasmas. The areas are labeled with the corresponding etch condition (UE = un-etched, AO = Argon only, ATO = Argon then oxygen, and O2O = Oxygen only).

The oxygen plasma had the greatest effect qualitatively on the film and removed the “soot” material on that portion of the substrate. Figure 9 shows SEM images from various areas of interest. The argon plasma appeared to have little effect on the film as the SEM images were very similar to images of the un-etched film as seen in Figure 9(b) and Figure 9(a) respectively. The image of the O2O area (Figure 9(c)) revealed “defects”

in the surface of the film (“pin holes”) which were most likely caused by the concurrent chemical and physical etching of the film. The argon plasma followed by the oxygen plasma did not appear to have an additive effect as shown in Figure 9(d).

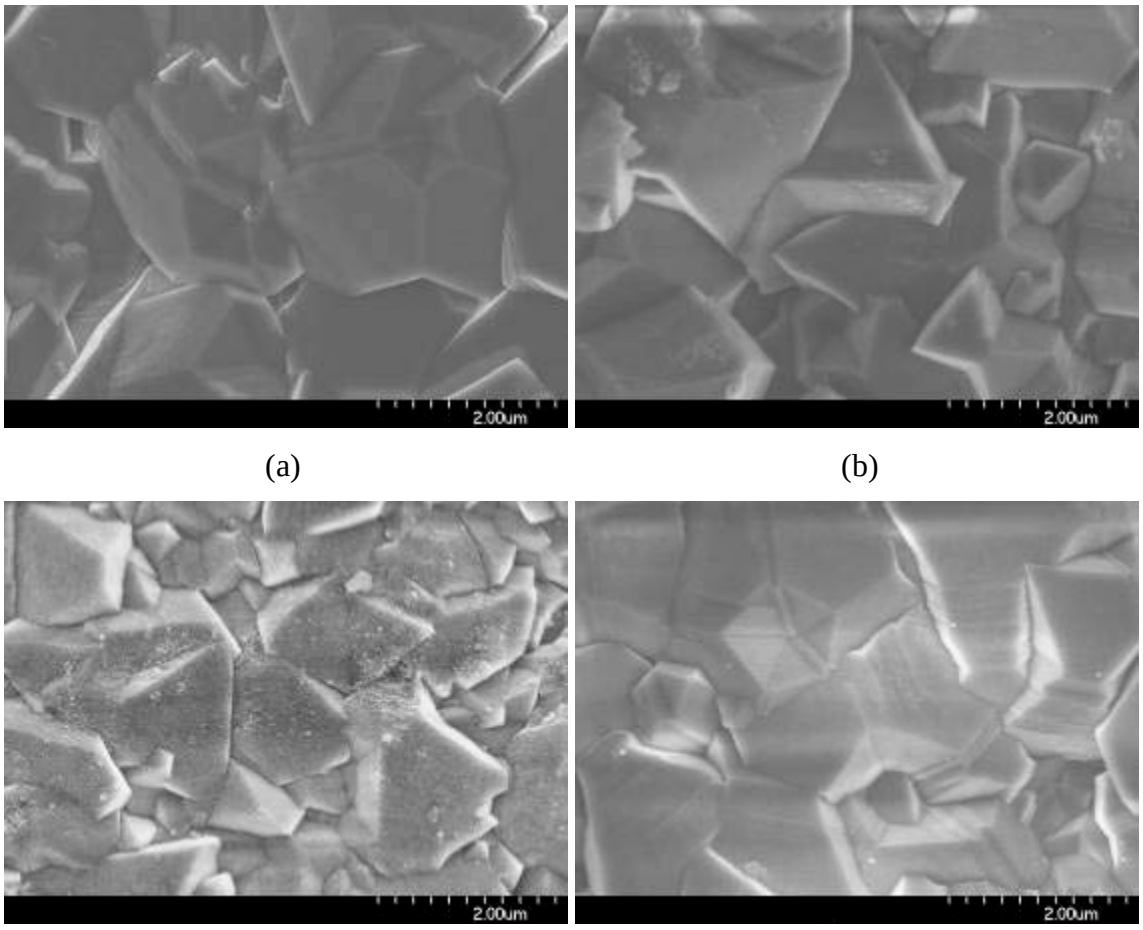

(a) (b)

(c) (d)

Figure 9: SEM image of diamond thin film exposed to (a) no post-deposition plasma, (b) argon only plasma, (c) oxygen only plasma and (d) argon followed by oxygen plasma.

The cross-section of diamond films deposited by a horizontally focused CO_2 laser-assisted combustion-flame method at UNL was investigated using SEM. The objective was to determine the effect of the horizontally focused CO_2 laser on the thickness, and subsequently, the deposition rate of the films. Figure 10 shows a representative SEM image. The surface of the WC substrates and the diamond film were too rough and uneven for thickness measurements with the standard stylus profilometer.

The WC substrates were sectioned using a diamond wafering blade and a low speed saw. The diamond film remained intact during the sectioning with the exception of a few areas near the cutting edge. The previous study of the films concluded that the laser irradiation led to larger diamond grains. That result was neither confirmed nor denied by the cross-section images. In general, the thicknesses of the films deposited with and without the CO_2 laser were between one and two microns thick, allowing for discrepancies from sample tilt and uneven topography. Also, the interface between the film and the substrate appeared to be smooth with no transition area readily apparent. Overall, it was determined that the adherence of the diamond films was adequate to survive cutting of the WC substrate for further characterization.

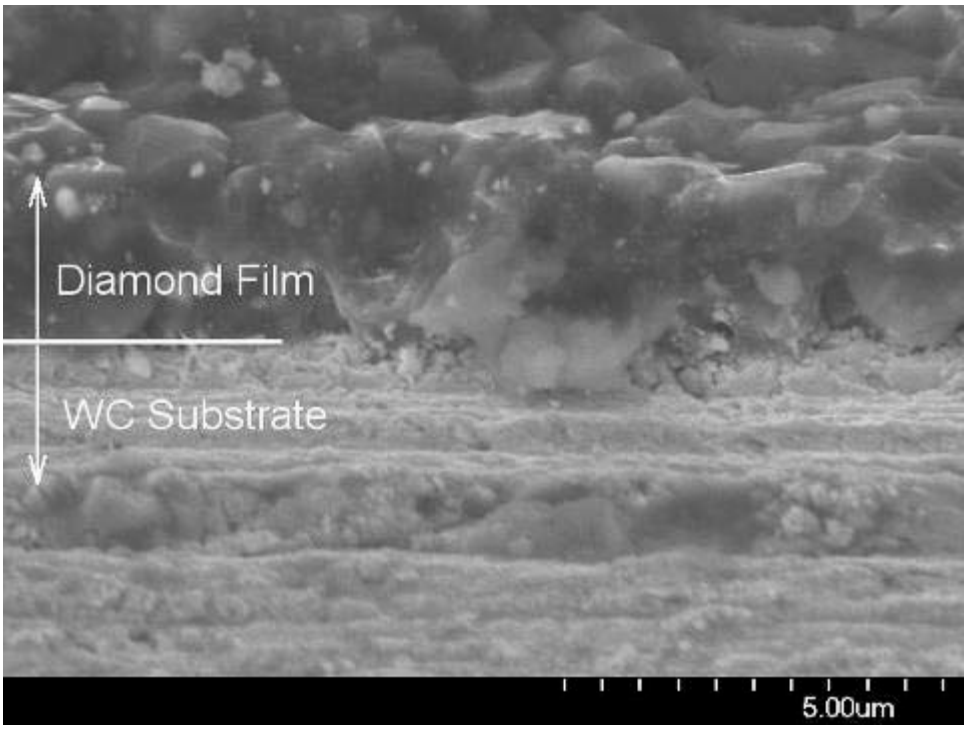

Figure 10: SEM image of cross-section of LACF deposited diamond film and WC substrate.

Carbon pillars

Samples from UNL included a carbon pillar deposited by the O_2/C_2H_2 combustion-flame method and a sample of soot from the combustion of C_2H_2. XRD and XPS analysis was completed on the pillar and soot. The XRD results are shown in Figure

11. The XRD spectrum of the soot, which was still on the WC substrate, displayed a broad peak near 26° and several peaks associated with WC that are labeled on Figure 11. The broad hump was in the area of the characteristic peak for the diffraction of the (002) planes of hexagonal graphite. The XRD spectrum obtained from along the side of the carbon pillar showed four characteristic peaks for hexagonal graphite. The most intense peak occurred near 26° of 2θ. It was concluded that the pillar was similar to the ultra-fast deposited pillars and composed of crystalline graphite. The soot was composed of an amorphous graphitic phase.

XPS analysis of the soot required removal from the WC substrate. The soot was scraped from the substrate surface and onto carbon tape onto a sample stub for analysis. The soot was pressed down and covered the entire surface of the tape. Figure 12 shows the XPS results for the soot and carbon pillar. The C 1s spectrum taken from the soot produced a peak near 285 eV that exhibited a one curve as seen in Figure 12(a). The C 1s spectrum from the pillar exhibited a slightly broadened peak centered near 285 eV resolved by one curve and was determined to be graphitic as seen in Figure 12(b).

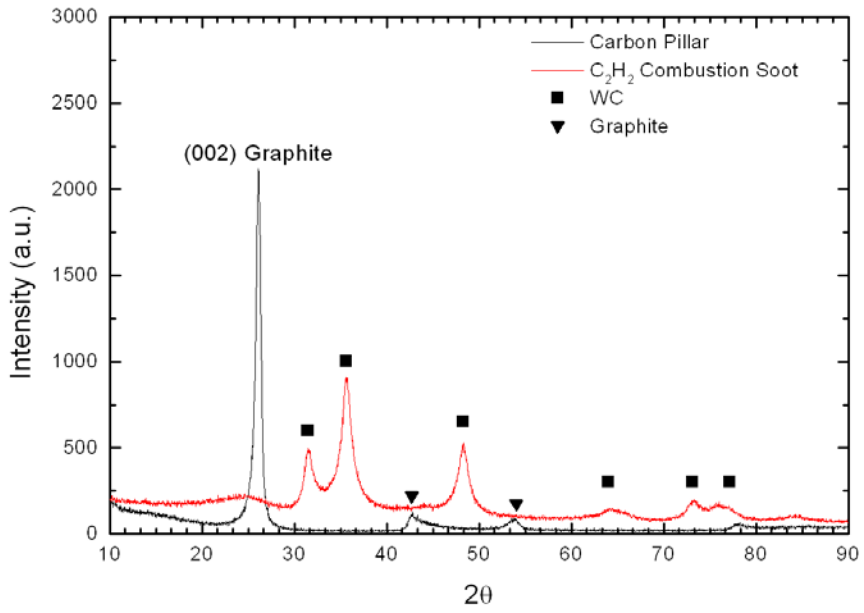

Figure 11: XRD comparison of combustion soot and carbon pillar.

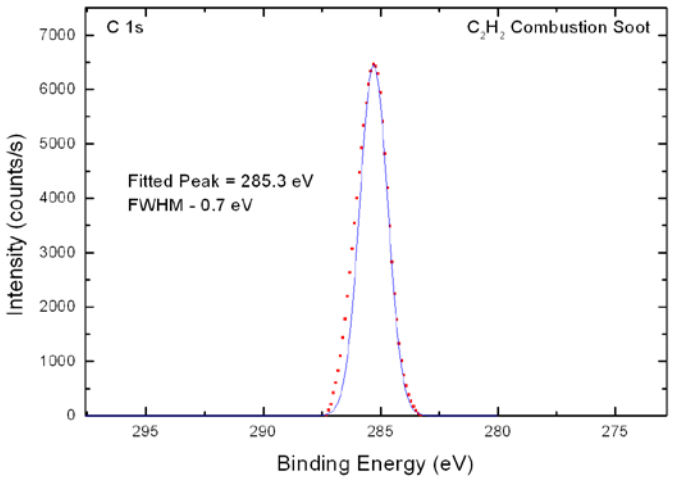

(a)

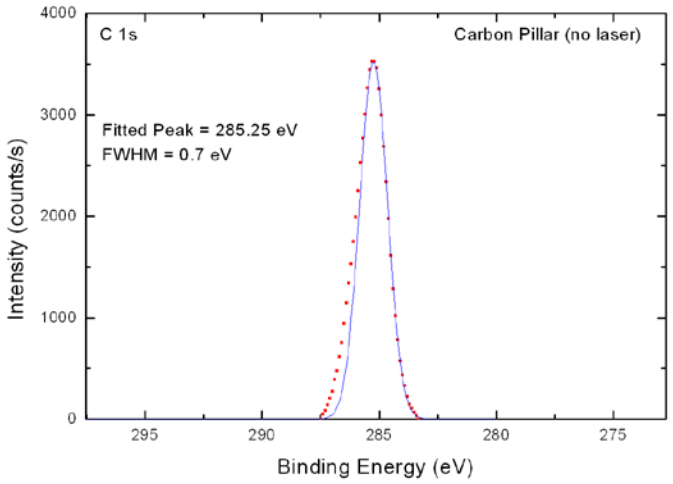

(b)

Figure 12: XPS C 1s spectra from (a) C_2H_2 combustion soot and (b) carbon pillar deposited by a combustion-flame method.

To further characterize the ultra-fast deposited combustion flames, representative samples were sent to the Air Force Research Labs (AFRL) for nanoindentation. The mechanical properties of hardness and modulus of the samples was determined. Table 1 summarizes the results. Figure 13 shows the samples and the areas tested by nanoindentation. The experimental values were relatively close to standards for graphite

and WC. The results confirmed the XRD analysis that determined the carbon pillars to be graphite.

Table 1: Mechanical properties of ultra-fast deposited carbon pillars as determined by nanoindentation

Sample	Location	E, GPa	H, GPa
340-1	Pillar Base	11.1	0.6
340-2	Pillar Base	10.8	0.6
340-3	WC Substrate	607.1	26
340P-1	Pillar (center)	3.4	0.2
320-1	Pillar Base	7.8	0.4
320-2	WC Substrate	567	26.9
S1-1	Pillar (center)	13	1.9
S3-1	Pillar (center)	5.7	0.7

Note: E and H are average over depth 400 ~ 500 nm

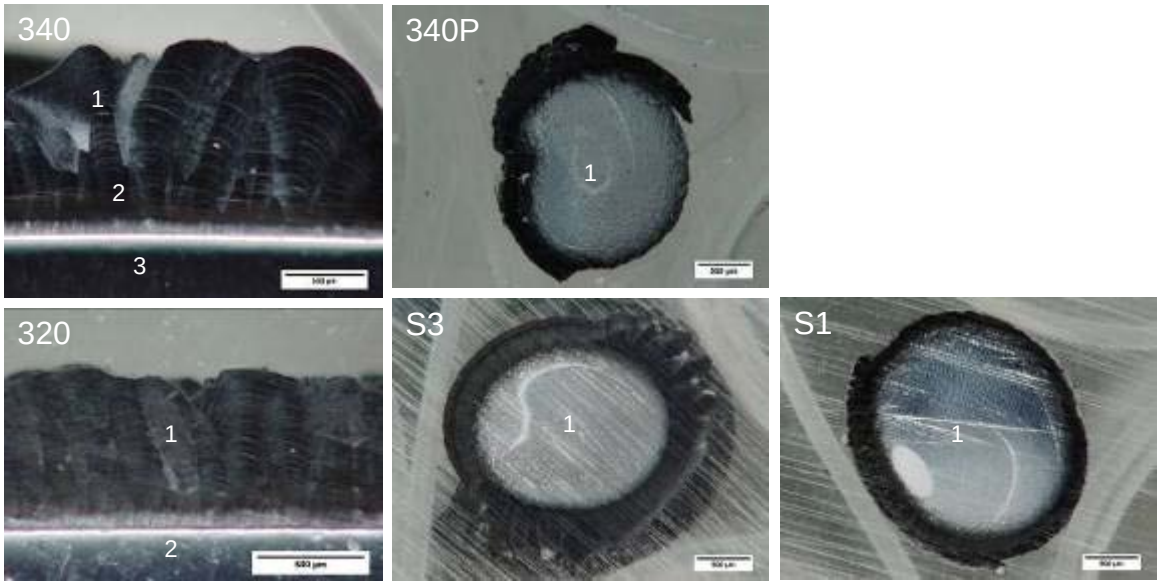

Figure 13: Digital micrographs of nanoindentation samples.

Depositions with O_2 + C_3H_6

The samples were horizontally focused CO_2 laser-assisted combustion-flame (LACF) deposited films on WC substrates. These experiments varied the incidence angle of the combustion-flame relative to the WC substrates as well as the location of the

incident laser beam on the combustion-flame. The O_2:C_3H_6 gas ratio was held constant at 1420:1250 sccm with the laser power set at 600 W. The flame was either vertical (0° incidence angle) or tilted (45° incidence angle). The films were characterized by XRD for phase identification.

When the flames were in the vertical position the distance between the WC substrate and laser beam was varied. Figure 14 shows the XRD spectra from all laser to substrate distances (no laser, 1, 3, 5 mm). Figure 14(a) shows the entire 2θ range and Figure 14(b) shows the spectra in the area of the cubic diamond (111) diffraction peak. The most intense peaks correspond to the WC substrate. The other major peaks were identified as various W_xO_y, $Co_xW_yO_z$ and Co_xW_yC species. There was a significantly less intense peak for cubic diamond. Given the signal intensity, there was little evidence that the CO_2 laser irradiation enhanced the diamond deposition. The higher peak intensity for the cubic diamond peak of the film deposited at a laser to substrate distance of 1 mm was attributed to the diffractometer conditions being slightly different since the entire spectrum was shifted to a higher intensity.

The effect of the laser to the combustion-flame nozzle distance was studied with the 45° tilted flames. Figure 15 shows the XRD spectra from all laser to nozzle distances (no laser, 0, 0.5, 1.0 mm). Figure 15(a) shows the entire 2θ range and Figure 15(b) shows the spectra in the area of the cubic diamond (111) diffraction peak. As with the vertical flames, the most intense peaks were identified as WC and the other oxides and carbides. The tungsten oxide peaks were more intense when compared to the vertical flames. Contrary to the vertical flames, the cubic diamond peak was not present. SEM images of the films did reveal faceted material, which typically has been associated with diamond peaks on XRD. It was possible that the diamond phase, if present, was too small and infrequent to be identified where the x-ray beam was focused. Figure 16 shows representative SEM images of the vertical and 45° tilted flame conditions in an area closest to that sampled during XRD. The faceted material in Figure 16(b) was much less evident. Another possibility was that the faceted material was crystalline tungsten oxide.

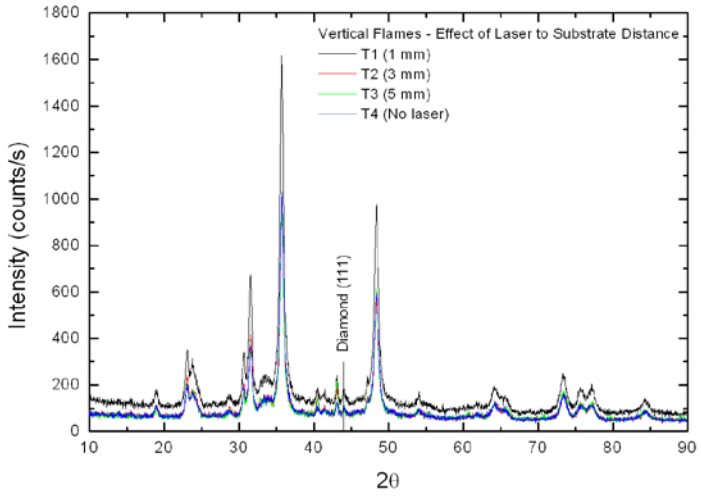

(a)

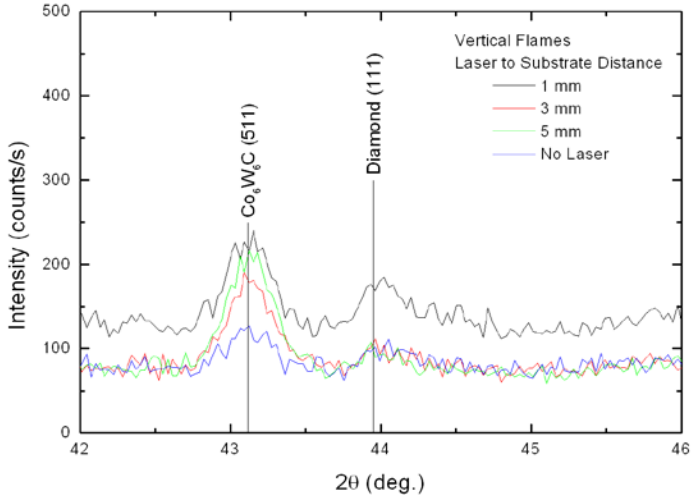

(b)

Figure 14: XRD spectra from LACF deposited film with vertical flames showing (a) entire 2θ range and (b) range associated with cubic diamond (111).

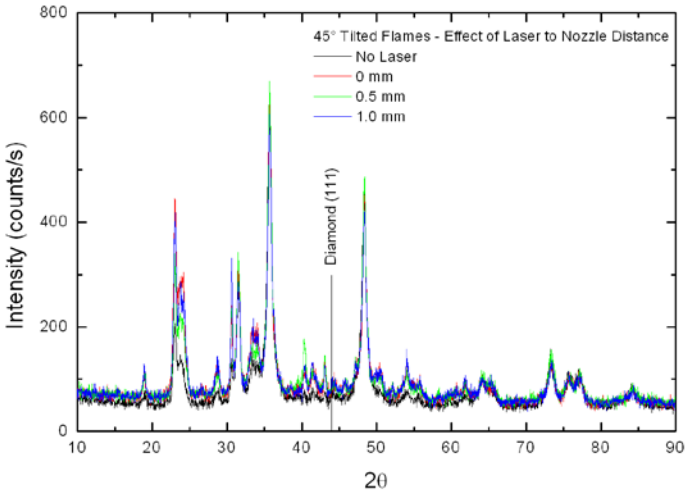

(a)

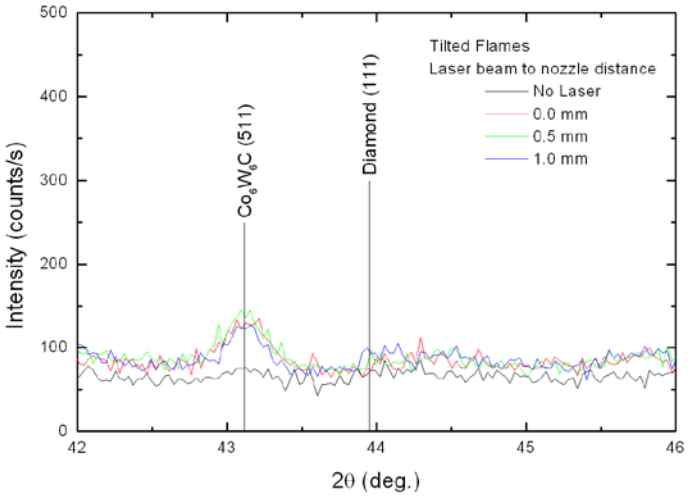

(b)

Figure 15: XRD spectra from LACF deposited film with 45° tilted flames showing (a) entire 2θ range and (b) range associated with cubic diamond (111).

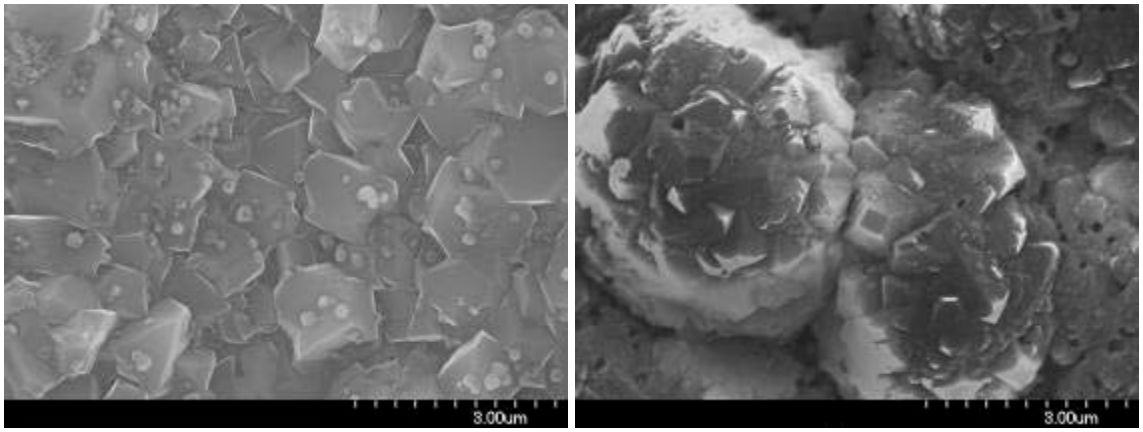

(a) (b)

Figure 16: SEM images from films deposited with (a) vertical flames and (b) 45° tilted flames.

MURI Annual Review 2009

Materials Characterization

Samples produced at UNL were characterized and analyzed throughout the year. The samples included films deposited by the CO_2 laser-assisted combustion-flame chemical vapor deposition (CVD) process. The effect of the deposition parameters, in particular the type of substrate and the laser wavelength and power, on the film morphology, microstructure and phases present was the primary focus of the work. Additionally, the effect of the laser energy on the film nucleation and growth was also investigated. The samples were characterized with optical microscopy, scanning electron microscopy (SEM), X-ray diffraction (XRD), micro-Raman spectroscopy, and scanning transmission electron microscopy (STEM) of cross-sectional specimens prepared using a focused-ion beam (FIB) system.

Laser wavelength and substrate effect

The samples were deposited on WC and silicon substrates for 30 minutes using a $O_2/C_2H_2/C_2H_4$ gas precursor (O_2:C_2H_2:C_2H_4 = 1200:620:620 sccm) and a tunable CO_2 laser. The laser power was 400 W and the wavelength was 10.532 μm. The wavelength was tuned to match the resonant frequency of the CH_2-wag vibrational mode of the C_2H_4 molecule. Optical micrographs of the as-deposited films are shown in Figures 1 and 2. The films deposited without the laser (Figures 1(a) and 2(a)) exhibited an approximately 1 mm circular area directly beneath the flame that was dark in color, which was soot-like in appearance. The dark area, labeled in Fig 1(a), was not apparent when the laser was used. It should be noted that deposit was circular in all cases except for the film deposited with the laser on silicon (Figure 2(b)) which had a non-uniform shape.

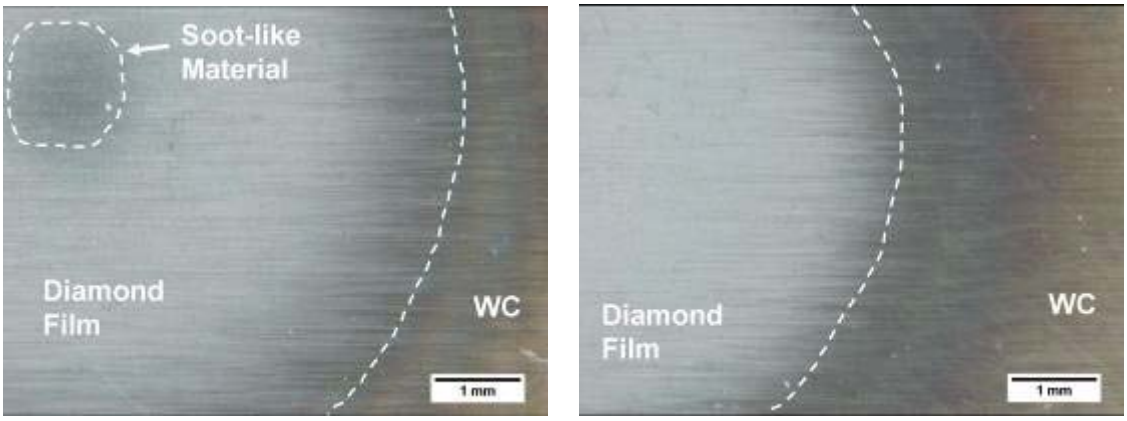

(a) (b)

Fig. 1. Optical micrographs from films deposited on WC substrates (a) without laser irradiation and (b) with laser irradiation.

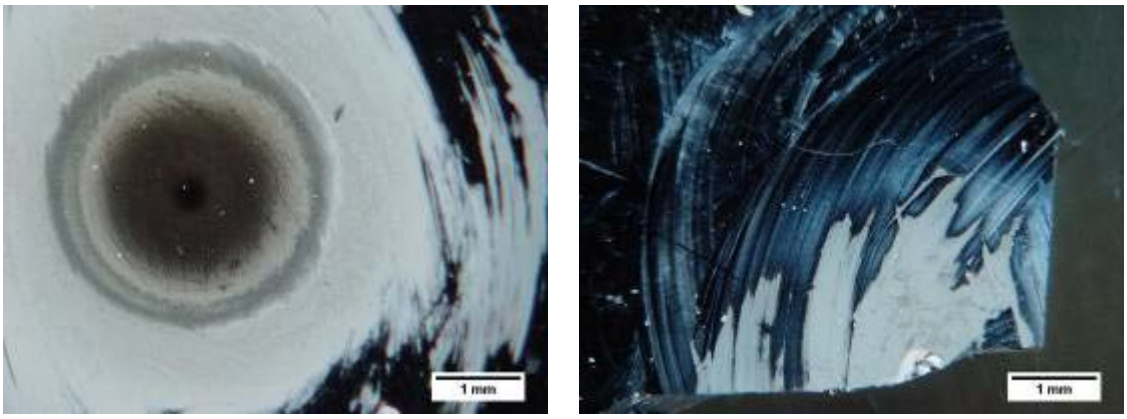

(a) (b)

Fig. 2. Optical micrographs from films deposited on Si substrates (a) without laser irradiation and (b) with laser irradiation.

The phases present in the films were investigated using both XRD and micro-Raman spectroscopy. Figure 3 shows the XRD spectra for films on both WC and Si with a more detailed view of the diamond (111) diffraction peak inset. The XRD spectra from the films deposited on WC shown in Figure 3(a) exhibited diffraction peaks from the substrate as well as from cubic diamond (111) (~44°) and (220) planes (~76°). The inset view shows the peak was slightly more intense and broader for the film deposited without the laser. The higher peak intensity was indicative of more diamond material diffracting the x-ray beam. However, there are other factors that affect the peak intensity, including

the surface topography of the sample and other instrumental factors such as beam intensity and alignment. Figure 3(b) shows the XRD spectra from the films deposited on silicon substrates. Again, the diamond (111) and (220) planes were apparent. The additional peak (~52°) and broad hump (~55°) were artifacts from the silicon substrate. From the inset view it was clear that the diamond (111) peak was significantly more intense, but also broader, without the laser irradiation. The sharper diffraction peak from the films deposited with the laser was indicative of a larger grain size.

Figure 4 shows the Raman spectra from the films deposited on both WC and Si. As seen in Figure 4(a), the first order Raman peak for diamond was clearly evident in the film deposited with the laser and less evident in the film deposited without the laser irradiation. The spectra from the film deposited without the laser had a significantly higher non-diamond (graphitic) component in agreement with Fig 2(a) that showed a large dark spot in the middle of the sample. Figure 4(b) details the Raman spectra from the films deposited on silicon that shows a sharp peak associated with diamond in the film deposited with laser irradiation. The film deposited without the laser exhibited a broad band located at approximately 1550 cm^{-1}. The band is known as the G-band and associated with the non-diamond, amorphous graphitic carbon phase in the film. The Raman results suggested that the addition of the tuned CO_2 laser was beneficial to the deposition of the diamond phase, regardless of the substrate. The Raman and XRD results differ in the relative amount of diamond detected, but the micro-Raman tests a much smaller area of the film which may account for the differences.

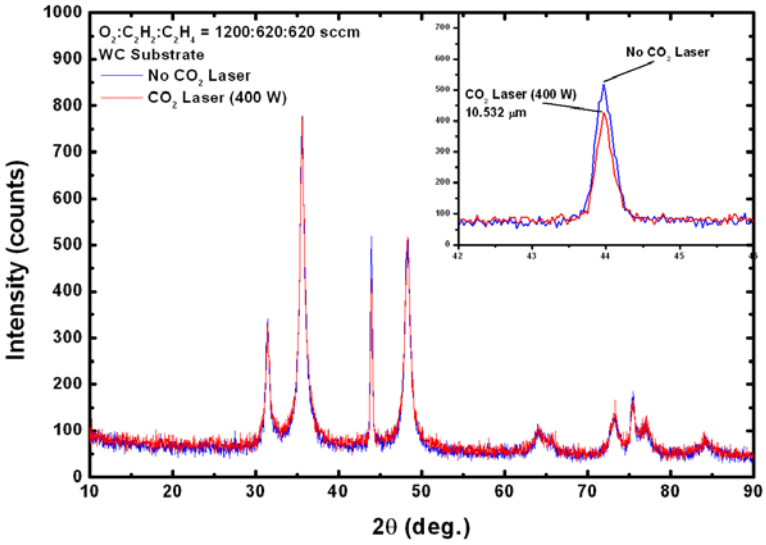

(a)

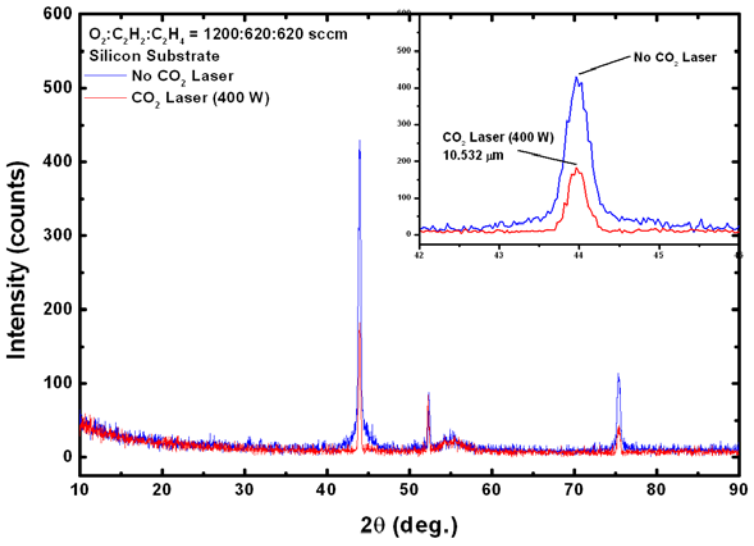

(b)

Fig. 3. XRD spectra demonstrating the effect of CO_2 laser irradiation with 2θ range associated with cubic diamond (111) inset on (a) WC substrates and (b) silicon substrates.

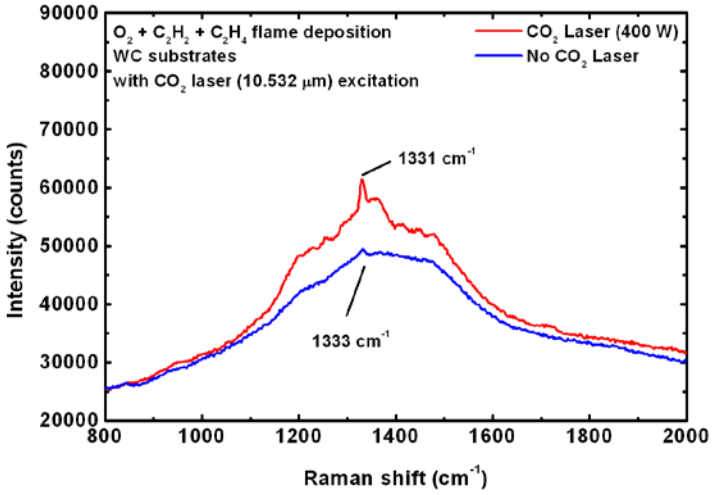

(a)

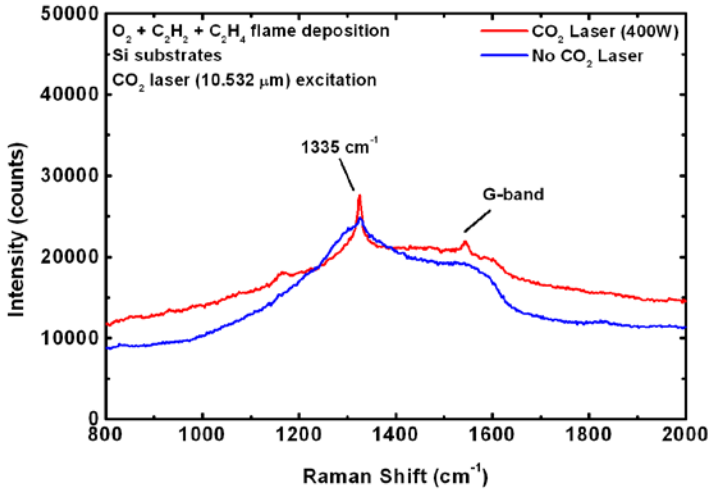

(b)

Fig. 4. Raman spectra of the diamond films showing the laser irradiation effect on (a) WC substrates and (b) silicon substrates.

STEM specimen were produced from each film using a dual beam FIB/SEM system by milling out a section of the film and substrate and attaching that piece to a copper grid. Figure 5 shows dark-field (DF) STEM images from the films deposited on WC. The image from the deposit without the laser (Fig 5(a)) showed a polycrystalline film approximately 2 μm in thickness with grains less than 1 μm in size. The grains

nearest the substrate/film interface appeared to be smaller than those nearer to the surface of the film. In Fig 5(b) the film deposited with the laser is 4 μm in thickness with some grains approaching 2-3 μm in size. The grains near the substrate/film interface appeared smaller and more randomly orientated, while several larger columnar grains were apparent toward the film surface. In terms of film nucleation, the substrate/film interface was very sharp with little interaction between the film and substrate. The smaller, darker particles near the interface were determined to be artifacts from ion milling during the sample preparation. The difference in thickness was attributed to the fact that the sample from the film deposited without the laser was from the edge of the deposit area where the film was thinner than in the area closer to the center.

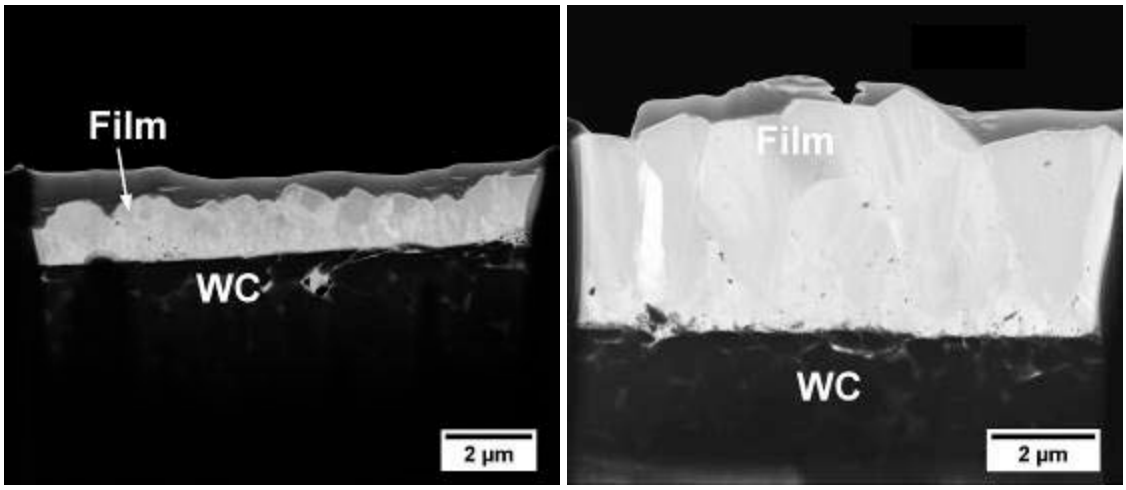

(a) (b)

Fig. 5. Dark-field STEM images from the diamond films deposited on WC (a) without CO_2 laser irradiation and (b) with CO_2 laser irradiation.

Figure 6 shows the STEM images from the films deposited on silicon. There were similar features in the images from the films deposited on silicon when compared to the films on WC substrates, namely the increase in grain size from the substrate to the film surface. Both films were ~3 to 4 μm in thickness, but with different microstructures. The film deposited without the laser (Fig 6(a)) appeared to have grains with several defects (twins), with some oriented parallel to the substrate surface. The grains in the film deposited with the laser (Fig 6(b)) were columnar and appeared to have fewer

defects. There was a defect from sample preparation in the center of the specimen which made grain morphology and microstructure difficult to discern. The STEM results indicated the use of the tuned laser resulted in a change in the growth morphology of the films, especially for the films deposited on silicon substrates.

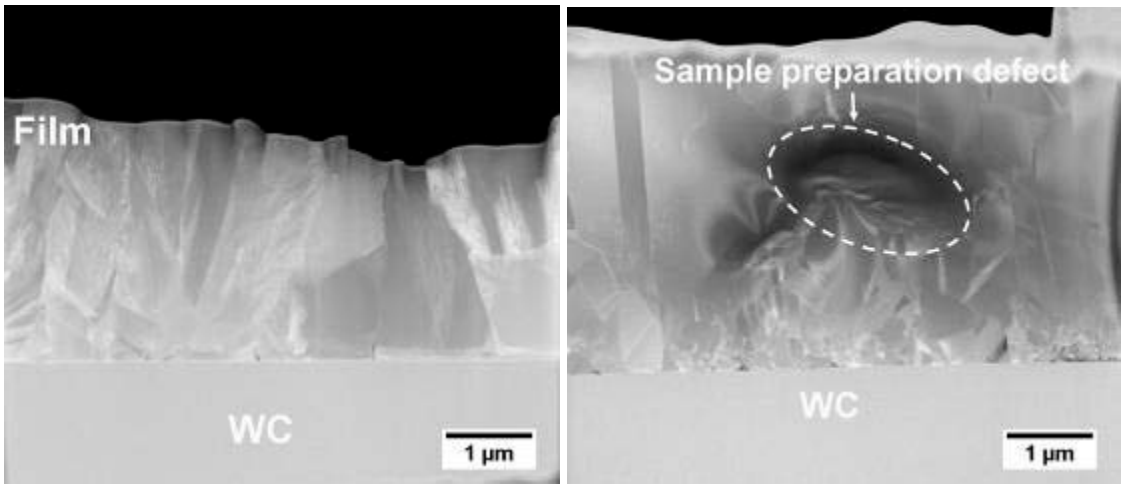

(a) (b)

Fig. 6. Dark-field STEM images from diamond films deposited on Si substrates (a) without CO_2 laser irradiation and (b) with CO_2 laser irradiation.

Laser wavelength and power effect

Films were deposited on WC substrates for 15 minutes using a $O_2/C_2H_2/C_2H_4$ gas precursor (O_2:C_2H_2:C_2H_4 = 1200:620:620 sccm) and a tunable CO_2 laser. The untuned laser wavelength was 10.591 µm (which is typical for a CO_2 laser) and the resonant excitation matched, tuned wavelength was 10.532 µm. The laser powers were 100, 400 and 800 W along with a film deposited without laser irradiation for comparison.

The deposited films covered a circular area, in the center of the WC substrate, approximately 10 mm in diameter. Plan view SEM images of the aforementioned area are shown in Figures 7 and 8. Fig. 7 shows the films deposited at each of the laser powers with the untuned CO_2 laser wavelength of 10.591 µm and the film deposited without laser irradiation for comparison. The films were continuous and consisted of overlapping, randomly oriented faceted crystals at all process conditions. The small, white particles on the surface of the films were identified as cobalt, which is used as a

sintering agent for WC, and most likely was redeposited from the substrate. The grain size of the film deposited without the CO_2 laser was approximately 1 µm. This was a lateral approximation to gain a qualitative comparison of the grain size between the various deposited films. At the lowest level of laser power (100 W, Fig. 7(b)) there was a noticeable increase in the grain size. When the laser power was increased to 400 and 800 W, Fig 7(c) and (d) respectively, the grain size increased to larger than 2 µm. The increase in surface grain size for the same deposition time indicated that the addition of the CO_2 laser irradiation promoted grain growth in the film.

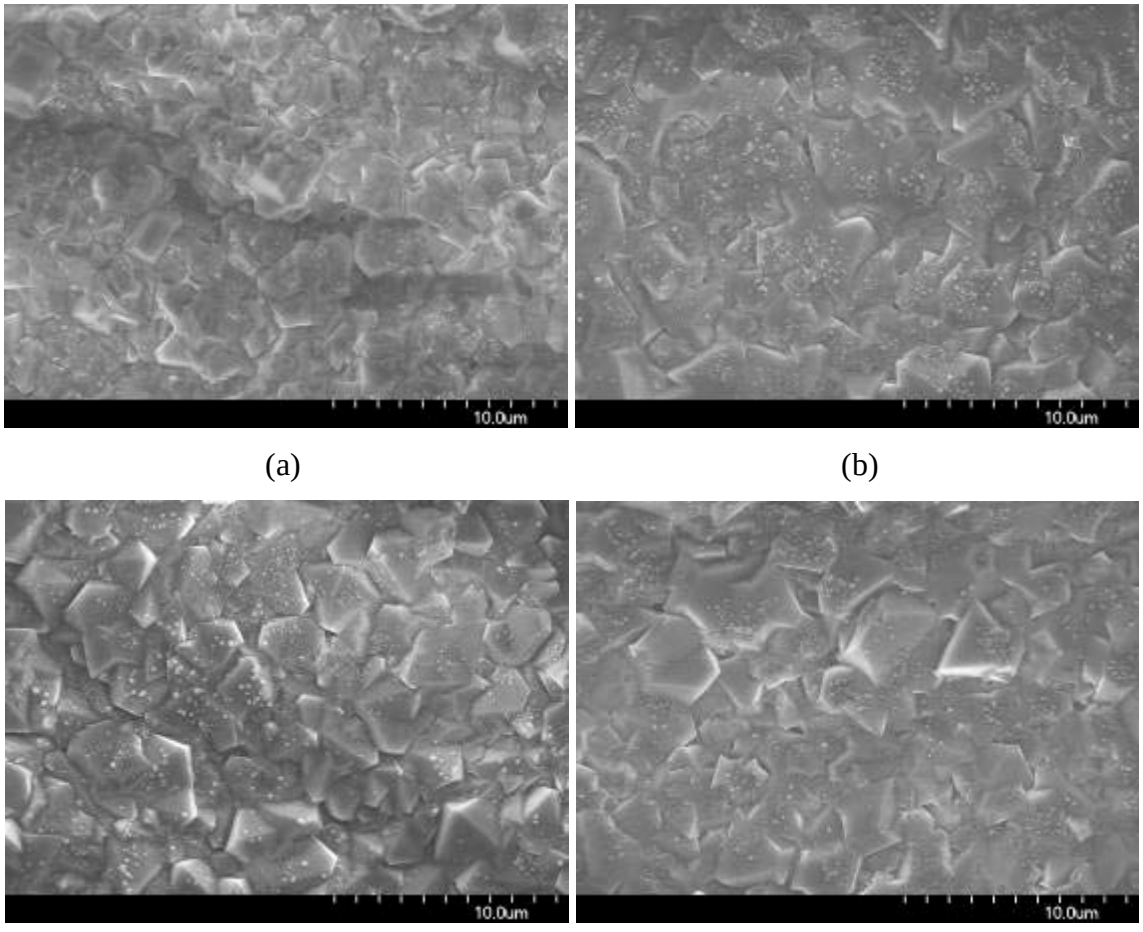

Fig. 7. SEM micrographs of as-deposited films, processed with the CO_2 laser wavelength of 10.591 µm and a laser power of (a) no laser, (b) 100 W, (c) 400 W and (d) 800 W.

Fig. 8 shows the films deposited at each laser power with the tuned CO_2 laser wavelength of 10.532 μm. In general, the films were similar in appearance to the films deposited with the laser wavelength of 10.591 μm in that the surface consisted of randomly orientated, overlapping faceted crystals with cobalt particles present on the top surface. The image of the film deposited without laser irradiation is included for comparison (Fig. 8(a)). Fig. 8(b) shows the film deposited at 100 W in which the grain size increased to approximately 1-2 μm versus the no laser case, though not as much as the film deposited with 100 W at 10.591 μm. The films deposited with a laser wavelength of 10.532 μm at 400 and 800 W, Fig. 8(c) and 8(d) respectively, had grain sizes that increased to greater than 2 μm and as much as 5 μm. Comparing the grain sizes of the films deposited at different laser wavelengths revealed that the tuned 10.532 μm condition resulted in significant grain growth, especially at the higher laser powers (400 and 800 W). The SEM results agreed with the UNL studies indicating resonant excitation of the gaseous precursors could increase the population of excited species responsible for diamond formation. If the manifestation of successful energy coupling is an increase in grain size for the same deposition time, then it follows that the 10.532 μm wavelength would produce larger grains since it is closer to the absorption band associated with the CH_2-wag vibrational mode of the C_2H_4 molecule.

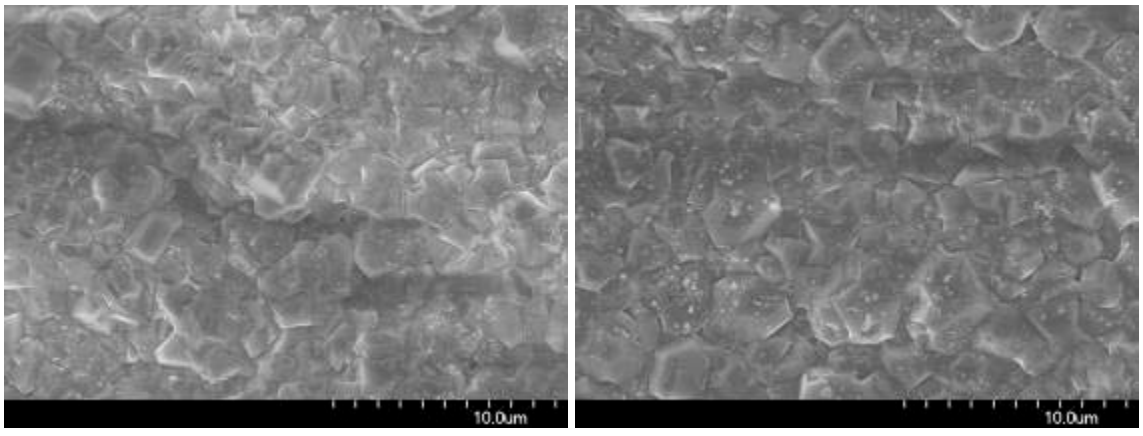

(a) (b)

Fig. 8. SEM micrographs of as-deposited films, processed with the CO_2 laser wavelength of 10.532 μm and a laser power of (a) no laser, (b) 100 W, (c) 400 W and (d) 800 W.

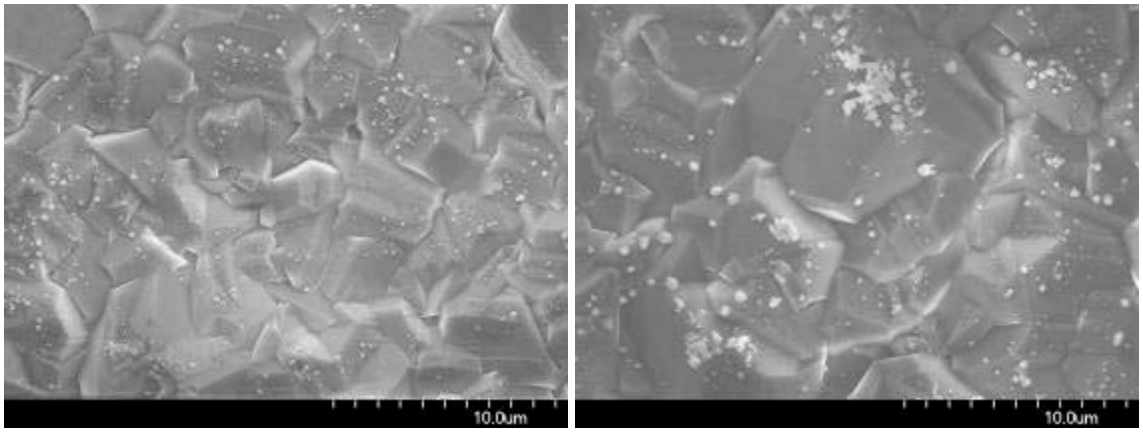

(c) (d)

Fig. 8. (Continued) SEM micrographs of as-deposited films, processed with the CO_2 laser wavelength of 10.532 µm and a laser power of (a) no laser, (b) 100 W, (c) 400 W and (d) 800 W.

Summary

The concept of multi-energy processing was investigated by coupling the energy from CO_2 laser irradiation with a combustion flame. Diamond thin films were deposited on WC and Si substrates by a CO_2 laser-assisted combustion-flame method. Subsequent characterization by various methods determined the effect of the CO_2 laser irradiation (wavelength and power) on the deposited films, specifically film surface morphology, phase, and film quality. It was concluded that regardless of power or wavelength the addition of the energy from the CO_2 laser was beneficial as the deposition area was more uniform and the film grain size increased. The diamond x-ray diffraction and Raman peaks were usually more intense when laser irradiation was used, indicating a greater amount of a diamond phase was detected. It was determined that for a given wavelength, when the laser power was increased the grain size increased, the diamond x-ray diffraction peak was more intense and the characteristic diamond Raman peak was sharper and more evident. For a given power, comparisons were made between the two different laser wavelengths. In general, the film grain size was larger, the diamond diffraction peak intensity increased and sharpened, and the Raman diamond spectra was more dominant when the films were deposited with a 10.532 µm tuned CO_2 laser wavelength than with an untuned 10.591 µm CO_2 laser wavelength.

VITA

Travis Kyle McKindra was born on January 25, 1980 in Kansas City, KS where he grew up with his parents and two sisters. He graduated from Sumner Academy of Arts and Science in May 1998. He enrolled at the University of Missouri-Rolla in the fall of 1998. He obtained his Bachelor of Science degree in Metallurgical Engineering at the University of Missouri-Rolla in December 2002. He earned his Master's degree in Metallurgical Engineering in May 2004. He has worked as a Graduate Research Assistant and as a Graduate Teaching Assistant. He earned his doctorate in Metallurgical Engineering in December 2010 under the advisement of Dr. Matthew J. O'Keefe.